Department of
Industry and Resources

RECORD
2007/3

STRUCTURAL AND LITHOLOGICAL EVOLUTION OF THE JACK HILLS GREENSTONE BELT, NARRYER TERRANE, YILGARN CRATON, WESTERN AUSTRALIA

by C. V. Spaggiari

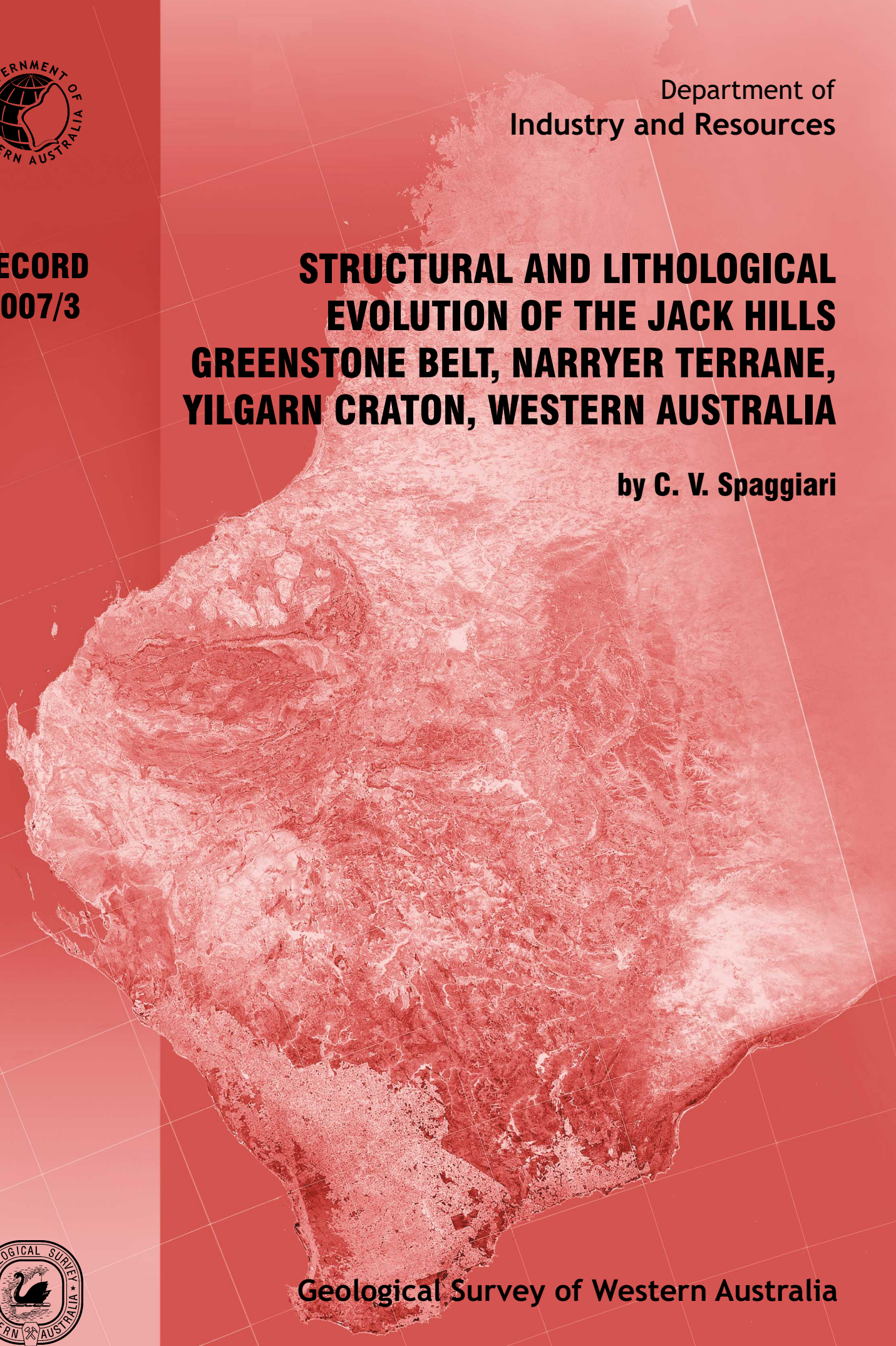

Geological Survey of Western Australia

GEOLOGICAL SURVEY OF WESTERN AUSTRALIA

Record 2007/3

STRUCTURAL AND LITHOLOGICAL EVOLUTION OF THE JACK HILLS GREENSTONE BELT, NARRYER TERRANE, YILGARN CRATON, WESTERN AUSTRALIA

by
C. V. Spaggiari

Perth 2007

MINISTER FOR RESOURCES
Hon. Francis Logan MLA

DIRECTOR GENERAL, DEPARTMENT OF INDUSTRY AND RESOURCES
Jim Limerick

EXECUTIVE DIRECTOR, GEOLOGICAL SURVEY OF WESTERN AUSTRALIA
Tim Griffin

REFERENCE
The recommended reference for this publication is:
SPAGGIARI, C. V., 2007, Structural and lithological evolution of the Jack Hills greenstone belt, Narryer Terrane, Yilgarn Craton, Western Australia: Western Australia Geological Survey, Record 2007/3, 49p.

National Library of Australia Card Number and ISBN 978-1-74168-094-2

Grid references in this publication refer to the Geocentric Datum of Australia 1994 (GDA94). Locations mentioned in the text are referenced using Map Grid Australia (MGA) coordinates, Zone 50. All locations are quoted to at least the nearest 100 m.

Cover image modified from Landsat data, courtesy of ACRES

Published 2007 by Geological Survey of Western Australia
This Record is published in digital format (PDF) and is available online at www.doir.wa.gov.au/GSWA/publications.
Laser-printed copies can be ordered from the Information Centre for the cost of printing and binding.

Further details of geological publications and maps produced by the Geological Survey of Western Australia are available from:
Information Centre
Department of Industry and Resources
100 Plain Street
EAST PERTH, WESTERN AUSTRALIA 6004
Telephone: +61 8 9222 3459 Facsimile: +61 8 9222 3444
www.doir.wa.gov.au/GSWA/publications

Contents

Appendices

Plates

1. Northeastern area of the Jack Hills greenstone belt
2. East-central area of the Jack Hills greenstone belt
3. Central area of the Jack Hills greenstone belt
4. West-central area of the Jack Hills greenstone belt
5. Southwestern area of the Jack Hills greenstone belt

Figures

Tables

Structural and lithological evolution of the Jack Hills greenstone belt, Narryer Terrane, Yilgarn Craton, Western Australia

by

C. V. Spaggiari

Abstract

The Jack Hills greenstone belt is about 70 km long and includes a significant component of metasedimentary rocks. It lies along the southern margin of the Narryer Terrane, in the northwest of the Yilgarn Craton. Structural, lithological, and geochronological data from the belt show that it has undergone a long and complex depositional and deformational evolution from c. 3000 to 1075 Ma.

The belt is hosted by Archean granitic gneiss and granitic rocks, and comprises at least three lithological associations: an association of banded iron-formation, chert, quartzite, and mafic and ultramafic rocks; an association of pelitic and semipelitic schist, quartzite, and mafic schist; and an association of mature clastic rocks. The mature clastic rocks host detrital zircons that are 4.0 Ga and older, and these have been the focus of most previous work on the belt. The majority of rocks in the belt are Archean, but some of the metasedimentary rocks are now known to be Proterozoic. No attempt has been made to create a stratigraphy for the Jack Hills rocks because of difficulties in dividing lithologically similar, strongly deformed, and extensively recrystallized rocks.

The dominant structural feature of the region is a major, east-trending shear zone (Cargarah Shear Zone) that cuts the belt and has produced the present-day sigmoidal geometry. This geometry, kinematic indicators, and shear-related structures indicate that it is a dextral transpressional zone. ^{40}Ar–^{39}Ar data and structural and metamorphic similarities to the nearby Errabiddy Shear Zone suggest that the shear zone formed during the 1830 to 1780 Ma Capricorn Orogeny. Coplanar and coaxial overprinting relationships make it difficult to assign specific foliations to tectonic events, but the preservation of multiple foliations in some outcrops, and fold relationships preserved in the banded iron-formation sequence, help define a structural chronology. This has been used to interpret ^{40}Ar–^{39}Ar data, where the dating of the main shear-related foliation by the in situ UV laser technique allowed comparisons to be made with age data from other foliation-forming micas and hornblende. This shows that the main phase of cooling, from predominantly greenschist-facies temperatures, occurred between c. 1800 and 1700 Ma.

The rare preservation of recumbent folds in banded iron-formation, and an early foliation in the older associations, but not the mature clastic rocks, are indicative of an early deformation event that occurred prior to, or possibly during, intrusion of voluminous Neoarchean monzogranitic rocks. This may have been related to amalgamation of the Narryer Terrane to the Youanmi Terrane (i.e. the Murchison Domain). The boundary of the two terranes has been previously interpreted as the Yalgar Fault, which is just south of the Jack Hills greenstone belt. However, it is not clear whether this structure was initially formed at that time, or whether it is a younger structure associated with major dextral shearing during the Capricorn Orogeny. Alternatively, the two terranes may have been amalgamated prior to deposition of the greenstone sequences, both at Jack Hills and in the Murchison Domain. The main foliation associated with formation of the Cargarah Shear Zone is overprinted by semibrittle and brittle structures, such as faults and kink folds, and the main shears show evidence of reactivation. The ^{40}Ar–^{39}Ar data suggest that this may have occurred at c. 1200 Ma, during intrusion of mafic dykes. The presence of a second generation of crosscutting mafic dykes, interpreted to be part of the 1075 Ma Warakurna large igneous province, indicates that the main phases of deformation had ceased by that time.

KEYWORDS: Jack Hills greenstone belt, Narryer Terrane, Yilgarn Craton, Capricorn Orogeny, ^{40}Ar–^{39}Ar data.

Introduction

Purpose and scope

This work was carried out while the author was a research fellow at the Department of Applied Geology, Curtin University, Perth, from 2003 to 2004. It was supported by Australian Research Council Grant DP0211706 (awarded to R. Pidgeon, S. A. Wilde, and A. A. Nemchim), the Tectonics Special Research Centre, and the Geological Survey of Western Australia. The aim of the study was to elucidate the structure, lithological relationships, and tectonic history of the Jack Hills greenstone belt, which is within the Narryer Terrane of the northwest Yilgarn Craton (Fig. 1). The belt is significant because the metasedimentary rocks contain detrital zircons that are 4.0 Ga and older. Most of these zircons are older than any known rocks on Earth, and their source is unknown, but they contain geochemical and isotopic evidence about the conditions of early Earth (Amelin et al., 1999; Mojzsis et al., 2001; Peck et al., 2001; Wilde et al., 2001; Valley et al., 2002; Cavosie et al, 2004; Harrison et al., 2005). Although much geochronological data have been generated, the geological history of the belt, including the relationship between the host rocks of the 4.0 Ga-and-older detrital zircons and surrounding rocks, is not well understood. Until recently all rocks in the belt were thought to be Archean, but it is now evident that some metasedimentary rocks are Proterozoic (Cavosie et al., 2004; Dunn et al., 2005). The extent of the Proterozoic rocks and their relationship to other units in the belt are unknown.

The purpose of this study is to determine the geological evolution of the Jack Hills greenstone belt to provide context for the pre-existing geochronological data. Five areas were chosen to be mapped in detail. Apart from the southwestern area, the areas were initially mapped as across-strike traverses to gain a general understanding of the geology along the length of the belt. These were then expanded to become the map areas shown in Plates 1–5. The northeastern and west-central areas were also chosen because they included the localities of both the 4.0 Ga-and-older detrital zircons and the Proterozoic rocks. The southwestern area was included in the second field season to provide further context along strike, and because it included intrusive relationships between various rock units and granitic rocks.

The Jack Hills greenstone belt differs from the greenstone belts in the Murchison Domain of the Youanmi Terrane in that it includes a significant proportion of siliciclastic metasedimentary rocks. Siliciclastic metasedimentary rocks are also abundant in the Mount Narryer region of the Narryer Terrane, (Williams and Myers, 1987) but, unlike the Jack Hills greenstone belt, mafic and ultramafic rocks are not. It is not clear to what extent a common geological history is shared by the greenstone belts of the Murchison Domain, the Mount Narryer region, and the Jack Hills greenstone belt, or how they relate to each other. The results of this study will enable comparisons of these regions to be made to help address these questions.

Location, physiography, and access

The Jack Hills greenstone belt outcrops over a range of northeast-trending hills and ridges (Jack Hills) in the Murchison River region of Western Australia (Fig. 1). The belt is about 70 km long, and straddles the Robinson Range*, Belele, and Byro 1:250 000 map sheets. It varies in width from about 2 km in the centre to about 6.5 km at its northeastern and southwestern ends. The Jack Hills are a series of strike ridges (Fig. 2) with major drainage feeding the Murchison River just to the north and Whela Creek to the south. The highest ridges are composed of banded iron-formation (BIF), chert, and quartzite. The highest peaks are in the northeast within BIF and chert, with the highest being Mount Hale at 697 m above sea level. Low-lying areas between ridges are dominated by mafic and ultramafic rocks that are predominantly schistose, and quartz–mica schist. The area is locally rugged and access is by pastoral lease tracks, most of which require four-wheel drive vehicles, and these may become impassable after heavy rains.

Map compilation methodology

This Record includes five plates of detailed structural and lithological interpreted bedrock geology maps presented at scales of about 1:11 000 to 1:7 000. They were compiled from field mapping, and aerial photography, satellite, and aeromagnetic imagery interpretation. Pre-existing maps (GSWA's Byro and Belele 1:250 000-scale geological series map sheets) provided some background information. The portion of the Jack Hills greenstone belt on Robinson Range was not mapped. Field mapping was conducted on rectified aerial photographs at a scale of about 1:5 000. The aerial photographs were scanned and rectified against planimetry (mostly creeks and tracks) supplied by the Department of Land Information (DLI). The field maps were scanned and compiled using standard graphics software (Adobe Illustrator).

Regional geological setting

The Narryer Terrane (Fig. 1), consists of granitic rocks and granitic gneisses ranging in age from early through to late Archean (e.g. Kinny et al., 1988, 1990; Nutman et al., 1991; Pidgeon and Wilde, 1998). These are interlayered with minor deformed and metamorphosed BIF, mafic and ultramafic intrusive rocks, and metasedimentary rocks (Williams and Myers, 1987; Myers, 1988a; Kinny et al., 1990). The Jack Hills greenstone belt is the only greenstone belt within the Narryer Terrane, although the Maitland greenstone belt is just east of the proposed tectonic boundary with the Murchison Domain of the Youanmi Terrane (Fig. 1).

The oldest component of the Narryer Terrane is a dismembered layered igneous complex (anorthosite–

* Capitalized names refer to standard 1:250 000 map sheets.

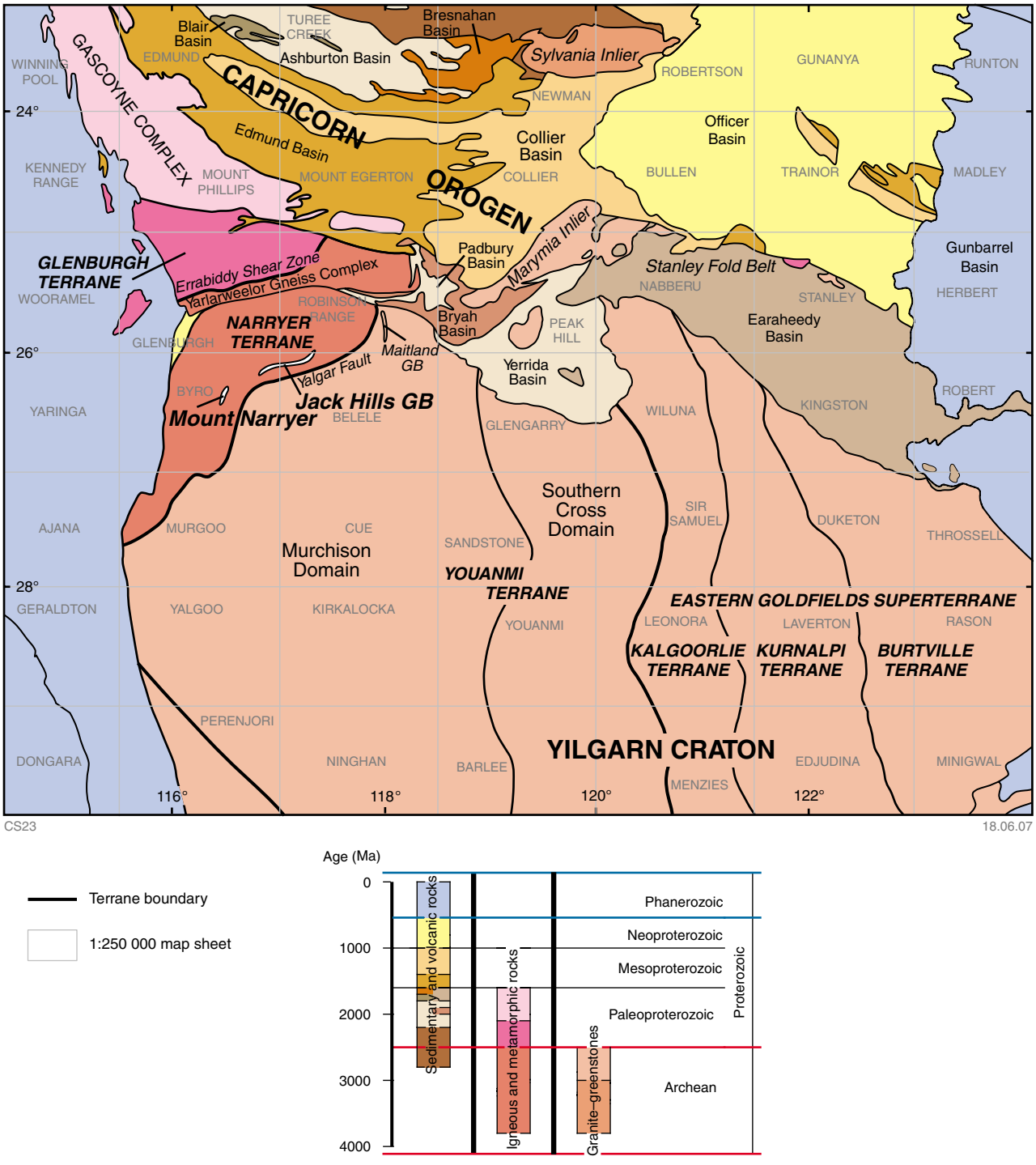

Figure 1. Map of the Yilgarn Craton showing the Youanmi Terrane, which is an amalgamation of the former Southern Cross and Murchison Terranes. The location of the Jack Hills greenstone belt and Narryer Terrane are shown (GB = greenstone belt). Modified from Cawood and Tyler (2004) and Cassidy et al. (2006)

gabbro–ultramafic intrusion) known as the Manfred Complex (Myers and Williams, 1985; Myers, 1988b). Leucogabbro and meta-anorthosite inclusions within syenogranitic gneiss (Dugel gneiss) that are part of the complex have a magmatic sensitive high-resolution ion microprobe (SHRIMP) U–Pb zircon age of 3730 ± 6 Ma (Kinny et al., 1988). The oldest felsic intrusive rocks, termed the Meeberrie Gneiss (Myers and Williams, 1985), are a complex mixture of various lithological associations (migmatite) where the oldest component has a maximum SHRIMP U–Pb zircon age of 3730 ± 10 Ma similar to the Manfred Complex (Kinny and Nutman, 1996). Both the Meeberrie Gneiss and the Manfred Complex were intruded by various felsic magmas (Dugel and Eurada gneisses) until a major magmatic event at c. 3300 Ma, accompanied by deformation and high-grade (amphibolite–granulite

CS57 23.05.07

Figure 2. View east from the central Jack Hills, showing topographic expression and curvature of the belt to the northeast

facies) metamorphism (Kinny et al., 1988; Myers, 1988a; Nutman et al., 1991, 1993; Pidgeon and Wilde, 1998). Further felsic magmatism is believed to have occurred at c. 3100 Ma (Nutman et al., 1991). These events occurred prior to the deposition of the supracrustal sequences predominantly exposed in the Jack Hills greenstone belt and the Mount Narryer region (e.g. Compston and Pidgeon, 1986; Maas and McCulloch, 1991).

The Yalgar Fault, which is a major fault inferred to separate the Narryer Terrane from the Murchison Domain of the Youanmi Terrane to the south, has been interpreted as a dextral strike-slip fault (Fig. 1; Myers, 1990; Myers and Hocking, 1998). However, little is known about the structural history of this fault, and whether it is a true terrane boundary. The Jack Hills greenstone belt is close and parallel to this structure. The basis for the terrane distinction is the presence of gneisses older than c. 3300 Ma in the Narryer Terrane only (Myers, 1990). However, understanding zircon systematics and inheritance is problematic and the terrane boundary is likely to be cryptic and disrupted by late Archean magmatism and subsequent deformation (e.g. Nutman et al., 1993). The early Archean gneisses of the Narryer Terrane have been interpreted as an allochthon that was thrust over c. 3000 to 2920 Ma granitic crust of the Youanmi Terrane, prior to late Archean magmatism (Nutman et al., 1993). Widespread Neoarchean granites that were emplaced between c. 2750 and 2620 Ma stitch both the Narryer and Youanmi Terranes, indicating that they were amalgamated by this time (Myers, 1990; Nutman et al., 1991; Pidgeon and Wilde, 1998). Although there is evidence of deformation prior to intrusion of the late Archean granitic rocks, the main deformation is believed to have occurred at amphibolite facies between 2750 and 2600 Ma, producing the main tectonic grain and affecting both the Narryer Terrane and Murchison Domain (Myers, 1990). Three phases of folding are recognized: recumbent folding associated with thrusting (D_1), followed by two phases of upright folding with generally northeasterly or east-northeasterly trending axes (D_2 and D_3; Myers, 1990).

The northern margin of the Narryer Terrane is defined by the Errabiddy Shear Zone (Williams et al., 1983b; Occhipinti and Reddy, 2004), along which the c. 2540 to 2000 Ma Glenburgh Terrane was accreted to the Yilgarn Craton during the Glenburgh Orogeny (2005–1960 Ma; Occhipinti et al., 2004). This boundary was reworked during the Capricorn Orogeny (1830–1780 Ma),

producing predominantly dextral transpressional structures at greenschist facies (Occhipinti and Reddy, 2004). The northeastern part of the Narryer Terrane — the Yarlarweelor Gneiss Complex (Fig. 1) — was deformed, metamorphosed, and intruded by granites and dykes during the Capricorn Orogeny. This involved a two-stage process between c. 1820 and 1795 Ma of intrusion during compression, followed by intrusion during dextral strike-slip deformation (Sheppard et al., 2003).

Jack Hills greenstone belt

Introduction and previous work

The dominant lithologies of the Jack Hills greenstone belt (Fig. 3) are BIF, chert, quartzite, mafic and ultramafic rocks, and siliciclastic rocks including quartz–mica schist, andalusite schist, quartzite, metasandstone, and pebble metaconglomerate (Elias, 1982; Williams et al., 1983a; Wilde and Pidgeon, 1990). Wilde and Pidgeon (1990) divided the supracrustal rocks of the Jack Hills greenstone belt into three informal associations:

- BIF, chert, mafic schist (amphibolite), and minor ultramafic intrusions;
- pelitic and semipelitic schists associated with mafic schists that were possibly part of a turbidite sequence;
- a more restricted sequence of mature clastic sedimentary rocks comprising metaconglomerate, metasandstone, quartzite, and metasiltstone.

The latter are interpreted by Wilde and Pidgeon (1990) to have been deposited as an alluvial fan, and are where the majority of 4.0 Ga-and-older detrital zircons have been found. It is not clear whether these associations were deposited at the same time or whether they are unrelated successions juxtaposed by deformation (Wilde and Pidgeon, 1990). Banded iron-formation, chert, some quartzite, mafic and ultramafic schist, and some pelitic and semipelitic rocks in the Jack Hills greenstone belt have been intruded by monzogranites and muscovite granite and pegmatite. However, there are no clear intrusive relationships with the mature clastic rocks that host the old detrital zircons. The monzogranites have SHRIMP U–Pb zircon ages of 2654 ± 7 and 2643 ± 7 Ma (Pidgeon and Wilde, 1998).

The supracrustal rocks of the Jack Hills greenstone belt have not undergone the same high-grade (granulite-facies) metamorphism as the gneissic rocks of the Narryer Terrane. The presence of grunerite in BIF and the association of calcic plagioclase and hornblende in mafic schists indicate that at least some supracrustal rocks were metamorphosed under amphibolite-facies conditions (Wilde and Pidgeon, 1990). Hornblende in the mafic schists is commonly overprinted by actinolite, suggesting some retrogression to greenschist facies. The majority of pelitic rocks are semipelites that lack diagnostic mineral assemblages, other than andalusite. Quartz–biotite–cordierite assemblages in some siliciclastic rocks indicate upper greenschist-facies metamorphism (Wilde and Pidgeon, 1990).

The following structural history was presented in Wilde and Pidgeon (1990), and was based on the work of Baxter et al. (1986). Five phases of deformation were recognized. D_1 produced isoclinal folding and the development of a strong mineral lineation. D_2 formed a major anticline across the belt, open to tight folds, and minor folds with a coaxial lineation. These were largely confined to the BIF and chert. D_3 produced gentle to open, upright folding with subhorizontal axes. These are the first folds to have formed in the mature clastic association. This, and the difference in metamorphic grade, led Wilde and Pidgeon (1990) to suggest that the mature clastic rocks were deposited after D_2. D_4 produced conjugate shear zones and minor shear folds that cut both the supracrustal rocks and granitic rocks outside the belt. D_5 produced localized kinks and buckles. This structural history shares some similarities with that described below (see **Deformation**), but there are also some major differences.

SHRIMP U–Pb detrital zircon geochronology

Both the Jack Hills greenstone belt and nearby Mount Narryer region (Fig. 1) are well known for their siliciclastic sequences that contain 4.0 Ga-and-older detrital zircons (e.g. Froude et al., 1983; Compston and Pidgeon, 1986; Wilde et al., 2001). A single detrital zircon has also been found in quartzite at Maynard Hills, in the Southern Cross Domain of the Youanmi Terrane, that has a SHRIMP U–Pb age of 4351 ± 7 Ma (Wyche et al., 2004). Previously, all metasedimentary rocks in the Jack Hills greenstone belt were thought to be Archean, but it has now been recognized that some are Proterozoic (Cavosie et al., 2004; Dunn et al, 2005). However, the extent of the Proterozoic sequence within the belt is not clear, and it is generally difficult to distinguish it from Archean metasedimentary rocks due to lithological similarity, deformation, and recrystallization. Although a significant number of detrital zircons have been analysed from the Jack Hills greenstone belt, most of the work has focused on zircons that are 4.0 Ga and older, and much of that material has come from a single pebble metaconglomerate outcrop in the mature clastic rocks at Eranondoo Hill (Figs 3, 4, and 5; Plate 4; commonly known as the W74 or discovery site). Therefore, the data are biased and do not fully describe the provenance of the mature clastic rocks or provide information about their depositional age. Research interests have focused on the 4.0 Ga-and-older zircons because they yield much information about early Earth processes. The W74 site has been targeted because it yields the greatest percentage of these old zircons, about 12% (Pidgeon and Nemchin, 2006).

The mature clastic rocks have yielded U–Pb detrital zircon ages up to 4.4 Ga (Wilde et al., 2001). However, analyses of more than 50 000 grains show that there is a complete spread of ages between 4.0 and 4.4 Ga, with the greatest percentage between 4.0 and 4.2 Ga (Cavosie et al., 2004; Harrison, T. M., 2005, written comm.). The mature clastic rocks also contain abundant detrital zircons between 3.7 and 3.0 Ga, indicative of deposition after that time (Compston and Pidgeon, 1986; Nutman et al., 1991; Cavosie et al., 2004; Dunn et al., 2005). However, it is

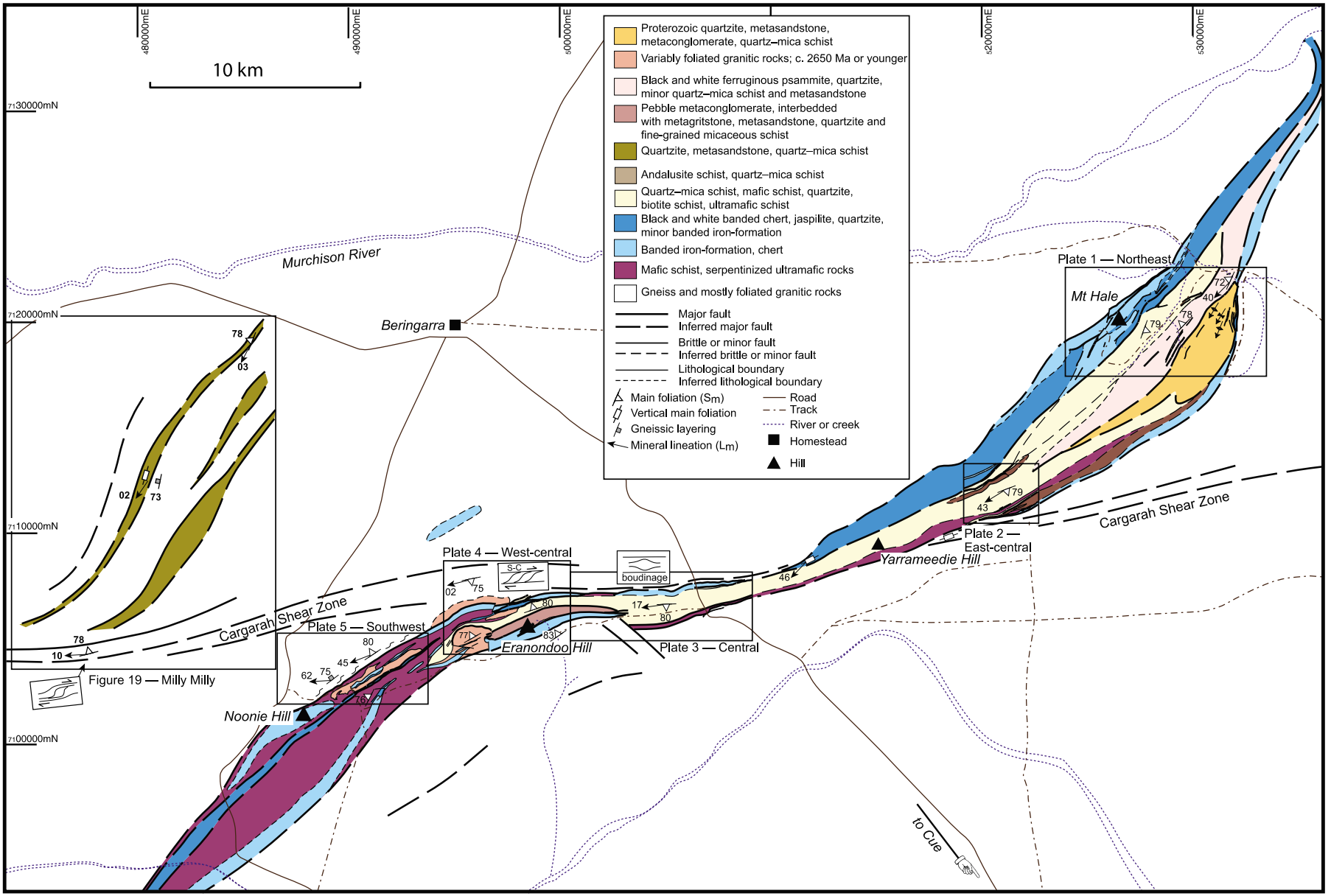

CS61 18.05.07

Figure 3. Simplified geological map of the Jack Hills greenstone belt, showing locations of areas mapped in detail (Plates 1–5), and the Milly Milly area

CS24 03.05.07

Figure 4. The W74 or Discovery site near Eranondoo Hill, Jack Hills. This is the most heavily sampled outcrop for 4.0 Ga-and-older detrital zircons

not clear from field relationships whether the association pre-dates the Neoarchean granitic rocks. A few zircons younger than 3.0 Ga have been reported, but their significance is not clear. Cavosie et al. (2004) analysed detrital zircons from two transects: a western transect that included the W74 site, and an eastern transect within more strongly deformed mature clastic rocks about 900 m to the east. Metaconglomerate sample 01JH47 (Plate 4) from the eastern transect yielded two grains with ages 2724 ± 7 Ma (12% discordant) and 2504 ± 6 Ma (6% discordant). Metaconglomerate sample 01JH42 (Plate 4) from the same transect also contained a single grain with an age of 2.3 Ga (Cavosie, A., 2005, written comm.). Although more data are needed, these results suggest that the mature clastic rocks are a separate succession that was deposited after intrusion of the Neoarchean granites. This is consistent with field observations and the inferred structural history (see **Deformation**).

The western transect of Cavosie et al. (2004) also yielded some Proterozoic detrital zircons. Quartzite sample 01JH63 (Fig. 5a) contained concordant* late Archean grains (2736 ± 6, 2620 ± 10, and 2590 ± 30 Ma), two concordant Paleoproterozoic grains (1973 ± 11 and 1752 ± 22 Ma), and a single concordant grain at 1576 ± 22 Ma. This quartzite is from the southern end of the western transect of Cavosie et al. (2004), close to the contact with the BIF, and is interpreted as part of a Proterozoic unit of predominantly micaceous schist and quartz–mica schist. Dunn et al. (2005) analysed a fine-grained micaceous schist from what appears to be the same unit (sample JH3, Fig. 5a; Plate 4). That sample contained concordant Paleoproterozoic grains ranging in age from c. 1981 to 1944 Ma, with a single youngest grain at 1791 ± 21 Ma. The sample also contained a significant proportion of concordant late Archean grains. These data suggest that the unit was potentially deposited during or following the Capricorn Orogeny, with a detrital contribution from rocks formed during the Glenburgh Orogeny to the northwest (Dunn et al., 2005). The single grain of 1576 ± 22 Ma (Cavosie et al., 2004) suggests that the unit may be even younger. However, this age does not correspond with any known sources of detritus from the region. Sample JH3 also contained a single concordant zircon with an age of 4113 ± 3 Ma, plus a few grains in the range 3500 to 3300 Ma (Dunn et al., 2005). This shows that a source of the 4.0 Ga-and-older zircons was still present and being eroded during the Paleoproterozoic, or that these zircons were recycled from other younger sources. Neoarchean granites could have provided some of this detritus because they do locally contain xenocrysts of 4.0 Ga-and-older zircons (Nelson et al., 2000).

Paleoproterozoic zircons were also found in a metaconglomerate (sample JH4, Plate 1) from the northeastern part of the belt, near the eastern margin (Dunn et al., 2005). The metaconglomerate differs from the association of mature clastic rocks at Eranondoo Hill in that it is a minor part of a thick unit of predominantly quartzite, pebbly sandstone, and metasandstone. The sample contained a similar range of ages to JH3, with the youngest concordant zircon at 1884 ± 32 Ma. Older zircons range from 3725 to 3500 Ma (Dunn et al., 2005). Dunn et al. (2005) argued that at least two sedimentary successions are present in the Jack Hills greenstone belt: an older succession (middle to late Archean) containing the metaconglomerate outcrop W74, and a younger succession (Paleoproterozoic), represented by the outcrops of JH3 and JH4, that is possibly similar in age and related to either the Mount James Formation or Earaheedy Basin sediments.

In summary, it is clear that at least two, but possibly four, metasedimentary successions or associations are present in the Jack Hills greenstone belt:

- an older succession of BIF, chert, quartzite, quartz–mica schist, and mafic and ultramafic rocks;
- an association of pelitic and semipelitic rocks, quartzite, and mafic schists;
- a mature clastic association that hosts the majority of the 4.0 Ga-and-older detrital zircons;
- a Proterozoic association of quartz–mica schist, quartzite, and metasandstone with local metaconglomerate.

Association 1 and at least part of association 2 were deposited prior to Neoarchean granite intrusion, and may be part of the same succession (see **Lithological units**).

The depositional age of the mature clastic rocks is not clear, but could be either between c. 3.0 Ga (the age of most of the youngest detrital zircons) and 2.7 Ga (if it was intruded by Neoarchean granites), or Paleoproterozoic, but not necessarily deposited as late as the Proterozoic unit represented by samples JH3 and JH4. The absence of late Archean detrital zircons from most samples suggests the former. However, it is possible that either the Neoarchean granites were not fully exposed and eroding at the time of deposition or that the rocks sampled do not contain the full suite of detrital zircons. The first rocks in the region to record a component of late Archean zircons are the sediments of the Yerrida Basin (Pirajno et al., 2004). The Windplain Group of the Yerrida Basin lies unconformably on Neoarchean granites of the Yilgarn Craton, indicating

* 'Concordant' in this Record refers to analyses that ≤10% discordant.

a)

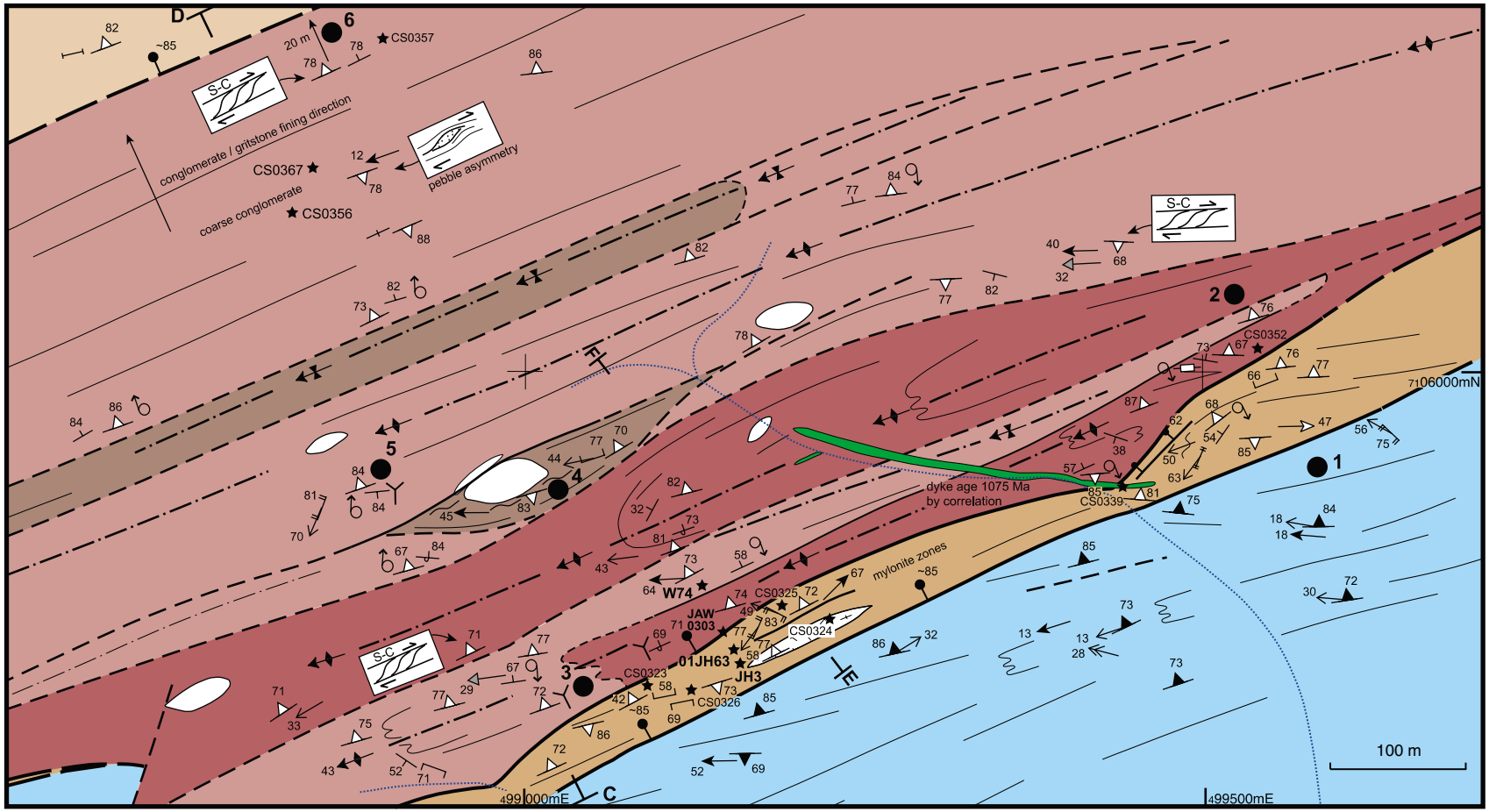

Lithological units

- Dolerite or gabbro plug, sill or dyke
- Felsic dyke
- Quartz veins
- (Proterozoic) fine-grained micaceous schist, quartz–mica schist, quartzite
- Fine-grained micaceous schist, quartz–mica schist, quartzite
- Pebble metaconglomerate, interbedded with metagritstone, metasandstone, quartzite and fine-grained micaceous schist
- Interbedded metasandstone, quartzite, metagritstone, minor pebble metaconglomerate, and fine-grained micaceous schist
- Fine-grained micaceous schist, quartz–mica schist, quartzite, sometimes interleaved with mafic or ultramafic schist
- Banded iron-formation, chert

Structural symbols

- Bedding (S_0); vertical; overturned
- Early foliation; vertical
- Compositional banding (BIF and chert); parallel to main foliation (S_m)
- Main foliation (S_m); vertical
- Crenulation cleavage (S_{cc}); vertical
- Fold with axial surface and plunge
- Antiform; synform
- Geological section lines
- Younging direction
- Fold vergence (to next antiform) S_0/S_m
- Intersection lineation (L_o/S_m)
- Crenulation intersection lineation (LS_{cc})
- Pebble elongation
- Mineral lineation
- Rodding lineation
- Sample locality
- Creek
- Major fault with dip; inferred
- Brittle or minor fault with dip; inferred
- Brittle fault zone
- Lithological boundary; inferred
- Axial trace of fold hinges
- Trend lines of bedding or foliation
- Trend lines of anastomosing foliation
- Lithological section line markers (see Fig. 13)

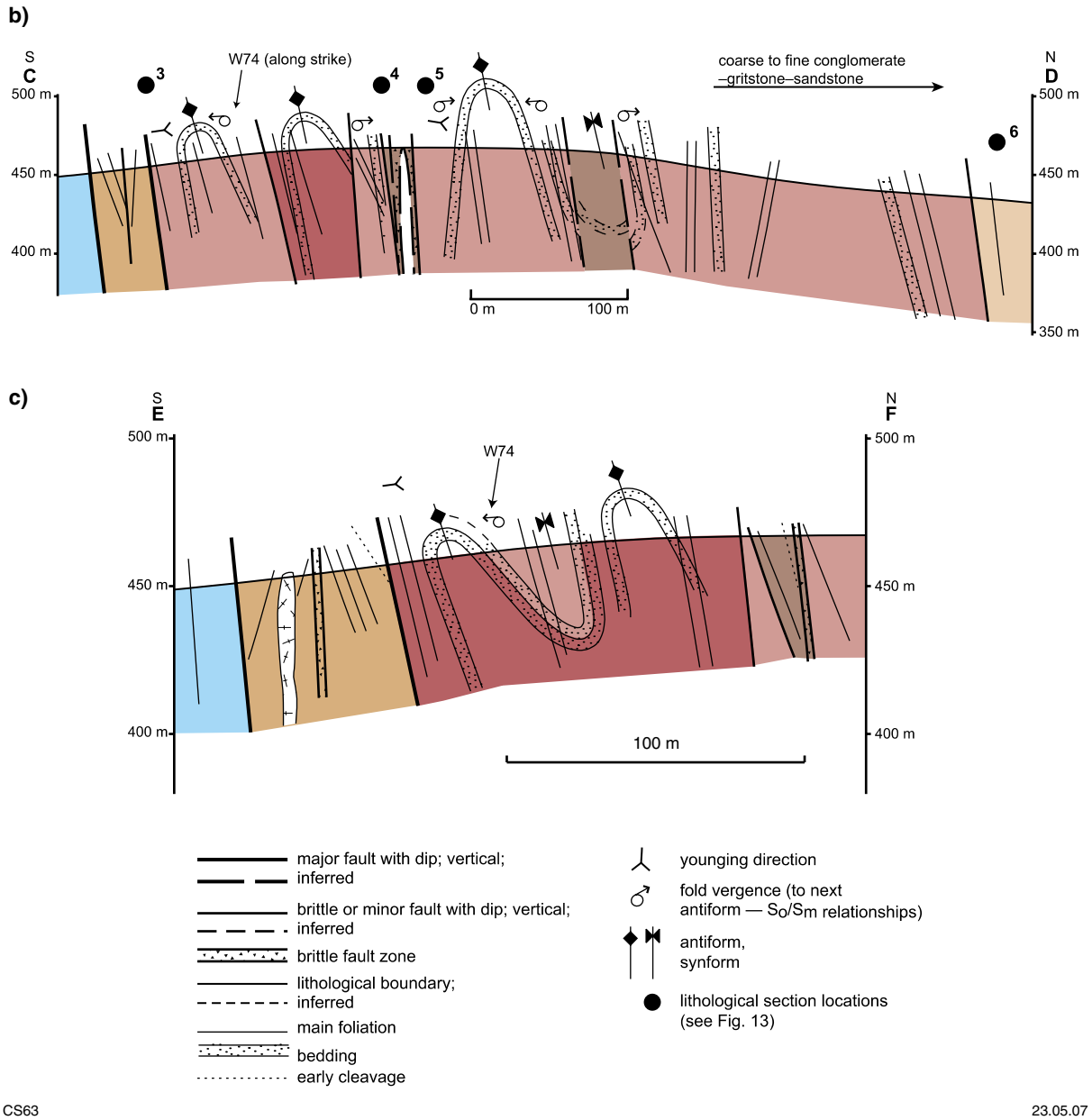

Figure 5. Map (previous page) and cross sections of the W74 site, west-central area (Plate 4); a) detailed geological map showing geochronological sample sites discussed in the text, and sites of cross sections C–D and E–F, and lithological sections; b) and c) cross sections C–D and E–F showing structural and lithological relationships in the W74 area

exposure of these rocks, at least locally, at the time of deposition, which is interpreted as 2.17 Ga (Pirajno et al., 2004). The Camel Hills metamorphic rocks, preserved in the Errabiddy Shear Zone, were deposited by c. 2.0 Ga and also contain a component of late Archean detritus (Occhipinti et al., 2004). This suggests that the late Archean granitic rocks were uplifted by at least 2.2 to 2.0 Ga. It is conceivable that the mature clastic rocks of the Jack Hills greenstone belt were deposited at about this time, or possibly during tectonism associated with the Glenburgh Orogeny. Alternatively, they may have accumulated after intrusion of the Neoarchean granites, but prior to their exposure, potentially as passive margin sediments.

Lithological units

The lithological units of the Jack Hills greenstone belt are described in this section in order of formation. The order is approximate only, because not all the age relationships between the units are adequately known. The three associations described by Wilde and Pidgeon (1990) are generally the same as those found in this study, excluding the Proterozoic metasedimentary rocks. These are:

- an association of BIF, chert, quartzite, and mafic and ultramafic rocks;
- an association of pelitic schist, semipelitic schist, quartzite, and mafic schist;
- an association of mature clastic rocks.

No attempt has been made to construct a stratigraphy for the Jack Hills rocks because of difficulties in dividing lithologically similar, strongly deformed, and extensively recrystallized rocks. Geochronological data has highlighted this, particularly for the metasedimentary rocks. The numerous shear zones and faults, and extensive silicification, also make stratigraphic subdivisions, and to some extent lithological unit subdivisions, problematic. Intrusive relationships are also difficult to determine for some units because of extensive tectonism. Because all the rocks have been metamorphosed, the descriptions include the metamorphic assemblages, and effects of metasomatism where present.

Granitic gneisses

The Jack Hills greenstone belt is surrounded by granitic gneisses that are heterogeneously deformed and metamorphosed. These gneisses are intruded by Neoarchean granitic rocks and pegmatite that partially intrude the belt itself (Pidgeon and Wilde, 1998). There are lenses of BIF, chert, quartzite, mafic schist (amphibolite), and ultramafic rocks throughout the gneissic rocks. Pidgeon and Wilde (1998) recognized four textural types of gneiss and granitic rocks: tonalite gneiss (in part equivalent to the Meeberrie gneiss of Myers and Williams (1985), porphyritic granodiorite, monzongranite, and muscovite granite (Fig. 6). The monzogranite and muscovite granite are described below (see **Granitic rocks**). The tonalite gneiss includes a variety of granitic phases, is widespread, and occupies the whole of the northern margin of the belt as well as part of the southern margin. Granitic phases include tonalite and trondhjemite, and more evolved phases such as granodiorite and monzogranite. All contain biotite and some also contain garnet and late-stage muscovite (Pidgeon and Wilde, 1998). The tonalite gneiss commonly has a strong pervasive gneissic layering, with subparallel pegmatite veins (Fig. 7). The gneissic layering is overprinted by a lower grade foliation defined by quartz, feldspar, mica, chlorite, and, locally, epidote. The porphyritic granodiorite contains microcline phenocrysts and is restricted to the southern margin of the belt (Pidgeon and Wilde, 1998). It is less deformed than the tonalite gneiss, except near the sheared margins of the belt, and has been intruded by Neoarchean monzogranite (Pidgeon and Wilde, 1998).

Mafic and ultramafic rocks — mafic schists

The Jack Hills greenstone belt contains a significant component of mafic and ultramafic rocks, most of which are strongly deformed and schistose (mafic schists or amphibolites). These rocks are widespread, but commonly

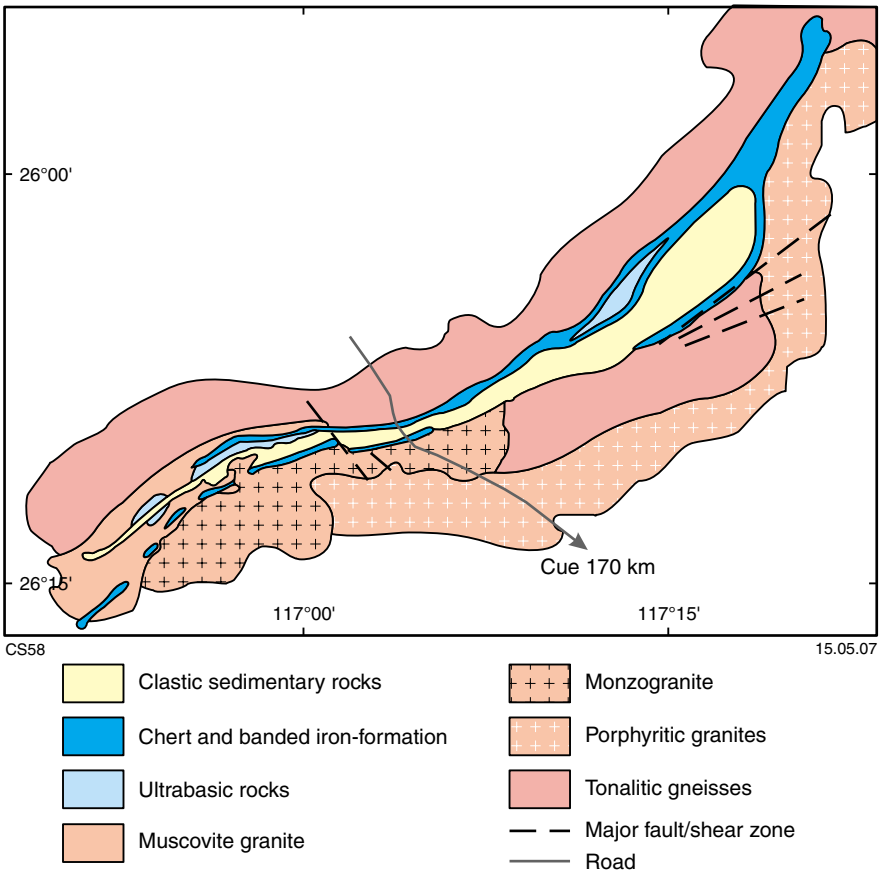

Figure 6. Geological sketch map of the Jack Hills greenstone belt showing the distribution of granitic host rocks (modified from Pidgeon and Wilde, 1998)


CS28 14.05.07

Figure 7. Granitic gneiss from the southwest area, near Pindar road (WP 48, MGA 487149E 7103134N; Plate 5)

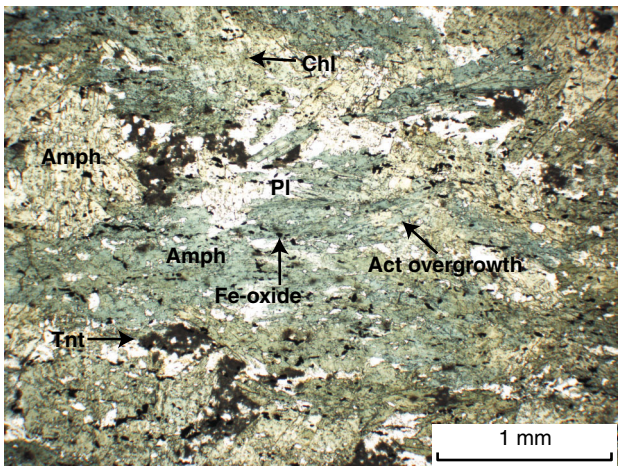

CS59 15.05.07

Figure 8. Mafic schist from the east-central area of the belt (Plate 2). Hornblende amphibole (Amph) is overgrown by actinolitic (Act) amphibole. Other phases are plagioclase (Pl), titanite (Tnt), chlorite (Chl), and Fe-oxide (sample CS0378, MGA 520847E 7111151N; plane-polarized light)

associated with BIF, chert, and quartzite, where they are interlayered as metre-scale to 100 m-scale slivers or lenses. Mafic schists are also commonly interlayered with pelitic or semipelitic schists. In most cases the protoliths are unknown, although some of the less deformed mafic schists are fine grained and have relict volcanic textures, such as lath-like phenocrysts of plagioclase in a fine-grained matrix, that suggest they were basalts. The mafic schists commonly comprise assemblages of hornblende or actinolite, plagioclase, titanite, and Fe-oxide, with or without chlorite, biotite, epidote, and quartz (Fig. 8). Hornblende is mostly overgrown by smaller actinolitic amphiboles that are commonly aligned with the main foliation. Both varieties of amphibole have strong yellow to blue-green pleochroism. Plagioclase is locally replaced by sericite. Some mafic schists are biotite rich. Others contain abundant garnet and amphibole, and titanite, quartz, chlorite, and minor epidote and white mica (Fig. 9). The garnets contain abundant quartz inclusions and are locally rimmed by quartz and amphibole. They are also partially overgrown by small amphibole grains (Fig. 9). Ultramafic rocks are commonly serpentinized, and locally contain either talc or amphibole or both. Relict grains of probable pyroxene or olivine are typically poorly preserved (Fig. 10).

Metasedimentary rocks

Banded iron-formation, chert, and quartzite

Interbedded BIF, chert, and quartzite are widespread and form a considerable component of the belt, typically

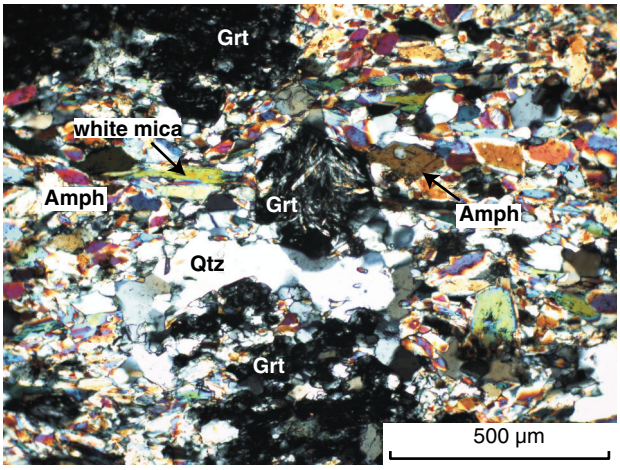

CS60 15.05.07

Figure 9. Garnet mafic schist from the central area (Plate 3). Garnet (Grt) is rimmed and partially overgrown by amphibole (Amph). Other phases shown are quartz (Qtz) and white mica (sample CS03100, MGA 505270E 7105938N; cross-polarized light)

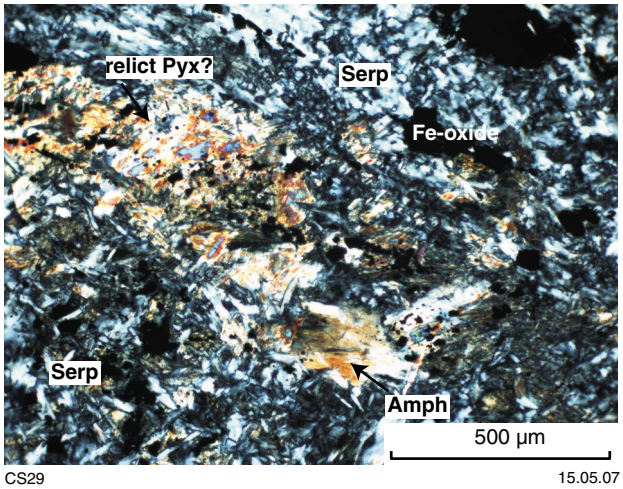

CS29 15.05.07

Figure 10. Ultramafic schist from the central map area (Plate 3). Possible relict pyroxene (Px) is overgrown by serpentinite (Srp) and amphibole (Amph; sample CS03101, MGA 505270E 7105938N; cross-polarized light)

forming long, high, strike ridges. Jaspilitic BIF is exposed locally. The BIF is locally interbedded with quartz–mica schist and quartzite and associated with lenses of mafic and ultramafic rocks. In the southwestern part of the belt (Plate 5), monzogranite, pegmatite, and muscovite granite have intruded this unit; therefore it was deposited prior to late Archean magmatism.

Extensive polydeformation and recrystallization has masked much of the primary texture of these rocks. They typically exhibit strong banding delineated by Fe-oxide-rich and Fe-oxide-poor layers. These layers may locally represent original bedding, but it is clear that in many instances they are secondary, and were produced by deformation and metamorphism (Fig. 11a). Deformation effects are evident where Fe-oxide layers have been remobilized into an oblique layering defining a crenulation cleavage (Fig. 11b). Where this is fully developed and accompanied by strong recrystallization, it is impossible to define the original layering.

The BIF is generally fine grained (1–2 mm grains) and shows pronounced effects of deformation and metamorphism. In thin section, quartz grains in chert commonly show evidence of static recrystallization, with straight boundaries and foam-structure texture (after Passchier and Trouw, 1996; Fig. 11c). Otherwise they typically show deformation effects such as undulose extinction, ragged grain boundaries, and grain-size reduction. Both the BIF and chert commonly contain aligned stilpnomelane needles in Fe-oxide-rich layers (Fig. 11c). The BIF locally contains grunerite, indicative of amphibolite-facies metamorphism (Wilde and Pidgeon, 1990). In quartzite, small sparse aligned white mica or fuchsite, or both, are locally present in the main foliation. Quartz grains in quartzite show some evidence of static recrystallization, but also strong deformation such as multiple grain sizes (subgrains), ragged grain boundaries, and undulose extinction.

The BIF includes horizons of hematite-rich lenses with crystals up to 1 cm. These lenses are secondary and crosscut the main layering of the BIF (Fig. 11d). Extensive quartz veins throughout the sequence indicate a significant degree of silicification, which may have been associated with remobilization of iron to form these lenses. This has also produced some quartzites (recrystallized and metasomatized chert) that can be difficult to distinguish from the siliciclastic quartzites. They typically contain small discontinuous bands of Fe-oxide, suggesting that they were originally part of the BIF and chert unit.

In the central part of the northeastern region (Plate 1) a unit of black and white ferruginous psammite and quartzite is interbedded with minor amounts of chert, metasandstone, and quartz–mica schist. The ferruginous psammite has diffuse, commonly discontinuous, black and white banding (Fig. 11e). It is typically silicified, with extensive, sometimes massive, quartz veins. Epidote is common near faults. The black bands contain a high percentage of small Fe-oxide grains, which may relate to original bedding layers. Alternatively, the black Fe-oxide layers may be at least in part derived by metasomatism with iron. In thin section the quartz grains show dynamic recrystallization textures, including bands and lenses of small grains that have undergone grain-size reduction during deformation (Fig. 11f). Iron-oxide grains are common in these layers. The banding is locally folded into small-scale isoclinal folds. The age of this unit, and its relationship to other lithological units, including the BIF, chert, and quartzite described above, is unknown. However, given its ferruginous character, it is possibly part of the same sequence as the BIF, chert, and quartzite unit, and is therefore included in association 1.

Pelitic and semipelitic rocks

Quartz–mica schist and andalusite schist are common, particularly in the northeastern and central parts of the belt. Their relationship to other units in the belt is unknown and contacts are typically sheared or faulted. They are commonly associated with mafic schists (or amphibolites), chlorite-rich schists, and quartzite. Andalusite is a common component of most of the pelitic and semipelitic rocks, particularly in schists in the east-central area (Plate 2). Quartzite is locally fuchsitic or chert-like, for example, in the southwestern area.

Quartz–mica schists are strongly foliated, with the foliation defined by white mica, quartz, and in some cases, by chlorite or biotite, or both (Fig. 12a). Stretched quartz rods are common; some are asymmetrical and indicate shear sense (Fig. 12b). In thin section, quartz or andalusite porphyroblasts, and sometimes Fe-oxide grains, typically have pressure shadows of mica and chlorite (Fig. 12c). Andalusite porphyroblasts are commonly poikiloblastic, in some cases showing chiastolite form (Fig. 12d), and are mostly overgrown by sericite, white mica, and quartz that form part of the main foliation. This suggests that andalusite grew prior to development of the main foliation. Quartz grains are commonly deformed and elongate, have undulose extinction, and some show effects of dynamic recrystallization (mylonitization). Elongate zones of larger and smaller grains (subgrains) were formed by grain-size reduction during deformation. However, quartz grains also typically show evidence of recovery and static recrystallization, with local development of foam-structure texture and straight grain boundaries. Quartz–mica schists contain two generations of white mica, with larger muscovite grains overgrown by smaller white-mica grains that define the main foliation (centre of Fig. 12a). Sericite also locally replaces some white mica grains. Other schists are rich in biotite and contain stretched lenses of quartz and muscovite, and numerous small grains of Fe-oxide. Biotite sometimes shows minor chloritization. Tourmaline grains in some biotite schists are probably detrital (Fig. 12e). Chlorite-rich schists have a strong foliation defined by chlorite and quartz and, locally, biotite (Fig. 12f). Tabular Fe-oxide grains are subparallel to the foliation. In the southwestern part of the belt, pelitic schist contains chloritoid, andalusite, staurolite, garnet, plus some chlorite, quartz, and an opaque phase. Both staurolite and garnet have ragged grain boundaries, suggesting that they are partly overgrown. The textures indicate an early assemblage of garnet, staurolite, and andalusite overgrown by chloritoid and chlorite, consistent with retrogression from amphibolite to greenschist facies.

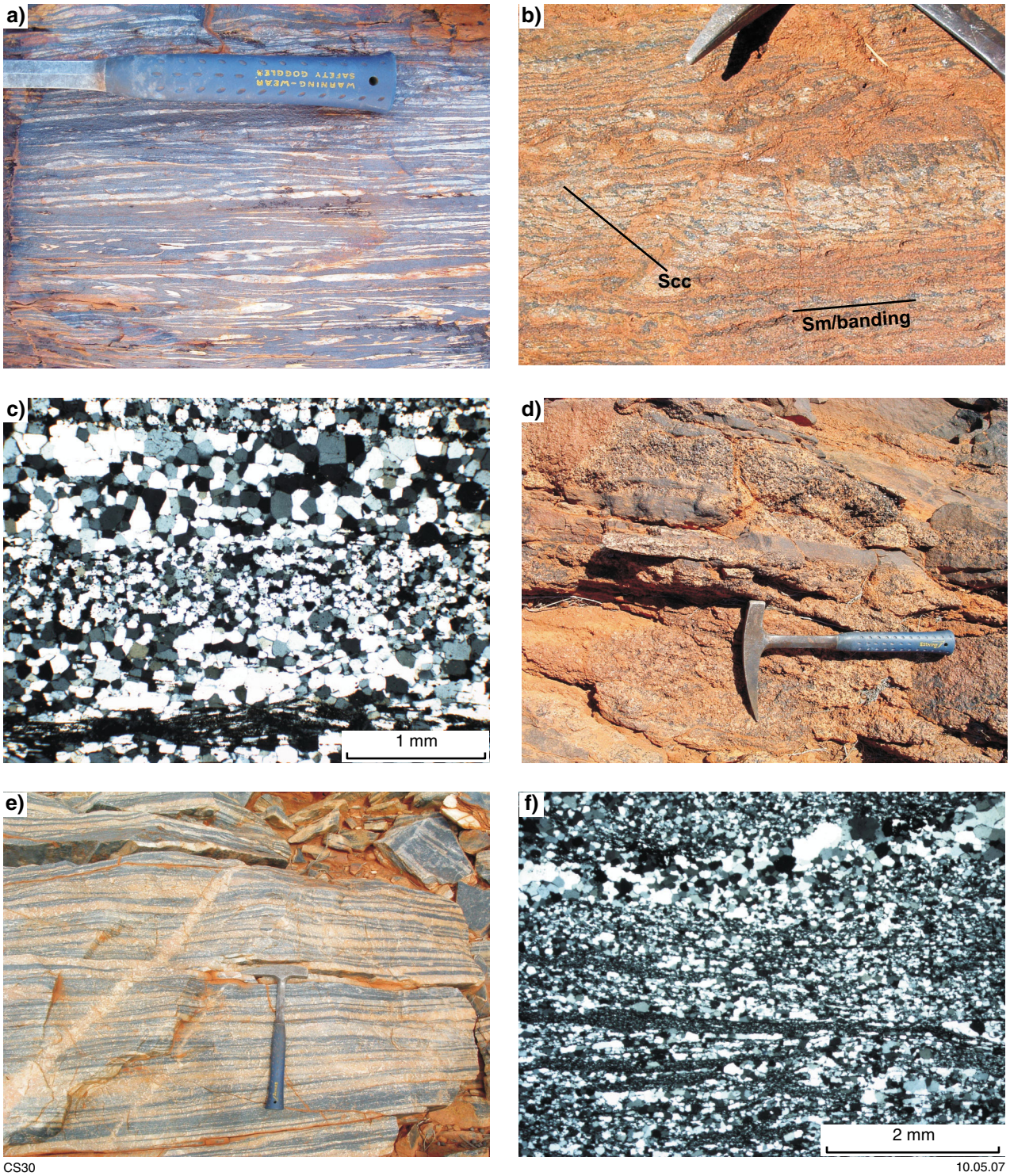

Figure 11. Banded iron-formantion (BIF), chert, and quartzite: a) transposed foliation in BIF from the northeastern area (Plate 1); b) incipient crenulation cleavage development in BIF, showing migration of Fe-rich layers into new cleavage planes, central area (Plate 3); c) chert from the central area (Plate 3). Many of the quartz grains have straight boundaries and show foam-structure texture, indicative of static recrystallization. The fine needles at the base of the photomicrograph are stilpnomelane (sample CS0388 near MGA 507624E 7107704N; cross-polarized light); d) BIF with horizons of hematite-rich lenses that crosscut the main layering, northeastern area (Plate 1); e) black and white banded quartzite, northeastern area (Plate 1); f) black and white banded quartzite, northeastern area (Plate 1). Quartz grains typically show dynamic recrystallization textures, including bands and lenses of small grains that have undergone grain-size reduction during deformation. Fe-oxide grains are common in these layers (sample CS0383; MGA 520325E 7113175N; cross-polarized light)

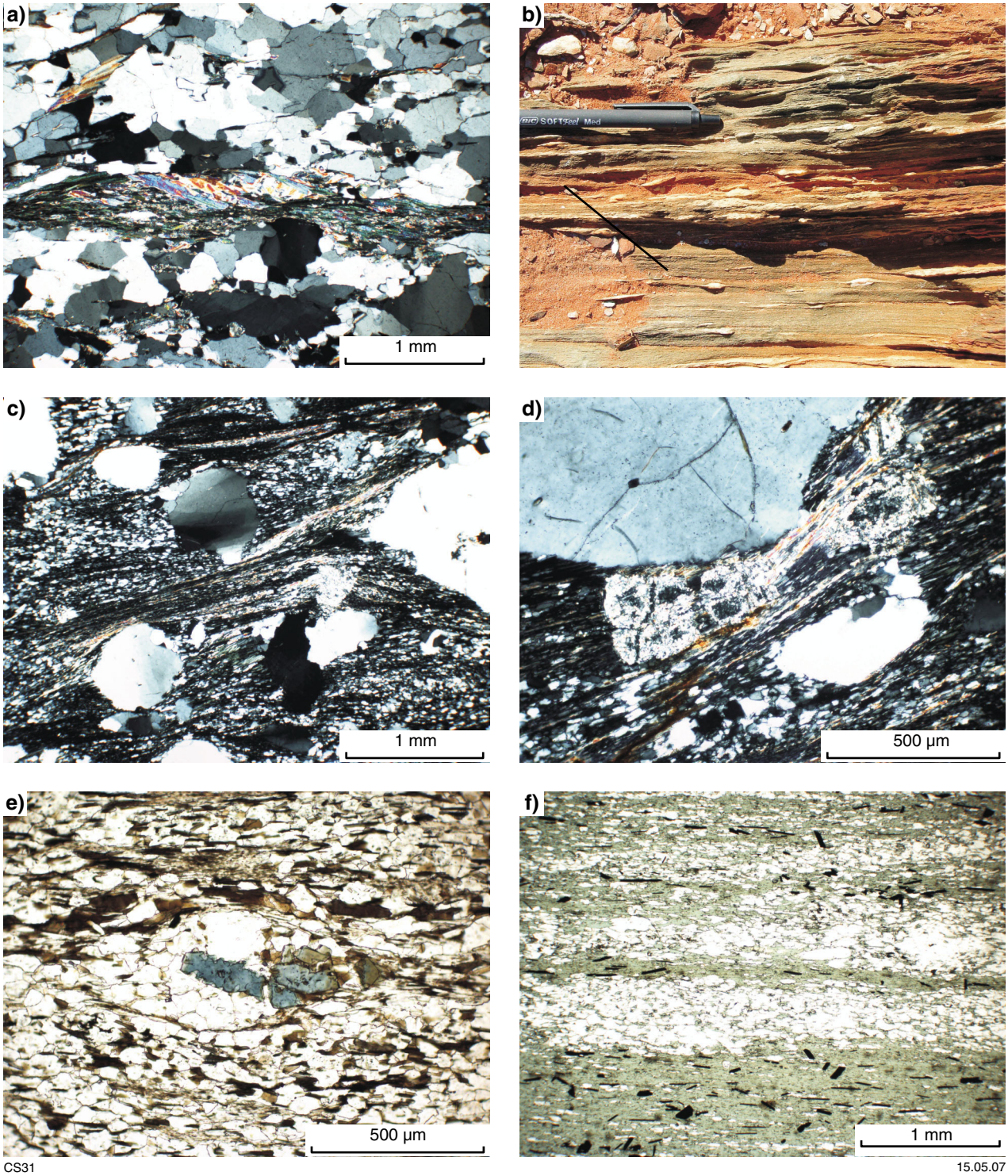

Figure 12. **Pelitic and semipelitic rocks: a) quartz–mica schist from the Milly Milly area (see Fig. 19), showing white mica as the main foliation-defining mineral. Two generations of mica growth are indicated by the different grain sizes (central part of picture; sample CS0341, MGA 485929E 7119422N; cross-polarized light); b) quartz–mica schist from the east-central area (Plate 2), showing dextral, asymmetric quartz-eyes; c) quartz–mica schist, showing andalusite porphyroblasts with micaceous and chloritic pressure shadows, northeastern area (Plate 1; sample CS0394, MGA 529034E 7118818N; cross-polarized light); d) chiastolitic andalusite porphyroblasts (centre of picture) in quartz–mica schist (cross-polarized light). Same sample as in (c); e) biotite schist from the west-central area (Plate 4), showing strong biotite and quartz foliation, and relict detrital tourmaline (sample CS0364, MGA 498818E 7106426N; plane-polarized light); f) chlorite–quartz schist from the east-central area (Plate 2), showing strong chlorite and quartz foliation, and tabular Fe-oxide grains subparallel to the foliation (sample CS0386, MGA 519568E 7112137N; plane-polarized light)**

Pebble metaconglomerate and associated mature clastic rocks

The association of mature clastic rocks is confined to the central and west-central areas of the belt (Plates 3 and 4). Similar rocks have been reported at Yarrameedie Hill (Fig. 3; Wilde and Pidgeon, 1990), but that area was not mapped during this study. No evidence of Neoarchean granitic intrusions has been found in the association, and its contacts with other associations are faulted. The association is well exposed over a series of ridges, extending from the Neoarchean granite intrusion in the west (known as the Blob; Wilde and Pidgeon, 1990; Plate 4), to close to the Cue–Beringarra road in the east (Plate 3). It consists of interbedded pebble metaconglomerate, metagritstone, metasandstone, metasiltstone, quartzite, and quartz–mica schist. Wilde and Pidgeon (1990) interpreted the association as a deltaic alluvial-fan deposit, based on well-preserved sedimentary structures (cross-bedding, graded bedding) and upward-fining sequences. Lithological sections constructed in the Eranondoo Hill area also show upward-fining sequences (Fig. 13a,b). However, thin beds of fine-grained rocks (quartz–mica schist) prevail throughout the association. In this area, pebble metaconglomerate, metagritstone, and metasandstone are the dominant lithologies. A faulted-out synform containing quartz–mica schist and minor quartzite (lithological section 5–6, Fig. 13b) suggests that a unit of mudstone-dominated rocks may have been deposited above the coarser grained, alluvial-fan sediments (see also Wilde and Pidgeon, 1990). This is supported by the gradual thinning and disappearance of conglomerate beds in quartz–mica schist towards the faulted contact with quartz–mica schist, quartzite, and mafic schist to the north (Plate 4). However, the facing direction near the faulted contact (assumed to be to the north, consistent with bedding dips) is not well constrained.

The metaconglomerate and metagritstone consist of rounded and flattened, mostly white quartz pebbles, minor chert, and sandstone pebbles, from about 0.5 to 30 cm long (Fig. 14a,b). Some of the pebbles have a similar appearance to the black and white ferruginous psammite described above (Fig. 14c). Black and white ferruginous psammite also locally forms thin lenses within the association (Fig. 14d), suggesting that the conglomerate may include clasts of metasedimentary rock derived from other units in the belt. The pebbles are supported by a sandy and micaceous matrix (Fig. 14e). Fuchsite is common throughout the association. In thin section the metaconglomerate typically has a strong foliation composed of quartz, white mica or fuchsite, or both. The foliation anastomoses around aggregates of quartz (pebbles or clasts; Fig. 14f). Grain-size reduction zones are evident in quartz, as are deformation effects such as undulose extinction and ragged grain boundaries. Quartz grains commonly show partial recovery and static recrystallization effects such as foam-structure texture and straight grain boundaries. The foliation is defined by quartz, and strongly aligned micaceous and locally chloritic or fuchsitic layers that are part of the matrix. Iron-oxides are locally cracked and pulled apart, or have pressure shadows of mainly quartz and white mica.

Granitic rocks

Neoarchean granitic rocks and pegmatite intrude granitic gneisses, BIF, chert, mafic and ultramafic rocks, and some quartzite and quartz–mica schist. The granites are mainly medium- to coarse-grained biotite monzogranites (Pidgeon and Wilde, 1998). Two of the best examples of these granites are a large mass in the west-central part of the belt (Plate 4), commonly known as the Blob, and a large outcrop on the southern margin of the central area of the belt, just east of the Cue–Beringarra road (Plate 3), commonly known as the Gallery. Rafts of granitic gneiss are preserved in monzogranite at the Gallery. Intrusive relationships between quartz–mica schist and Neoarchean granite are exposed on the eastern edge of the Blob, where rafts of the schist and thin-bedded quartzite are preserved in the granite (Fig. 15a). However, the mature clastic rocks, which appear to overlie the quartz–mica schist at this locality, do not show any evidence of intrusion by the granite.

In the southwestern and west-central areas of the belt (Plates 4 and 5), low-grade muscovite granite and pegmatite clearly intrude the BIF, chert, and quartzite unit, mafic and ultramafic rocks, quartzite, and quartz–mica schist (Fig. 15b). The muscovite granite commonly has a crumbly texture, and is locally pegmatitic. It is cut by pegmatites that contain coarse books of muscovite (Fletcher et al., 1997). Small zones of dynamically recrystallized feldspar and quartz are associated with a heterogeneously developed foliation (Fig. 15c). Some feldspar crystals also show effects of brittle deformation in the form of microfaults (Fig. 15d).

Proterozoic metasedimentary rocks

Two areas of Proterozoic rocks have been recognized by SHRIMP U–Pb detrital zircon dating (sample 01JH63, Cavosie et al., 2004; samples JH3 and JH4, Dunn et al., 2005; see **SHRIMP U–Pb detrital zircon geochronology** above). Two thin lenses, about 50 to 100 m wide, of quartz–mica schist with minor interbedded, mostly thin beds of quartzite outcrop between BIF and the mature clastic rocks for a combined strike length of about 4 km (Plates 3 and 4). The lenses are fault bound and have been sampled at sites 01JH63 and JH3 (Fig. 5). It should be noted that the geographic coordinates for the JH3 sample locality given in Dunn et al. (2005) do not correspond to the location plotted on their map. The map position is assumed to be the correct position because the sample was collected before GPS was used. The schist is indistinguishable from other quartz–mica schists in the belt. They are mostly mylonitic (Fig. 16a), and contain boudinaged quartz veins (Fig. 16b). In thin section the schists show evidence of both dynamic and static recrystallization, where a mylonitic foliation is partly overgrown by quartz with straight grain boundaries and foam-structure texture (Fig. 16c). Lithological section 1–2 (Fig. 13a) shows boudinaged quartzite beds at the northern end of the Proterozoic unit. This may indicate a change in depositional conditions, but it is not clear which way the unit youngs.

Metaconglomerate sample JH4 (Dunn et al., 2005) is from the northeastern part of the belt (Plate 1) from a unit

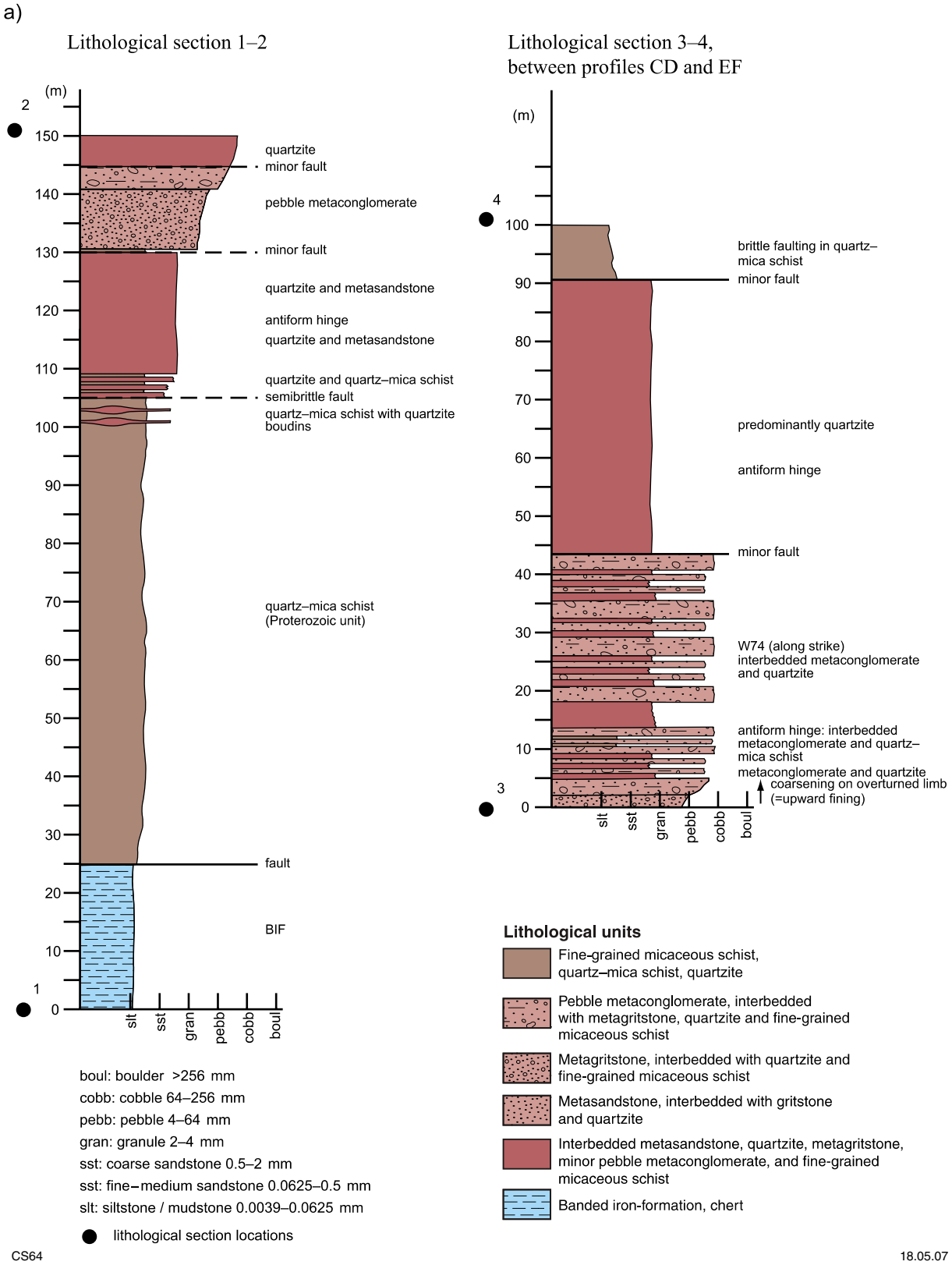

Figure 13. Lithological logs from the west-central area (see Fig. 5 for location): a) lithological logs of the sections between points 1 and 2, and points 3 and 4); b) (next page) lithological logs of the sections between points 5 and 6, and a 60 m-section commencing with outcrop W74. Sedimentary grain and lithic size definitions are after Boggs (1987)

b)

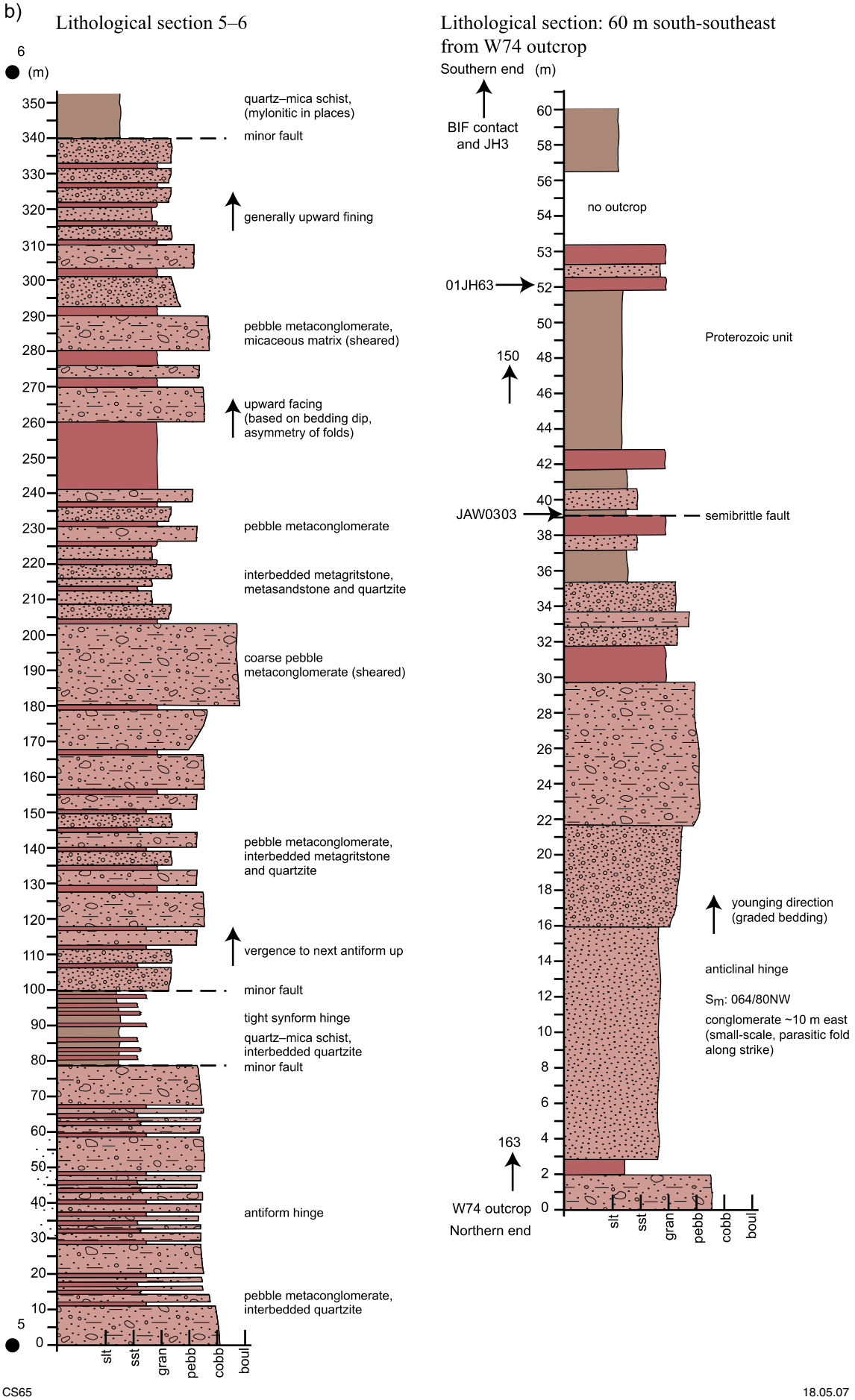

CS65 18.05.07

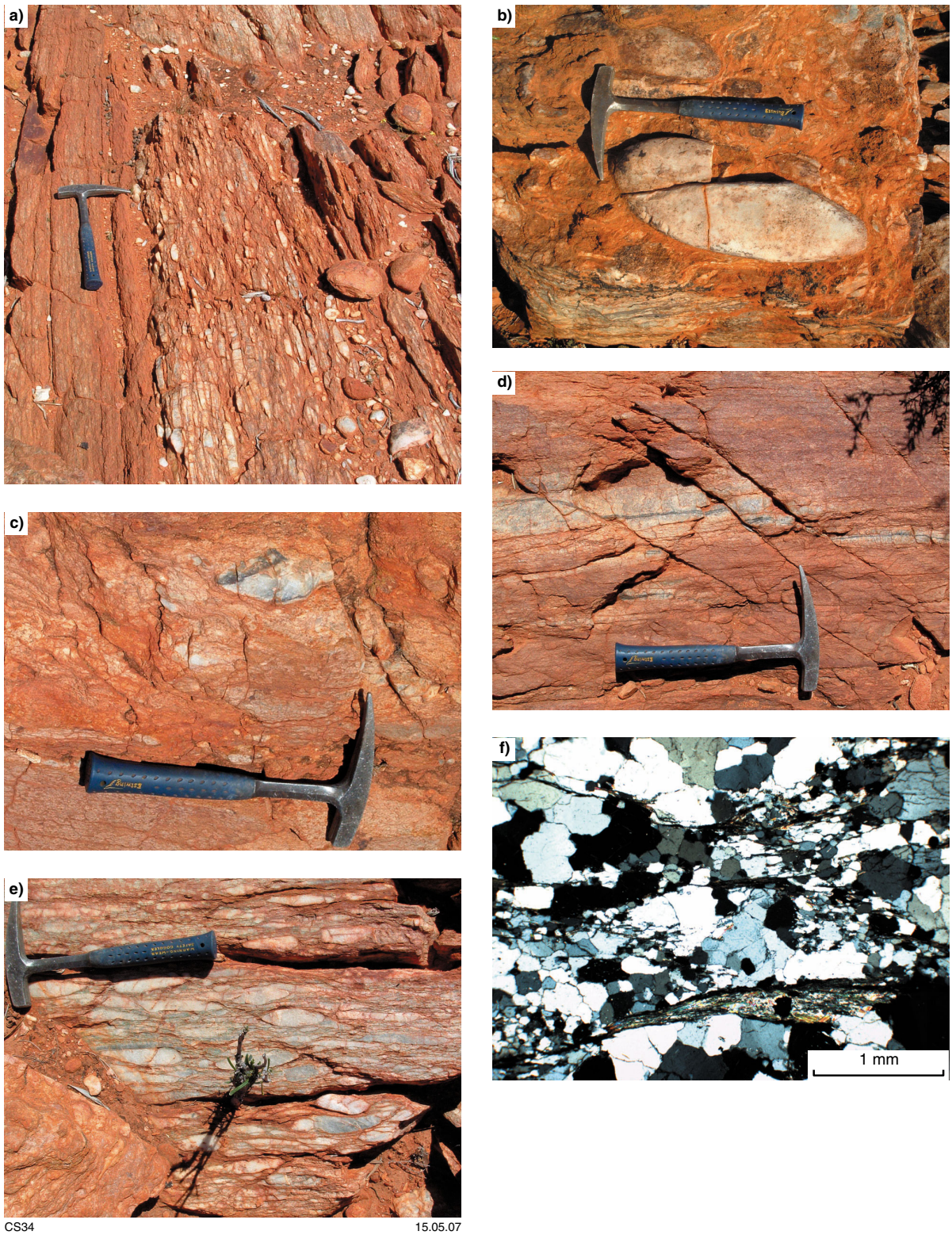

Figure 14. The mature clastic association: a) interbedded metasandstone, metagritstone, and pebble metaconglomerate from the mature clastic association in the west-central area (Plate 4); b) large quartz pebble in metaconglomerate from the west-central area (Plate 4). This pebble is about the maximum size in the association; c) clast (upper centre) of black and white quartzite in metasandstone and metaconglomerate in the west-central area (Plate 4); d) lenses of black and white banded quartzite interbedded with metasandstone in the mature clastic association from the west-central area (Plate 4). Small, west-northwesterly trending brittle faults offset the layering; e) sandy and micaceous matrix supporting stretched quartz pebbles in metaconglomerate from the west-central area (Plate 4). The greenish colour is due to fuchsitic micas in the foliation (WP 379, MGA 497261E 7105495N); f) metaconglomerate showing the quartz, white mica, and fuchsite foliation anastomosing around aggregates of quartz (from pebbles or clasts) from the west-central area (Plate 4; sample CS0322, MGA 499135E 7105844N; cross-polarized light). Note, this is from the same outcrop as W74 (see Fig. 5)

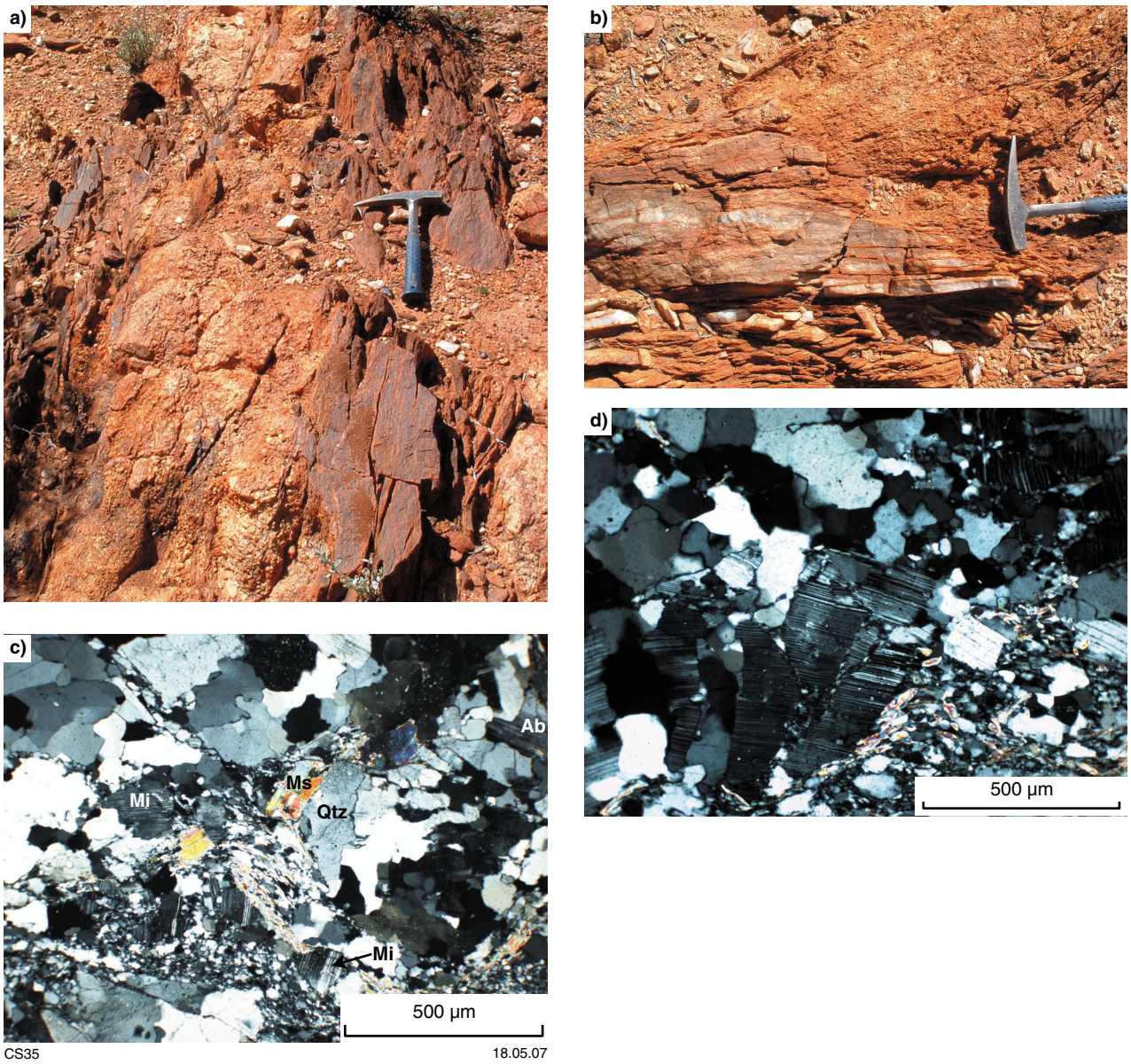

Figure 15. Metasedimentary rafts and muscovite granite: a) quartz–mica schist intruded by granite near the eastern margin of the main granite body known as the Blob, from the west-central area (Plate 4); b) muscovite granite (upper right) intruding quartzite and quartz–mica schist, in the southwestern area (Plate 5); c) muscovite granite from the southwestern area (Plate 5; cross-polarized light). The rock consists of microcline (Mi), albite (Ab), quartz and quartz megacrysts (Qtz), and muscovite (Ms). Small zones of dynamically recrystallized feldspar and quartz, and some muscovite (e.g. lower part of picture), define the foliation (sample CS0416, 30 m north of MGA 491092E 7103606N); d) muscovite granite showing brittle microfaults in microcline crystals (same sample as (c); cross-polarized light)

of folded interbedded quartzite, metasandstone, pebbly sandstone, metaconglomerate, and quartz–mica and ferruginous schist. It should be noted that the geographic coordinates for the JH4 sample locality given in Dunn et al. (2005) do not correspond to the location plotted on their map, nor to the correct lithology. The position plotted on their map does, however, match lithologies in the field and this is assumed to be correct. The metaconglomerate is locally strongly deformed and outcrops within a small shear zone, not far from the faulted eastern margin of the greenstone belt. Near JH4 it is clearly conformable, and folded in, with the other metasedimentary rocks in this area, and therefore the whole unit is interpreted as Proterozoic (Plate 1). The metaconglomerate contains clasts of mainly quartz pebbles, some of which are fuchsitic, and black and white banded quartz-rich rocks similar to the black and white banded ferruginous psammite. These are supported by a micaceous matrix (Fig. 16d). The quartzite is commonly massive, and some is veined and silicified. The rocks in this unit have been metamorphosed to at least greenschist-facies temperatures, as indicated by the presence of andalusite. The sequence as a whole is very similar to the mature clastic rocks (association 3).

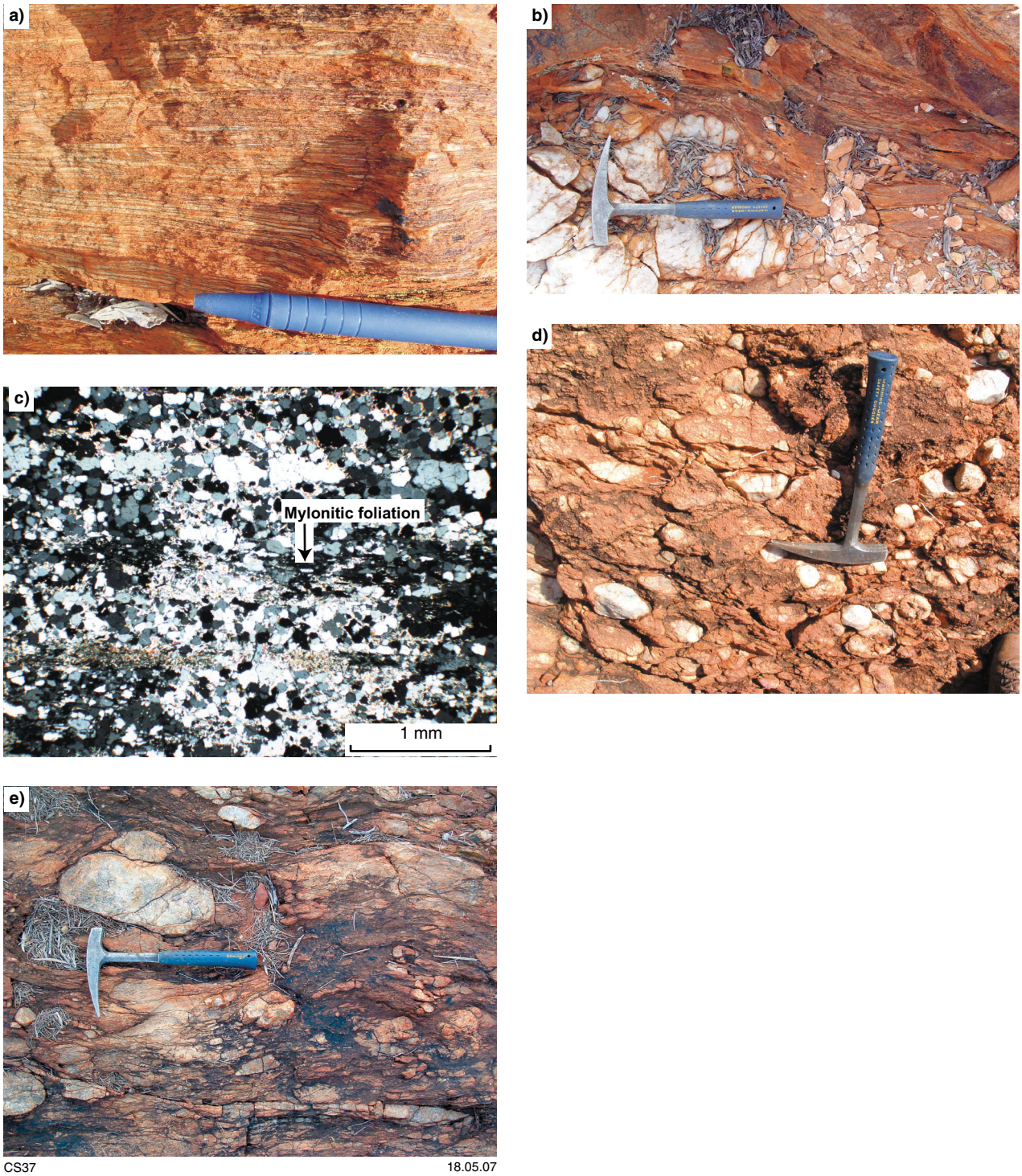

Figure 16. Proterozoic rocks: a) mylonitic Proterozoic quartz–mica schist from the west-central area (Plate 4); b) boudinaged quartz veins in Proterozoic quartz–mica schist, within the fault contact with the mature clastic association. This is also the locality of ^{40}Ar–^{39}Ar sample JAW0303, from the west-central area (Plate 4; Figs 5 and 16b; MGA 499135E 7105844N); c) Proterozoic quartz–mica schist showing statically recrystallized quartz overgrowing the mylonitic foliation, from the west-central area (Plate 4; sample CS0325, MGA 499135E 7105844N; cross-polarized light); d) possible metaconglomerate in a small shear zone in the northeastern area (Plate 1); e) tectonically disrupted quartzite and quartz–mica schist from the northeastern area (Plate 1). This is the locality of ^{40}Ar–^{39}Ar sample CS0395 (MGA 529034E 7118818N)

Near locality waypoint (WP) 318 (MGA 529128E 7118858N), an outcrop of disrupted interbedded and veined quartzite and quartz–mica schist has the appearance of a metaconglomerate, but is interpreted as a fault mélange because it has a variety of clast sizes in an approximately 8 m-wide horizon adjacent to a major zone of shearing overprinted by brittle faulting (Fig. 16e). This is near the western contact of the Proterozoic unit.

Quartz veins

Quartz veins and silicification are common throughout the Jack Hills greenstone belt. Veins range in width from centimetre-scale up to 50 m. The large veins have strike lengths up to 2 km, and are typically associated with brittle faults. Good examples are northwest-trending, large quartz veins and brittle faults that offset the southern margin of the belt with dextral sense in the central area (Plate 3). Quartz veins are mostly white (milky quartz), but some also contain black, grey or smoky quartz. Some veins are also associated with epidote alteration in host rocks, particularly where faults are present. There are clearly at least two generations of quartz veins because late crosscutting veins overprint folded veins in some outcrops. The first generation veins are commonly folded or sheared, or both. The second-generation veins are commonly vuggy, with well-formed quartz crystals in the cavities. These are either weakly deformed or undeformed.

Widespread silicification has affected most rocks in the belt, but less so the mature clastic rocks. Much of the chert interbedded with BIF may have been formed by this mechanism, rather than by chemical precipitation. High, competent strike ridges of chert and quartzite have also been affected by silicification, as marked by the diffuse banding (Fig. 17). Silicification has probably contributed to the production of serpentinites from the ultramafic rocks, and secondary quartz in mafic schists. Much of the fluid activity is likely to have occurred during major shearing across the belt (see **Deformation** below), and its effects may help explain why much of the belt has significant topographic relief compared to many other greenstone belts in the Yilgarn Craton. It is not clear whether some of the metasedimentary units, especially the Proterozoic rocks, were solely confined to the belt or covered a much wider area prior to erosion. Therefore, silicification may have played a role in their preservation.

CS39 16.05.07

Figure 17. Diffuse black banding in quartzite from a strike ridge in the southwestern area (Plate 5)

Mesoproterozoic mafic dykes

Dolerite dykes that intrude the Jack Hills greenstone belt and surrounding granitic rocks crosscut major structures and most lithological units. Major deformation and folding is constrained to have occurred prior to the intrusion of these dykes. The dykes mostly have easterly trends and locally appear to have used pre-existing major structures. For example, in the central area (Plate 3), an undeformed, east-trending dolerite dyke trends parallel to the main foliation in sheared gneiss and granite, near the southern margin of the belt. At least two phases of intrusion are recognized: dolerite and gabbro that typically show some chlorite and epidote alteration, and fresh unaltered dolerite. A leucogabbro dyke in the southwestern part of the belt has a precise SHRIMP U–Pb zircon age of 1211 Ma (Wingate et al., 2005). This dyke (which trends 080°) is at a high angle to, and may crosscut, this part of the belt and link up with similarly trending gabbroic and dolerite dykes within the belt (Plate 5, southern area, WP 341, MGA 490876E 7102231N). A similar dyke that intruded granite 30 km south of the belt has a SHRIMP U–Pb age of 1213 Ma (Wingate et al., 2005). These dykes have been included in the 1210 Ma Marnda Moorn large igneous province by Wingate et al. (2005).

Other east-trending dolerite outcrops east and south of the Jack Hills greenstone belt have been dated at 1075 ± 10 Ma using combined SHRIMP U–Pb and paleomagnetic techniques, and are related to the Warakurna large igneous province (Wingate et al., 2004). A west-northwesterly trending dyke that cuts across fold structures in the mature clastic and Proterozoic rocks in the Eranondoo Hill area (Fig. 5; Plate 4) is correlated with the 1075 Ma dyke suite (Wingate, M. T. D., 2004, written comm.). Discontinuous outcrops of east-northeasterly trending dolerite dykes in gneiss and granite just southeast of the Eranondoo Hill area are probably part of the same intrusion.

Deformation

Large-scale structure and geometry

The geometry of the Jack Hills greenstone belt is well illustrated by ASTER satellite imagery (Fig. 18). It shows that the approximately 70 km-long belt has a pronounced sigmoidal curvature, with a relatively narrow central section and wider sections at both ends, particularly the northeastern end. The geometry is typical of a dextral shear zone, where the northeastern and southwestern parts of the belt are within fault splays off a major east-trending shear zone that cuts the belt. The major shear zone is not confined to the belt itself, but cuts through gneiss and granite just north of it on the western side, and south of it on the eastern side (Figs 3 and 18). Fault splays off the

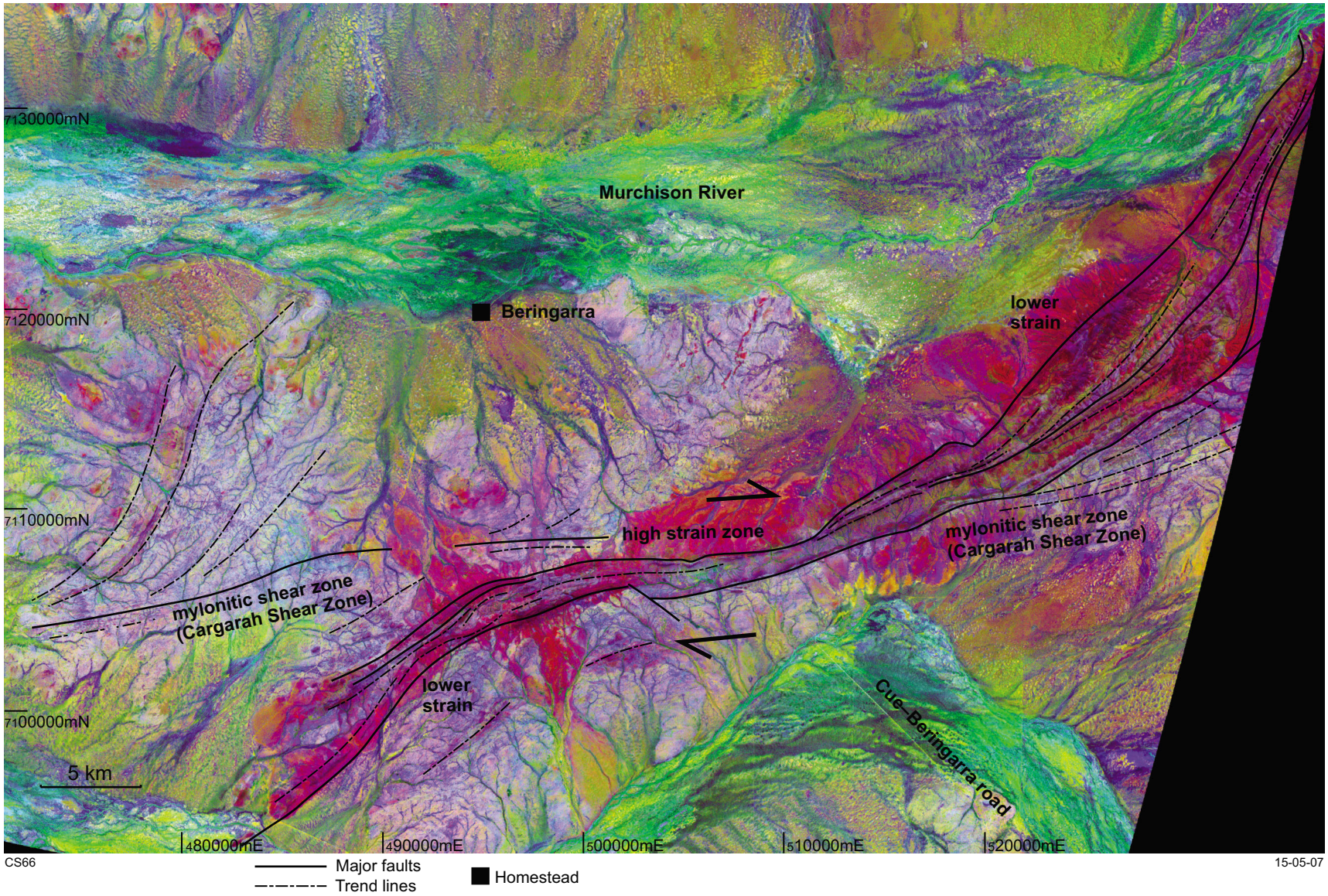

Figure 18. ASTER satellite image (decorrelation stretch of bands 2, 3, and 1) of the Jack Hills greenstone belt. The annotation is based on both image interpretation and field observations

western end of the shear zone (Milly Milly area, Figs 3 and 19) contain lenses of quartzite, mafic schist, BIF, and chert within gneiss and granite. This part of the shear zone is shown in Williams et al. (1983a) and Myers (1997), and was named the 'Cargarra Shear Zone' or 'Cargarra Fault'. It is here renamed the Cargarah Shear Zone, after Cargarah Bore, and the name is used here to apply to the entire shear zone. The continuation of the shear zone east of the belt is evident in aeromagnetic images (Fig. 20), with fault splays that contain slices of BIF and ultramafic rocks to the east (Fig. 21). The interpretation of the satellite and aeromagnetic images is consistent with field data that show that the central region of the belt is dominated by high strain, including pronounced stretching and boudinage, whereas the fault splays contain areas of lower strain with more localized high-strain zones (Fig. 18).

The margins of the belt are sheared and have steep dips, indicating that the belt itself is steeply dipping. Cross sections constructed through the mapped areas (Plates 1 to 5), and analysis of aerial photography, satellite imagery, and aeromagnetic imagery, indicate that the belt is a series of internally folded fault slices. Across strike the belt is interpreted to have a wedge-like form, pinching out within the gneiss at depth. This interpretation differs from that of Elias (1982), who interpreted the belt as a synformal structure. This study has shown that the belt has undergone a long and complex structural history to produce the present-day geometry. This involved an early phase of folding, including recumbent folding at least locally, possibly related to thrusting, followed by upright folding and shearing. Most shears are reworked and overprinted by widespread brittle and semibrittle faulting and localized folding.

Foliations

Interpreting overprinting relationships between the various foliations in the Jack Hills greenstone belt is not straightforward because they are commonly coplanar, and in many places the rocks have been silicified and statically recrystallized. All units within the belt are deformed and show at least one well-developed foliation (Table 1). This main foliation (S_m) is generally penetrative, and of upper greenschist or, locally, amphibolite facies. It post-dates formation of gneissic banding in the surrounding granitic gneisses. This relationship is evident at, and close to, the margins of the belt, where the main foliation is more intense. The main foliation does not relate to one specific set of structures, and is a composite foliation related to both folding and shearing, although these did not necessarily form at the same time. For example, in the west-central area (Plate 4), within the mature clastic rocks, the main foliation is axial planar to southwest-plunging, tight inclined folds, whereas in the eastern part of the west-central area and in the central area (Plates 3 and 4) the main foliation is anastomosing or mylonitic, and clearly related to development of S–C structures and shearing (Fig. 22a,b). In general, shearing post-dates the folding where the main foliation is axial planar, and could therefore represent either tightening of shear-related folds or overprinting of an earlier folding event. The main foliation defines the geometry of the belt and is mostly subparallel to the contacts between the various lithological units (Fig. 20).

Within the BIF, ultramafic rocks, mafic schist, and pelitic and semipelitic rocks, an earlier foliation (S_1) is typically evident, and the main foliation (S_m) is a crenulation cleavage (Table 1; Plates 1–5). It is not clear whether this early foliation is of a different metamorphic grade because mineral assemblages are generally the same. However, in some mafic schists, hornblende and plagioclase assemblages are overprinted by actinolitic amphiboles that probably represent a transition from amphibolite- to greenschist-facies conditions. The early foliation is not evident in the mature clastic rocks that host the 4.0 Ga-and-older detrital zircons, nor in metasandstone and quartzite in the northeastern area (Plate 1). The main foliation is overprinted by a less penetrative crenulation cleavage (S_{cc}), generally related to locally developed, open to tight folds (Fig. 23a). This cleavage is mostly spaced, and is no higher than greenschist facies.

Lineations

The Jack Hills greenstone belt contains a widespread moderately plunging mineral lineation that ranges in direction from southwest (dominant) to northeast (stereonets on Plates 1–5). In the central part of the belt, where it narrows, the lineation has a shallower plunge, and is mostly subhorizontal (Plate 3). The lineation is also developed within gneiss and granitic rocks that host the belt, and is subparallel to the gneissic lineation where developed. In the BIF the lineation is generally parallel to second-generation fold axes (Fig. 24a) and is a composite stretching and intersection lineation. In zones of higher strain the folds are obliterated and the lineation increases in intensity. Mineral lineations are variably developed in mafic schist, quartzite, and pelitic and semipelitic rocks that show S–C fabrics. In quartzites that form distinct strike ridges the mineral lineation is generally well developed, and varies in plunge along strike on scales of several metres or more. For example, in the southwestern area (Plate 5), the plunge changes gradually from about 60° northeast to 20° northeast, to 40° northeast, and back to 60° northeast, on a consistently oriented foliation plane over a distance of about 1 km. Plunge variations of this type have also been observed in BIF, where over a distance of about 20 m the lineation plunge changes by 50°.

Stretching is also evident in metaconglomerate within the mature clastic rocks, where pebbles are elongated parallel to mineral stretching directions (predominantly southwest, Plate 4; Fig. 24b). The pebbles are also commonly flattened with vertical elongation (Fig. 24c). Intersection lineations are variably developed, and are most prevalent in the BIF, pelitic and semipelitic rocks, and mafic schist.

Fold style and chronology

Fold geometry and style is variable throughout the belt, and also between the various lithologies. The most informative sequence is the BIF, which preserves at least

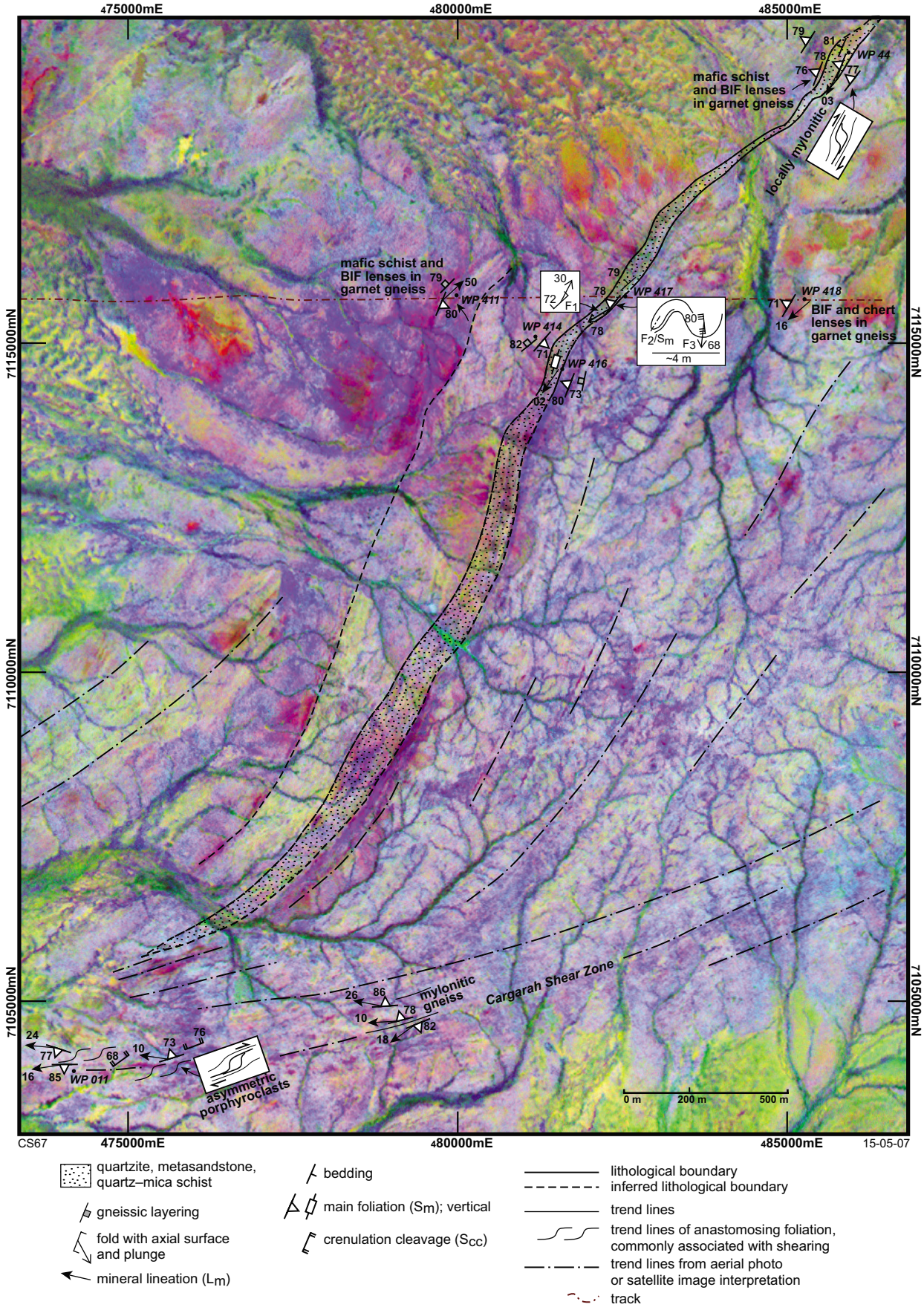

Figure 19. Simplified geological map of the Milly Milly area, overlain on an ASTER satellite image (decorrelation stretch of bands 2, 3, and 1; see Fig. 3 for location)

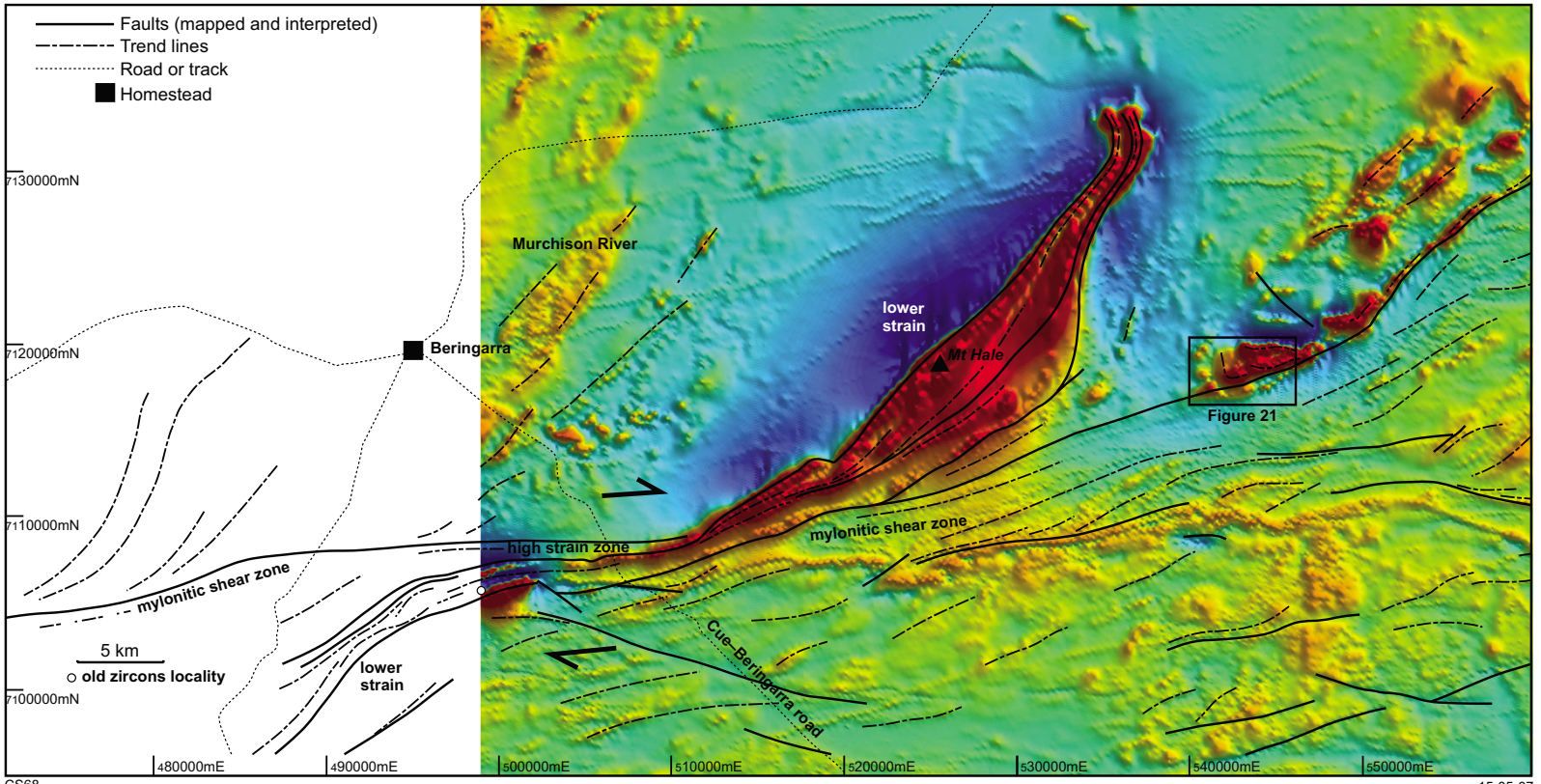

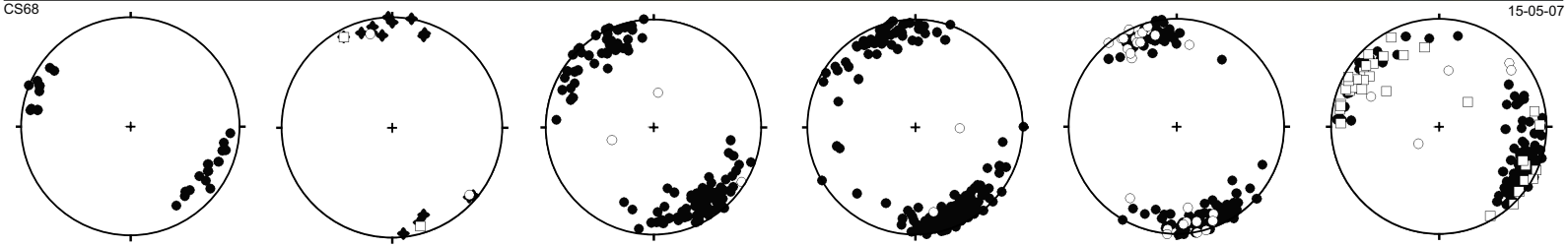

Milly Milly north: S_m = black dots, n=23

Milly Milly south (Cargarah Shear Zone): Granite, mafic schist, S_m, squares, n=2; Gneissic layering, open dots, n=2; Gneiss S_m, crosses, n=15

Southwest: S_m = black dots, n=120; BIF and chert: banding = open dots, n=3

West-central: S_m = black dots, n=214; BIF–chert: Sm / banding = open dots, n=2

East-central and Central: S_m = black dots, n=129; BIF–chert: S_m / banding = open dots, n=26

Northeast: S_m = black dots, n=111; S_m / banding = squares, n=36; BIF–chert: Banding = open dots, n=5

Figure 20. Annotated aeromagnetic image (total magnetic intensity, reduced to pole) showing the continuation of the Cargarah Shear Zone to the east. Note that 400 m or less line-spacing aeromagnetic data is not available west of the Belele sheet. Stereonets are equal angle. S_m refers to the main foliation

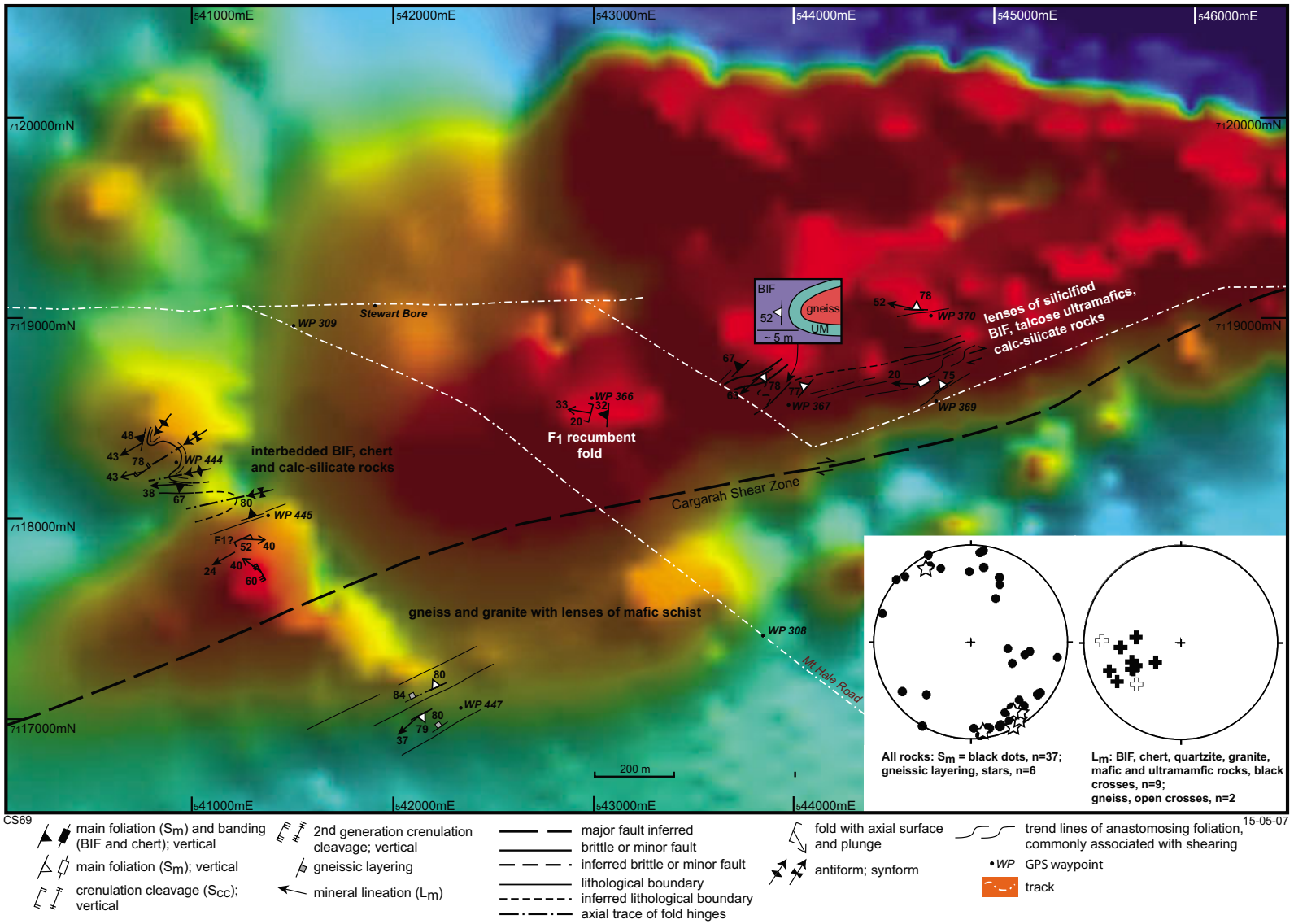

Figure 21. Simplified structural map of the area northeast of the main belt, showing the main fault between gneissic and granitic rocks and BIF, chert, ultramafic and calc-silicate rocks. Note the F_1 recumbent fold described in the text in the centre of the map, at WP 366. The map is overlain on an aeromagnetic image (total magnetic intensity, reduced to pole, see Fig. 19 for location)

Table 1. Chronology of structures in the Jack Hills region

Rock units	*Main mineralogy and type of foliation; associated structure(s)*				
Gneiss and granitic rocks	Gneissic layering (probably pre-dates S_1 below; pre-3000 Ma); Tight inclined folding of gneissic layering (possibly pre-dates folding below)	Intrusion of monzogranite and pegmatite	Main foliation (S_m) ± S–C foliations: Qtz, ± Bt, ± white mica, ± feldspar; Shear zone and folds	Localized and minor crenulation cleavage: Qtz, white mica Upright open or kink folds	Localized low-grade small shears and brittle faults
Mafic and ultramafic rocks	S_1 foliation (mostly schistose or slaty): mafics = Hbl ± Act, Bt, ± Chl, ± Qtz, ± Ep ultramafics = Serp, ± talc Inclined to recumbent folds?	Localized crenulation cleavage: mafics = Act, Plag, ± Bt, ± Chl, ± Qtz, ± Ep, ultramafics = Serp, ± talc Upright folds?	Main foliation (S_m) ± S–C foliations: mafics = Act, Plag, ± Bt, ± Chl, ± Qtz, ± Ep ultramafics = Serp, ± talc; Shear zone and tight folds	Localized crenulation cleavage: mafics = Act, Plag, ± Chl, ± Qtz, ± Ep Ultramafics = Serp, ± talc? Kink folds, upright folds	Localized low-grade small shears and brittle faults
BIF, chert, and quartzite	S_1 foliation ± banding: Qtz, Fe-oxide, ± stilpnomelane Inclined to recumbent folds (F_1)	Crenulation cleavage ± banding: Qtz, Fe-oxide, ± stilpnomelane Axial planar to inclined to upright chevrons (F_2)	Main foliation (S_m) ± S–C foliations: Qtz, Fe-oxide, ± stilpnomelane; Shear zone and tight to isoclinal folds	Localized crenulation cleavage: Qtz, Fe-oxide, ± pressure solution Upright kink folds, open folds, conjugates	Localized low-grade small shears and brittle faults
Pelite and semipelite	S_1 foliation (mostly schistose or slaty): Qtz, white mica, ± Bt, andalusite, ± Chl Inclined to recumbent folds?	Axial planar to upright folds (F_2) crenulation cleavage: Qtz, white mica, ± Bt, ± Chl Axial planar to upright folds (F_2)	Main foliation (S_m) ± S–C foliations: Qtz, white mica, ± Bt, ± Chl; Shear zone and tight to isoclinal folds	Localized crenulation cleavage: Qtz, white mica or sericite, ± Chl, ± pressure solution Upright kink folds, open folds, conjugates	Localized low-grade small shears and brittle faults
Mature clastic rocks: (metaconglomerate, quartzite, metasandstone, Qtz–mica schist)	`	Spaced foliation (slaty or schistose in Qtz–mica schist): Qtz, white mica, ± Chl, ± andalusite Axial planar to inclined to upright folds (F_1)	Main foliation (S_m), may be spaced, ± S–C foliations: Qtz, white mica, ± Chl, ±andalusite; Shear zone and tight folds	Localized crenulation cleavage: Qtz, white mica or sericite, ± Chl, ± pressure solution Upright kink folds, open folds, conjugates	Localized low-grade small shears and brittle faults
Proterozoic siliciclastic rocks: sandstone, quartzite, Qtz–mica schist		Spaced foliation (slaty or schistose in Qtz–mica schist): Qtz, white mica, ± Chl, ± andalusite Axial planar to inclined to upright folds (F_1)	main foliation (S_m), may be spaced, ± S–C foliations: Qtz, white mica, ± Chl, ± andalusite Shear zone and tight folds	Localized crenulation cleavage: Qtz, white mica or sericite, ± Chl, ± pressure solution Upright kink folds, open folds, conjugates	Localized low-grade small shears and brittle faults
Mesoproterozoic mafic dykes					Intrusion of mafic dikes
TIME	3000 Ma	2650 Ma	c.1800 Ma	1210 Ma	1075 Ma

NOTES: Hbl = hornblende
Act =actinolite
Bt = biotite
Chl= chlorite
Qtz = quartz
Ep = epidote
Serp = Serpentinite
Plag = plagioclase

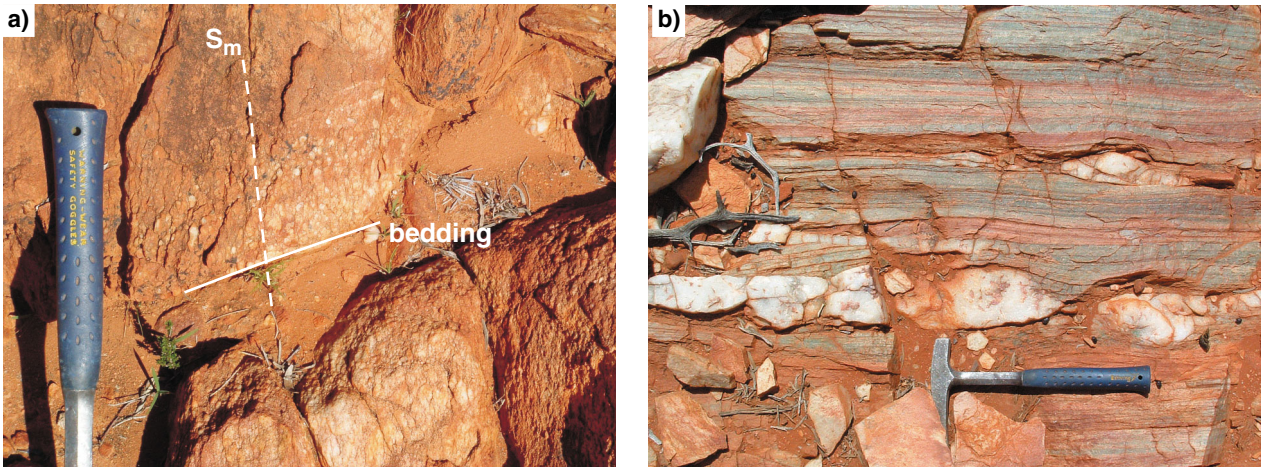

Figure 22. Foliations in the mature clastic association: a) simple bedding and cleavage (S_m) relationships in a fold hinge in the mature clastic rocks, in the west-central area (Plate 4); b) mylonitic foliation (S_m) and boudinage in mature clastic rocks in the central map area, near WP 402 (Plate 4). This is where the mature clastic association pinches out within the Cargarah Shear Zone

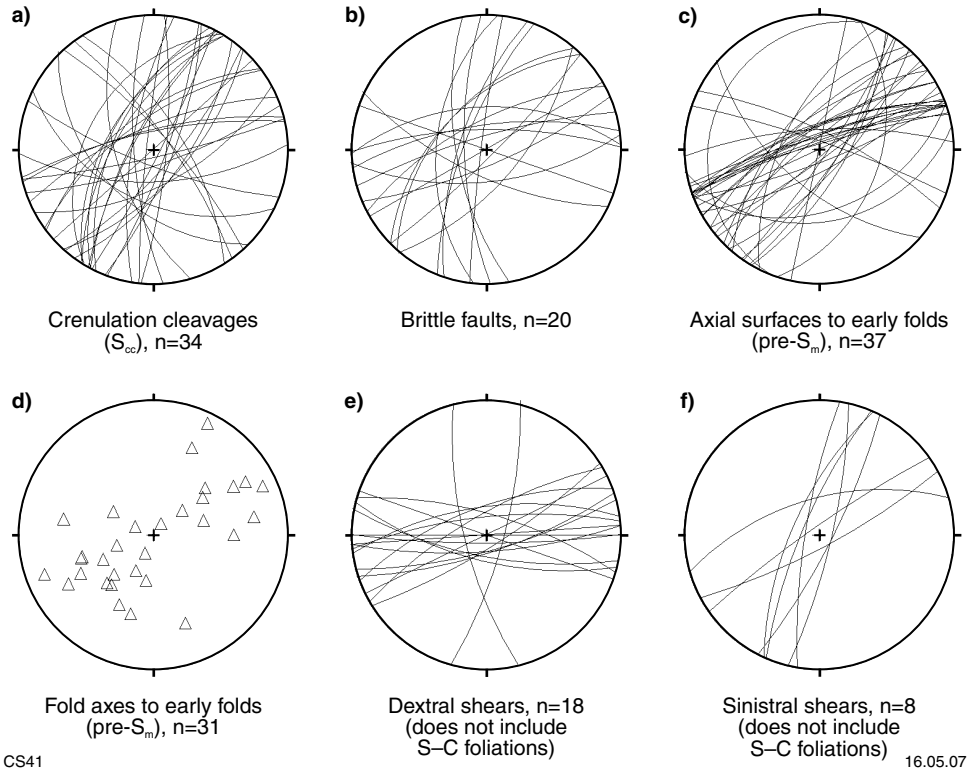

Figure 23. Stereonets showing early folds, faults, shears, and crenulation cleavages: a) stereonet showing crenulation cleavage (S_{cc}) plane orientations throughout the belt. This cleavage post-dates the main foliation (S_m) and varies in orientation from predominantly northeast trending to northwest trending; b) stereonet showing orientations of late small brittle faults; c) and d) stereonets showing axial surface and fold axis orientations of early pre-S_m folds within the belt; e) and f) stereonet showing orientations of dextral and sinistral small shears throughout the belt. All stereonets are equal angle

Figure 24. Linear fabrics in the mature clastic rocks and BIF: a) composite mineral lineation (L_m) and intersection lineation ($0L_{int}$) in BIF in the west-central area (Plate 4). L_{int} is the intersection of banding on the main foliation plane (S_m). In the photograph both L_m and L_{int} are parallel to steeply plunging fold axes (note the fold closure just below the hammer); b) pebble elongation parallel to mineral lineation (same as pen) in metaconglomerate near the W74 outcrop (Plate 4, see Fig. 5 for location); c) stretched quartz pebble in metaconglomerate, showing vertical elongation and flattening. Photograph taken near WP 56, Plate 4 (MGA 498661E 7106077N)

three generations of folds. First-generation folds are recumbent, with a well-developed axial-planar cleavage. These are rare and only preserved in low-strain zones or hinges of later folds, or both. The best example is east of the main belt, within a fault slice to the northeast (Figs 21 and 25a,b). Here, parasitic folds to a recumbent fold are well developed, and show the typical chevron form seen in refolded folds throughout the belt. Within most of the belt the recumbent folds have been refolded into either southwest- or northeast-plunging, tight to isoclinal, upright folds, with S_m axial planar to the folds. The strong overprinting due to S_m and these second-generation folds mostly obscures the earlier folds, but the development of S_m as a crenulation cleavage is clear as is refolding of early folds (Fig. 25c,d). Remobilization of iron-rich bands into a new foliation is common (Fig. 11b) and has also obliterated the earlier structures, as has localized, but widespread, strong overprinting from shearing, and silicification and veining. The main foliation (S_m) is folded by small-scale, upright kink folds, commonly developed as conjugates (Fig. 25e). S- or Z-type folds of this generation are also widespread.

Recumbent folds have not been identified in other lithologies apart from a shallowly dipping inclined fold in granitic gneiss just north of the central area. The presence of an earlier foliation suggests that at least the mafic and ultramafic rocks, and some of the pelitic and semipelitic rocks, have also undergone a similar or related early deformation event. Most folds that formed prior to the main foliation (S_m) are northeast trending with steeply dipping axial planes, and have variably plunging fold axes (Fig. 23c,d). This geometry is most probably due to reorientation during formation of the main foliation, either during subsequent folding or shearing, or both.

Second-generation folds as seen in the BIF are the dominant fold structures throughout the belt. However, in the mature clastic rocks they are first-generation folds. Here, they are inclined towards the southeast and plunge moderately to the southwest, parallel to mineral stretching lineations and pebble elongation (Fig. 5a; Plate 4). As in the BIF the axial-planar foliation to these folds (S_m) is folded by localized upright kink folds, commonly as conjugate pairs. These late folds are widespread throughout the Jack Hills area, and are commonly either northeast or northwest trending and typically associated with brittle faults (see stereonets on Plates 1–5).

Shear zones

The Jack Hills greenstone belt is dominated by strike-parallel shears that cut the main sets of folds. These shears can have long strike lengths, up to 50 km or so, and in mafic schist, pelitic and semipelitic rocks, quartzite, and granitic rocks typically have S–C foliations developed within them. The S–C foliations predominantly show dextral shear sense. At some localities low-angle shear bands show both dextral and sinistral shear sense in the one outcrop and are interpreted as conjugate shear bands indicative of flattening (Fig. 26; e.g. McClay, 1987). Small dextral shears are predominantly east trending, whereas most small sinistral shears are north trending (Fig. 23e,f). Locally, a strong rodding lineation is developed. This is

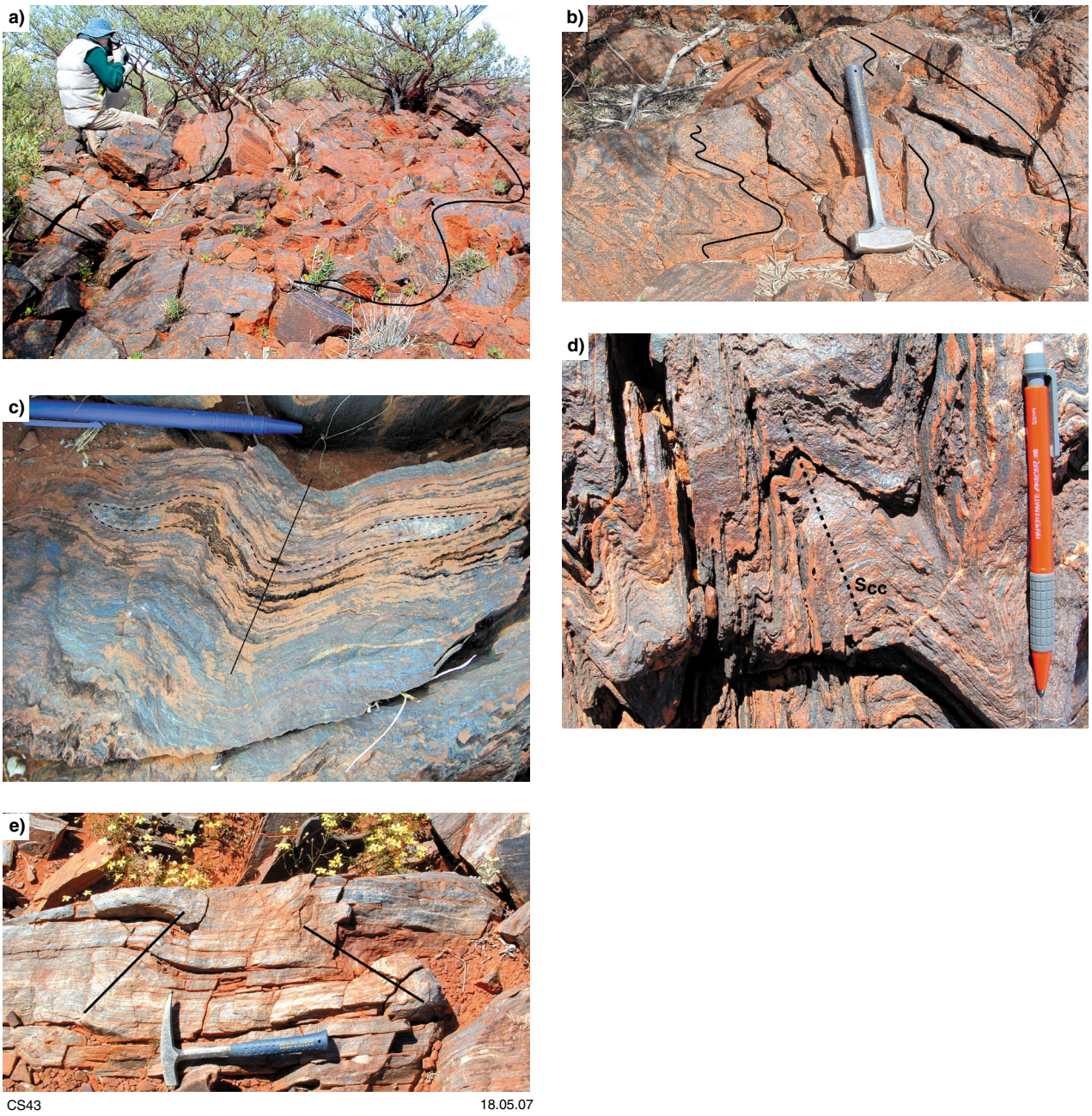

Figure 25. Fold relationships in BIF: a) recumbent fold preserved in BIF in the northeast of the main belt (see Fig. 21 for location, WP 366, MGA 542997E 7118630N); b) close-up of folded banding in recumbent fold in (a), showing parasitic folds with chevron form; c) refolded layer-parallel isoclinal fold in BIF, annotated with dashed line for clarity. The solid line denotes the axial-planar crenulation cleavage of second-generation folds. Photograph taken in the central area (Plate 3); d) the main foliation (S_m) is a crenulation cleavage (S_{cc}) in BIF, axial planar to typical chevron folds throughout the belt. This is the same cleavage as that shown in (c) by the solid line. These folds are interpreted as refolds of the recumbent folds in (a) and (b). Same locality as (c); e) conjuegate kink folds in BIF and chert, folding the main foliation (S_m). The axial planes are annotated for clarity. Photograph taken in the west-central area (Plate 4)

particularly evident in some quartzites, granitic rocks, and gneiss along the Cargarah Shear Zone. The strike-parallel shears sometimes show evidence of reactivation, marked by brittle or semibrittle structures such as reidel shears, shear bands, and local kink or drag folds. Some strike-parallel faults may also be younger faults that post-date the main phase of shearing. This has produced a complicated network of linked fault lenses throughout much of the belt.

The Cargarah Shear Zone is locally marked by mylonites. These are particularly well developed in the western part of the belt within gneiss and granitic rocks, where they contain feldspar porphyroclasts and S–C foliations indicative of dextral kinematics (Fig. 27a,b). Where the shear zone cuts the belt in the central region, BIF and quartzite lenses are boudinaged up to scales of tens of metres, and mafic and pelitic schists typically

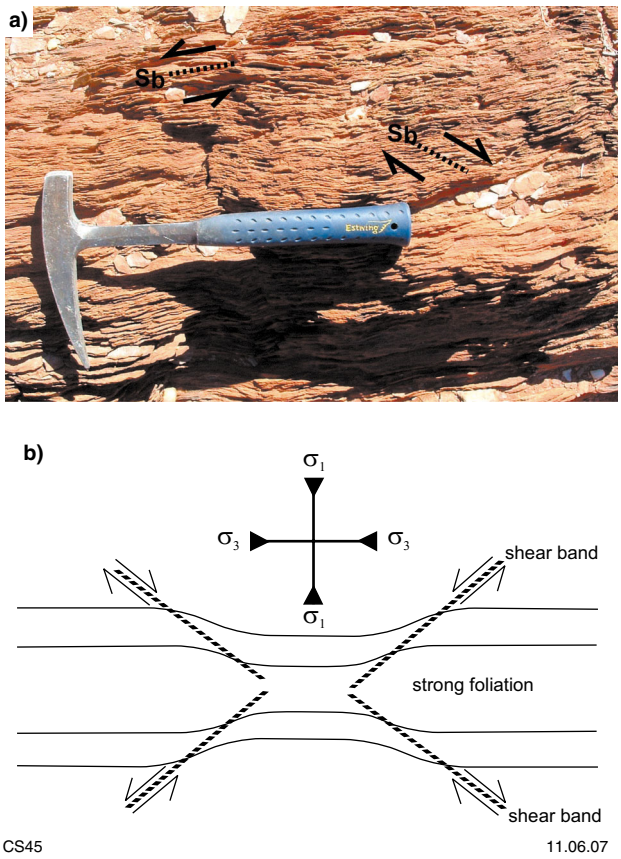

Figure 26. Low-angle conjugate shear bands (S_b): a) in quartz–mica schist in the east-central area (Plate 2); b) diagram showing the formation of low-angle shear bands in mylonitic rocks that show both sinistral and dextral shear sense. The shear bands are conjugates produced by flattening (after McClay, 1987)

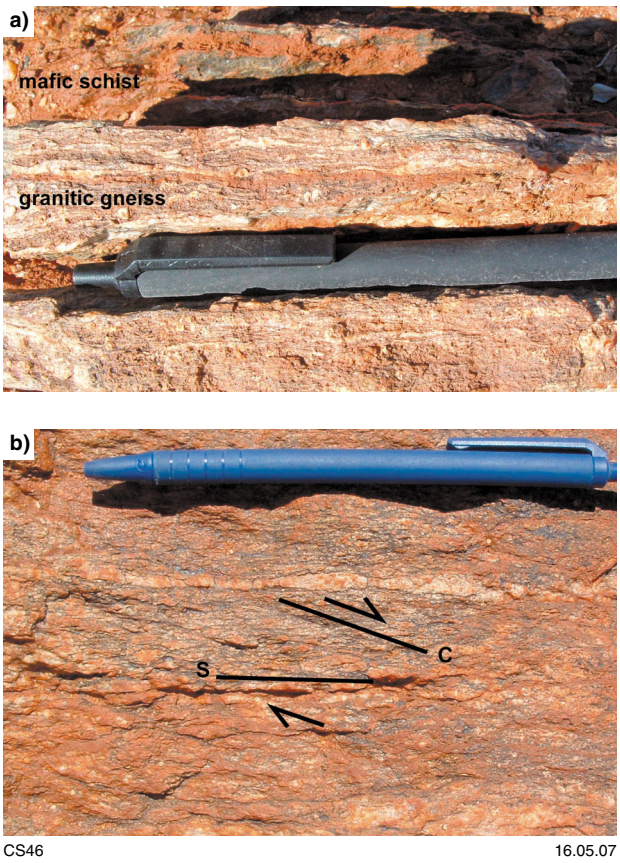

Figure 27. Mylonitic granitic gneiss and S–C foliations: a) mylonitic mafic schist and granitic gneiss in the Cargarah Shear Zone, west of the main belt in the Milly Milly area (see Fig. 19 for location); b) mylonitic granitic gneiss with dextral S–C foliations, from the Cargarah Shear Zone, near (a)

contain dextral S–C foliations (Plate 3). In this area the mature clastic rocks are boudinaged, mylonitic, and pinch out within the mafic and pelitic and semipelitic schists (Fig. 22b). A gap in the BIF and quartzite lenses suggests that they have been pulled apart by the shearing. Competent ridge outcrops of the BIF and quartzite disappear along strike for about 1 km, coinciding with breaks in the magnetic highs formed by the BIFs (Fig. 20, edge of belt on left). This is also the narrowest section of the entire belt. To the east, in the east-central area, the shear zone cuts through gneiss and granitic rocks, and the belt to the northeast is part of a fault splay (Plate 2). Large-scale boudinage is still evident along the southern part of the belt here (e.g. in the ultramafic rocks), but the strain is more variable towards the northern side of the belt.

The Cargarah Shear Zone is interpreted as a dextral shear zone because it is dominated by dextral kinematic indicators such as S–C foliations, asymmetric pebbles, and porphyroclasts, and because of its dextral sigmoidal geometry. These features, and the presence of low-angle conjugate shear bands (Fig. 26), indicate both a rotational and a flattening component during shearing that is interpreted to be related to transpression. Flattened pebbles in metaconglomerate are commonly found where shearing is intense, suggesting that they mainly formed because of the shearing rather than folding. Major folds throughout the belt are typically cut by shears. These either formed in relation to the transpressional shearing or pre-date it, or both. The presence of a strong rodding lineation (l-fabric), particularly in some quartzite and granitic gneiss outcrops, indicates variable strain conditions at scales of several metres. This suggests that some lithologies were preferentially flattened and squeezed horizontally (s-fabric, e.g. metaconglomerate, Fig. 25c; quartz–mica schist with low-angle shear bands, Fig. 26a), whereas others were stretched with little or no flattening component. The strain within the belt can therefore be characterized as having elements of both apparent flattening and apparent constriction (after Ramsay and Huber, 1983). The presence of large-scale boudinage in the central part of the belt also indicates a major stretching component along the length of the belt, and a flattening component perpendicular or oblique to it.

Late-stage faults

Late-stage brittle faults and shears that overprint the major shearing are particularly evident in granitic rocks and gneiss to the south, and also cut the belt at high angles along its length (Fig. 23b). There are several northwest-trending, steeply dipping brittle faults that show dextral displacement, some of which are coincident with large quartz veins (e.g. Plate 3). Northeasterly trending faults may be conjugate structures. There is no evidence to suggest displacements of more than a few hundred metres on any of these late-stage faults. Small-scale, semibrittle east-trending shears and faults are also common.

Summary of map areas

Northeastern area — Plate 1

The northeastern area (Plate 1), from northwest to southeast, consists of folded BIF and chert with some ultramafic rocks, strongly deformed quartzite and quartz–mica schist, variably deformed black and white banded quartzite, and a unit of folded metasandstone, quartzite, and quartz–mica schist. The latter is interpreted to be Proterozoic. Because the exact locality of the sample containing Proterozoic detrital zircons (JH4, Dunn et al., 2005) was unknown at the time of mapping, it is not clear whether it is from an isolated infaulted sequence similar to that in the west-central area (Plate 4) or representative of the metasandstone and quartzite unit mapped in this area. However, given that no separate units were distinguishable in this section in the field, it is mapped as Proterozoic. The contact between the BIF and chert unit and granitic gneiss to the northwest is a steeply northwest-dipping fault. The BIF and chert outcrop as high strike ridges that are cut by narrow gullies that 'vee' downstream, highlighting the steep northwesterly dips of the main foliation and faulted contact. The Proterozoic rocks to the southeast are flanked by a thin lens of mafic schist, which in turn is adjacent to strongly deformed BIF and chert. It is not clear how far the BIF and chert extend to the east because outcrop is poor, but the aeromagnetic data indicate that the contact with granitic gneiss is nearby. The Proterozoic rocks taper out to the north and are truncated by BIF and chert. The strain throughout the area covered by this map is generally lower than in other areas mapped, although there are localized high-strain zones, particularly in the BIF on the northwestern side, near the contact with the granitic gneiss.

The faulted contact between the BIF and chert unit and the quartzite and quartz–mica schist shows evidence of late-stage brittle behaviour with sinistral displacement inferred from reidel shears (Fig. 28a). These are probably reactivation structures that post-date the main phase of ductile shearing across the belt. A major strike-parallel fault in the central part of the northeastern area that separates the black and white banded ferruginous psammite unit from Proterozoic metasandstone, quartzite, and quartz–mica schist has S–C foliations indicative of normal fault sense, with the northwest side (Proterozoic rocks) down. Where exposed the fault has a steep northwest dip (~80–85°). Because of this it is difficult to determine if it initially formed as a normal fault because it may have been rotated from a vertical or steep southeast dip. It may also anastomose or change dip at depth. The fault cuts folds in the Proterozoic rocks and is overprinted by brittle structures such as small-scale faults with intense veining, and fault breccia. The same S–C kinematics have also been observed in adjacent parallel faults within the black and white banded ferruginous psammite, and in localized sheared outcrops nearby (Fig. 28b).

East-central area — Plate 2

The east-central area (Plate 2), from northwest to southeast, consists of folded BIF and chert, a wide zone of steeply dipping, mafic, ultramafic, pelitic, and semipelitic schist that make up most of the central part of the belt in this area, a strike ridge of strongly deformed quartzite near the northwestern edge of the central zone, and a strongly deformed zone of mafic and ultramafic rocks, pelitic schist, quartzite, chert, and BIF adjacent to the southern contact with the gneiss and granitic rocks. This contact is parallel to, and forms part of, the Cargarah Shear Zone. It is where the main part of the shear zone leaves the belt and cuts through granitic rocks to the east (Figs 3 and 18). The contact has a steep northerly dip that becomes vertical to the west, where the strain is very high. There, the BIF and chert pinch out and the unit is tectonically thinned. Lenses of ultramafic rocks along the eastern part of this contact are strongly boudinaged, indicating a high degree of stretching during shearing in this area.

S–C foliations locally developed in the southern part of the map area, including the southern part of the central zone, indicate dextral kinematics. Low-angle conjugate shear bands are common, particularly in quartz–mica schist and are interpreted to indicate flattening (Fig. 26; McClay, 1987). Zones of mylonite are also common, right across this section of the belt. Granitic rocks and gneiss close to the contact on the southern margin are also locally mylonitic, and have dextral S–C foliations (Fig. 29).

Central area — Plate 3

The central area (Plate 3), from north to south, consists of boudinaged strike ridges of strongly deformed BIF, chert, and quartzite; a wide central zone of strongly deformed mafic and semipelitic schist; and strike ridges of predominantly mafic and ultramafic rocks along the southern contact with gneiss and granitic rocks. This part of the belt is coincident with the Cargarah Shear Zone, is steeply dipping, and dominated by high-strain, boudinage, tight to isoclinal folds, and predominantly dextral S–C foliations. Mylonite is locally developed, particularly in BIF, chert, and quartzite on the northern margin. The mineral lineation plunges shallowly to moderately, either to the east or west. The main foliation is locally folded by northeast-trending upright folds. In the western part of the area, strike ridges of strongly deformed, locally mylonitic mature clastic rocks, BIF, and chert pinch out within the narrowest part of the belt. This is interpreted to have been caused by stretching during shearing. Late-stage, northwest-and northeast-trending, steeply dipping brittle

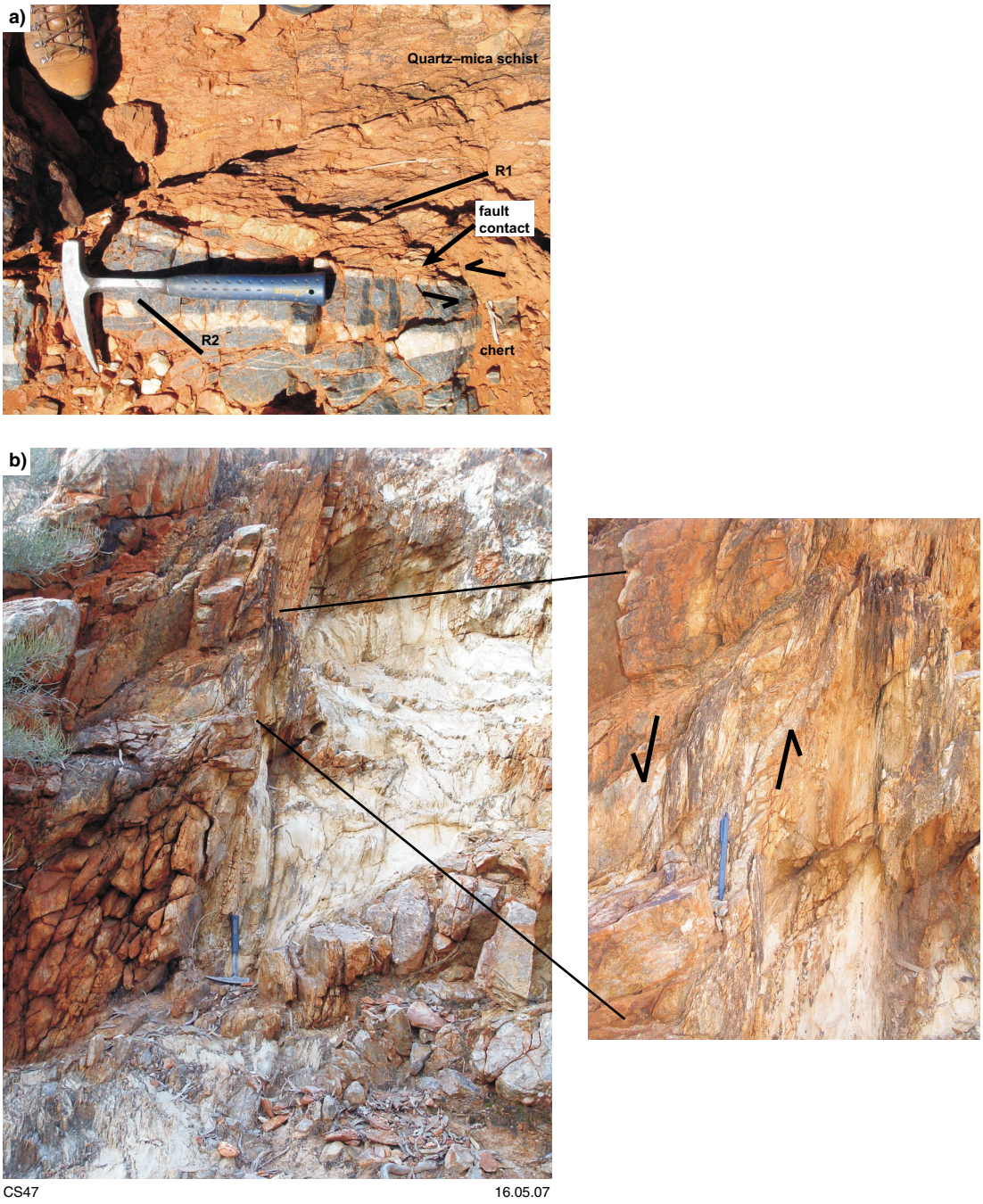

Figure 28. Semibrittle faults in the northeastern area: a) interpreted reidel shears indicating sinistral movement sense on the brittle fault contact between quartz–mica schist and chert in the northeastern area (Plate 1; WP 128, MGA 527428E 7120113N); b) fault within black and white banded quartzite in the northeastern area (Plate 1; sample CS0394, MGA 529000E 7118920N). The main break is in line with the hammer, and strongly foliated and disrupted rocks outcrop on either side of it for several metres.The fault has both ductile and brittle characteristics and has most probably been reactivated. Inset shows detail of fault lozenges in the immediate hangingwall, with top (northeast side) down asymmetry

CS48 16.05.07

Figure 29. Dextral S–C foliations in mylonitic gneiss from the southern margin of the belt, in the east-central area (Plate 2)

faults that cut the margins of the belt have an average displacement of about 100 m, but displacements up to 1 km are present.

Near the southern margin of the belt, in the eastern part of the area, rafts of gneiss are preserved in monzogranite and pegmatite (e.g. WP 133, MGA 507382E 7105831N). Relatively undeformed domes and tors of monzogranite flank the Cue–Beringarra road, but towards the southern contact the granite and pegmatite are strongly deformed and sheared. The contact with mafic and ultramafic rocks is a steeply dipping shear zone with complex small-scale folds and both sinistral and dextral kinematic indicators. Stretched lenses of BIF and chert outcrop within mafic and ultramafic rocks near the contact.

West-central area — Plate 4

The west-central area (Plate 4) is adjacent to the central area (Plate 3) and contains the majority of outcrop of the mature clastic association. The unit is folded into tight southwest-plunging folds that are inclined towards the south. It is fault-bound by lenses of Proterozoic rocks, BIF, chert, and quartzite to the south, and mafic, pelitic and semipelitic schists to the north. An intrusion of late Archean monzogranite, known as the Blob, outcrops to the southwest, but the nature of its contact with the mature clastic rocks is not clear. The granite contains lenses or rafts of metasedimentary rocks, but it is not clear which unit these belong to. The intrusive relationship of the granite to BIF and chert, and quartz–mica schist on the eastern side of the granite, is evident (Fig. 15a), but the mature clastic rocks, which overlie the quartz–mica schist in this area, may be in faulted contact or unconformable or both. The granite is predominantly weakly foliated, but sheared and locally folded on its margins (Fig. 30). The folding may have been related to the shearing. The shears and strong foliation wrap around the granite, much like a large-scale porphyroclast. Strongly deformed, steeply dipping, mafic, pelitic and semipelitic schists outcrop to the north of the granite. Banded iron-formation, chert, and quartzite strike ridges and lenses of mafic and ultramafic rocks define the northern margin of the belt in this area, and are intruded by muscovite granite. The granite also intrudes granitic gneiss along the margin (e.g. WP 439, MGA 495880E 7106770N).

The Cargarah Shear Zone cuts through gneiss and granitic rocks north of the belt in this area, and is locally marked by mylonites, small-scale isoclinal folding, and large quartz veins. In this area the belt is part of the southwestern fault splay off the shear zone, and links to the shear zone in the central area (Plate 3). Mylonitization increases to the east, but local high-strain zones with predominantly dextral S–C foliations are common throughout. Small late-stage brittle faults cut all rocks, including the Proterozoic rocks.

The southern contact of the mature clastic rocks is complex, and is folded and faulted with BIF, chert, and quartzite. Two fault-bound lenses of Proterozoic quartz–mica schist and quartzite are mostly mylonitic and contain slivers of ultramafic schist (e.g. WP 375, MGA 497464E 7105183N). Near the W74 outcrop (Fig. 5) the faulted contact between the mature clastic rocks and the Proterozoic unit shows evidence of late-stage, brittle or semibrittle movement, such as a sharp irregular contact, small duplexes that suggest sinistral displacement, and quartz veins (Fig. 16b). This fault may be either a reactivated structure or a late structure formed after the main phase of shearing. In the west-central area the southern margin of the belt is a steeply dipping sheared contact between BIF and granitic rocks and gneiss. Mylonite zones are exposed locally within granitic rocks and gneiss parallel to the belt. The BIF is internally folded with tight to isoclinal, mostly second-generation folds, which are locally refolded into tight folds, parallel to the trend of the belt (e.g. just north of WP 384, MGA 496838E 7106498N, and WP 292, MGA 496474E 7105003N).

CS49 16.05.07

Figure 30. Granite lens within quartz–mica schist near the margin of the main granite body known as the Blob, from the west-central area (Plate 4). Both the granite and quartz–mica schist are sheared, therefore shearing occurred after the granite intrusion

Southwestern area — Plate 5

The southwestern area (Plate 5) consists of ultramafic and mafic schists, interlayered with BIF, chert, and quartzite, and a minor component of pelitic and semipelitic schist. These are intruded by muscovite granite and pegmatite that contain a weak to moderate foliation that can be traced into all adjacent units. However, the muscovite granite and pegmatite do not appear to be folded in the same manner as the adjacent units, and folding in the latter is interpreted as having occurred prior to granite intrusion. Folded BIF, chert, and quartzite are truncated by muscovite granite and pegmatite, producing an irregular intrusive map pattern (e.g. near and southwest of WP 262, MGA 491266E 7103376N). The BIF, chert, and quartzite also contain an early foliation or banding, or both (overprinted by S_m), that is mostly steeply dipping, but is locally subhorizontal in fold hinges (see stereonets on Plate 5). Much of this early foliation has been reoriented by subsequent shearing.

The northwestern margin of the belt in this area consists of mafic and ultramafic schists in faulted contact with gneiss and granitic rocks. The fault has a steep northwest dip. Gneissic layering in the granitic gneiss is subparallel to, and overprinted by, a lower grade anastomosing foliation (S_m), also present in all other units in this area. The southern margin is not exposed in this area, but is interpreted as a faulted contact between BIF and gneiss and granitic rocks, similar to that in the west-central area (Plate 4). BIF, chert, quartzite, and mafic and ultramafic schists are tightly folded into south- to southwest-plunging folds in the southeastern part of the map area. These are cut by small east-trending shears, possibly related to the main phase of shearing or to intrusion of east-trending dykes. A distinctive strike ridge of strongly deformed banded quartzite outcrops along the central part of the belt. It is locally mylonitic, contains dextral S–C foliations, and is interpreted as a major steeply northwest-dipping fault.

^{40}Ar–^{39}Ar geochronology

Thirteen samples were dated using both infrared and UV-laser techniques. Four of these samples are presented in this Record, and the others are documented in Spaggiari et al. (in prep.). Eleven of the samples were white micas from quartz–mica and andalusite schists, sheared pegmatite, granite, and granitic gneiss. The other two samples were biotite from sheared granite and hornblende from mafic schist. The primary aim was to try to constrain the age of the main deformation related to shearing and formation of the Cargarah Shear Zone by determining the cooling ages from the sheared rocks. Most of the samples were chosen from sheared rocks that appeared to be completely recrystallized and contained only shear-related foliations that included fresh white mica or biotite. Others, such as the pegmatitic rocks and granitic gneiss, were chosen to see if any older or younger cooling ages were preserved, or whether the belt cooled uniformly. The samples were chosen to cover most areas of the belt, including the Milly Milly area (Fig. 3). The mafic schist was chosen because hornblende from the rock had given an old age of 3248 ± 64 Ma by the K-Ar method (see **Sample descriptions** below), and using the ^{40}Ar–^{39}Ar method would allow a comparison of results. The different techniques were chosen primarily primarily based on material type, for example grain size and mineralogy. Where possible, in situ UV-laser dating was undertaken on thick sections of schist to target the micas in the main shear-related foliation. Using different techniques also allowed some cross-checking of results.

Sample descriptions

Sample CS-491 (GSWA 184303) is from a sliver of mafic schist within gneiss from the western end of the Cargarah Shear Zone, in the Milly Milly area (Fig. 19). The sample was collected by H. Zwingman (CSIRO Petroleum Resources) for K–Ar dating of hornblende within about 100 m of site CS0309 (lower left in Fig. 19, WP 11, MGA 474180E 7103939N). The K–Ar dating gave an age of 3248 ± 64 Ma (Zwingman, H., 2004,written comm,). The rock consists of hornblende, plagioclase, biotite, Fe-oxide, minor chlorite, and quartz (Fig. 31a). The hornblende is pleochroic from yellow to blue-green and has grown in aggregates, most probaby replacing pyroxene. It is partially chloritized. Biotite is locally present along cleavage planes within hornblende, and also as small grains throughout. Plagioclase laths are about 1 mm long and have an interlocking texture with relict grains that were probably pyroxene. The protolith is interpreted as a dolerite that was probably a dyke within the granitic gneiss. Six grains of hornblende from the sample were dated using the infrared laser step-heating technique (Appendix 1). The average grain size was 300 × 150 μm, the largest was 370 × 240 μm, and the smallest was 170 × 160 μm.

Sample CS0416 (GSWA 184301) is from foliated muscovite granite in the southwestern area (Plate 5; 30 m north of MGA 491092E 7103606N). The sample consists of quartz and twinned feldspar with an interlocking texture, and interstitial muscovite (Fig. 15c). Muscovite grains range from approximately 100 μm to 1 cm (Fig. 31b). The foliation is defined by zones of recrystallized feldspar and quartz that have undergone grain-size reduction, and aligned white mica. Some feldspar crystals have brittle microfaults with small offsets (Fig. 14d). A muscovite flake from the sample was dated using the infrared laser step-heating technique (Appendix 1).

Sample CS0341 (GSWA 184302) is a sheared granite from the contact with mafic and ultramafic schist on the southern margin of the central part of the belt (Plate 3; MGA 503737E 7105724N). The granite contains a strong foliation defined by quartz and biotite (Fig. 31c). Relict grains of K-feldspar are locally preserved. Laths of K-feldspar aligned perpendicular to the foliation are kinked, indicative of shortening. Biotite laths have an average length of 500 μm, and are mostly fresh, although some show minor chloritization. Quartz is elongate and exhibits undulose extinction, but, like most samples in the Jack Hills area, shows some evidence of recovery such as straight grain boundaries and foam-structure texture. Two biotite grains from separates of the sample were dated using the infrared laser step-heating technique (Appendix 1).

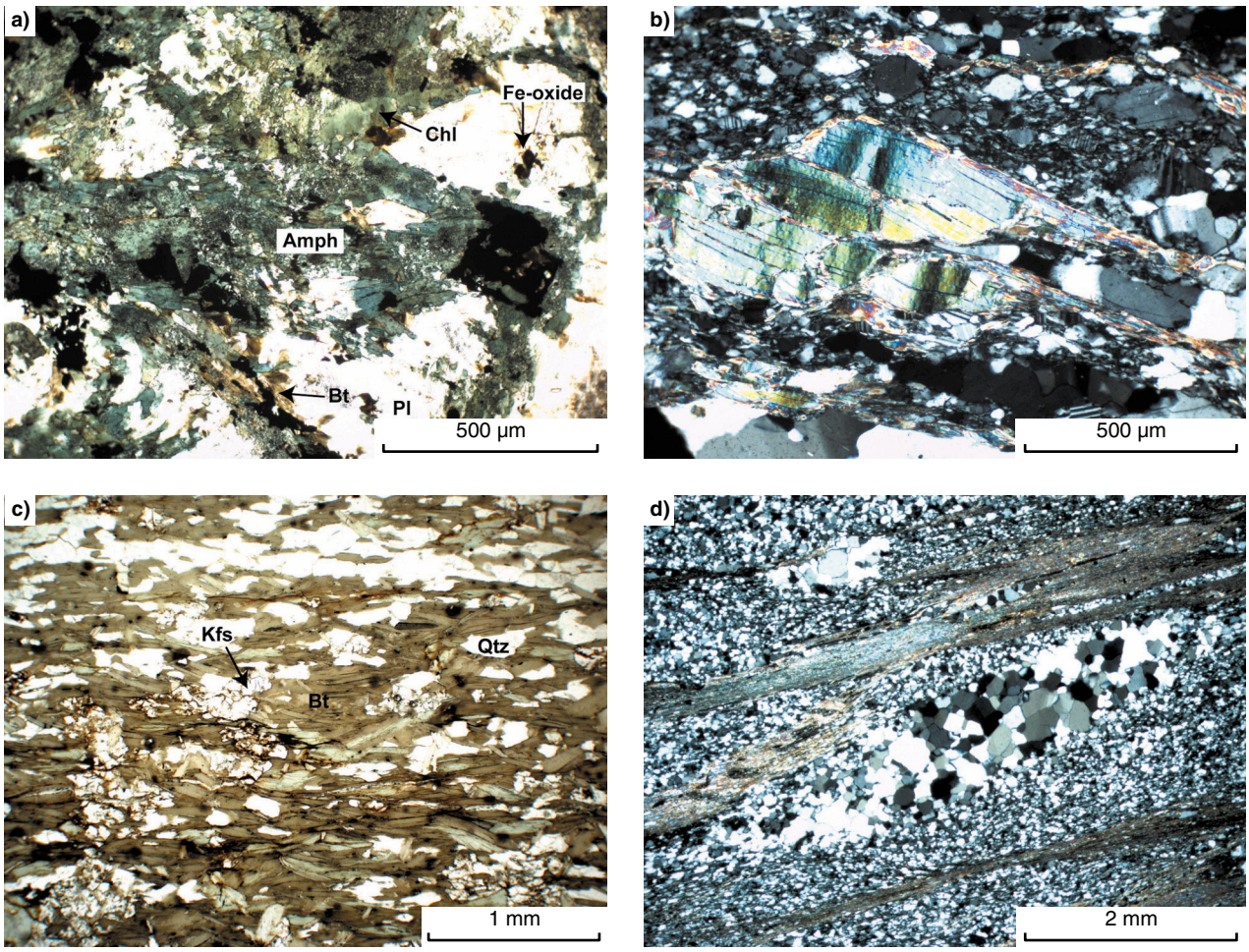

Figure 31. Samples dated by the ^{40}Ar–^{39}Ar method:
a) mafic schist (plane-polarized light) showing hornblende (Amph) growing in clusters, most probably replacing pyroxene (large mass in centre of photo). Small biotite (Bt) grains occur throughout. Other phases shown are plagioclase (Pl), Fe-oxide, and chlorite (Chl). Sample CS-491, from the Milly Milly area (see Figs 3 and 19 and text for location);
b) sample CS0416, showing typical muscovite grain similar to that dated. The muscovite is kinked, and shows evidence of new smaller grain growth parallel to the foliation on the right-hand side of the grain (southwest area, Plate 5; MGA 491092E 7103606N; cross-polarized light);
c) sheared granite (biotite schist) from the central area (Plate 3). The strong foliation is defined by biotite (Bt) and quartz (Qtz). Relict K-feldspar (Kfs) occurs throughout (sample CS0431, MGA 503737E 7105724N; plane-polarized light);
d) quartz–mica schist from the northeastern area (Plate 1). The strong mica fabric was targeted with in situ dating by the UV-laser technique (sample CS0395, MGA 529034E 7118818N; cross-polarized light)

Sample CS0395 (GSWA 184306) is from tectonically disrupted quartzite and quartz–mica schist adjacent to a major fault in the northeastern area (Plate 1; MGA 529034E 7118818N). The outcrop was described in **Proterozoic metasedimentary rocks** (near WP 318, MGA 529034E 7118818N, see also Fig. 16e). The sample is quartz rich, with elongate aggregates of quartz up to up to 1 to 2 cm, wrapped by a micaceous foliation (Fig. 31d). Andalusite forms small porphyroblasts and is also wrapped by the foliation. Foliation-forming white mica was dated in situ from a thick section (~200 µm), using the UV-laser spot analysis technique (Appendix 1).

Results

Infrared laser step-heated samples

The six hornblende grains from sample CS-491 produced complex results and a disturbed spectrum (Fig. 32, Table 2). The first six steps produced apparent ages between c. 2052 and 1932 Ma, and yielded a plateau age of 2041 ± 4 Ma (1σ, mean squares of deviates (MSWD) = 2.0) for steps 3–6 with 64.2% of the total ^{39}Ar. The remaining six steps yielded apparent ages that increase gradually to the highest temperature age of

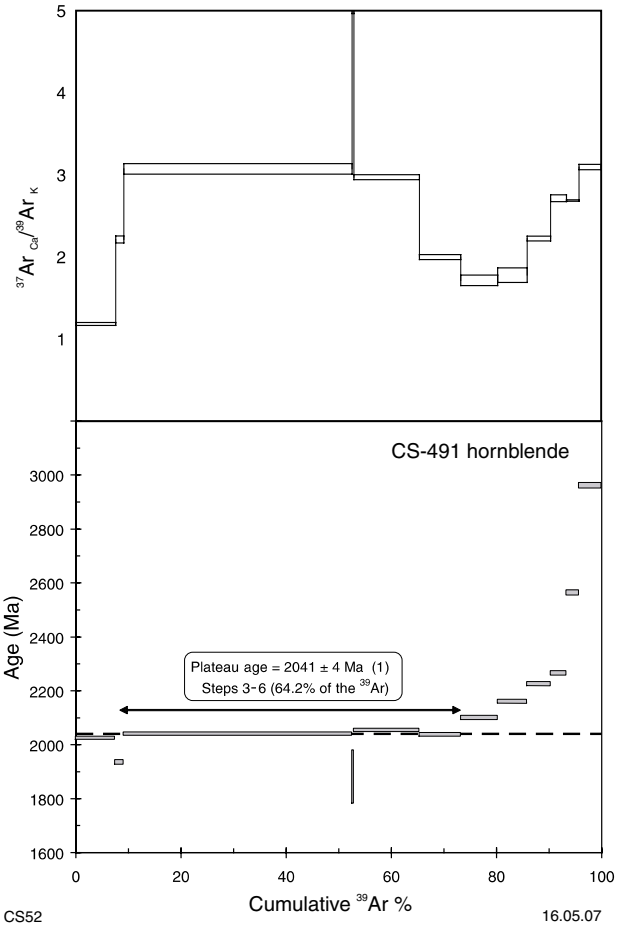

Figure 32. Sample CS-491 (hornblende) ^{40}Ar–^{39}Ar age spectrum and $^{37}Ar_{Ca}$–$^{39}Ar_K$ versus cumulative ^{39}Ar % plot. Individual errors area 1σ (denoted by box height on the age spectrum)

2961.4 ± 10.4 Ma (1σ). Step 4 (1878.76 ± 99.55 Ma) has a large uncertainty reflecting the low amount of gas released.

The complexity in the data may be due, in part, to biotite partially overgrowing cleavage planes in hornblende, in which case the apparent ages would reflect a mixture of two phases of different age. Because biotite and hornblende have different closure temperatures (i.e., ~300 ± 50°C for biotite: Harrison, 1981; and ~500 ± 50°C for hornblende: Harrison, 1981) the phases would have retained different ages if they were not cooled rapidly (McDougall and Harrison, 1999). The progressive increase in apparent ages produced by the step-heating process is reflected by younger ages from the rims (heated first), and older ages from the cores. However, this may also be an artefact caused by phase changes occurring during the step-heating process (e.g. Kuiper, 2002). Excess ^{40}Ar may also be a contributing factor to the complexity of the results, although excess ^{40}Ar in hornblende typically yields U-shaped age spectra (e.g. Wartho et al., 1996).

Muscovite from sample CS0416 produced apparent ages between c. 1837 and 1776 Ma (Fig. 33, Table 2). Even though the spread of apparent ages is less than for CS-491, the spectrum is disturbed and does not define a plateau. This is most likely due to partial resetting within different domains of the muscovite grain. However, excluding the youngest age in step 1, a weighted mean of steps 2–10 yielded an age of 1827.7 ± 5.8 Ma (95% confidence, MSWD = 13). The lack of an age plateau may be due to the presence of multiple phases, as steps 5 and 6 contain higher $^{37}Ar_{Ca}/^{39}Ar_K$ ratios, indicating the possible degassing of a calcium-bearing phase (Fig. 33). The muscovite is interpreted to have cooled through its argon closure temperature (i.e., 300–420°C; Lister and Baldwin, 1996) by 1827.7 ± 5.8 Ma (95% confidence).

Two biotite grains from sample CS0431 produced variable ages between c. 1869 and 1805 Ma (Fig. 34, Table 2). Grain 1 yielded a plateau age of 1817.8 ± 3.3 Ma (1σ, MSWD = 0.76) for steps 2–6, representing 79.1% of the ^{39}Ar gas released (Fig. 34a). The uncertainty on step 6 is large because of the small amount of gas released as only a small portion of the grain remained for this step. The age spectrum for grain 2 defined a plateau age of 1814.3 ± 3.5 Ma (1σ, MSWD = 2.2) for steps 2–4, representing 92% of the ^{39}Ar released (Fig. 34b), which is within error of the plateau age from grain 1 (Fig. 34c). These biotite grains are interpreted to have cooled through the biotite argon closure temperature of 300 ± 50°C (Harrison, 1985) by 1817.8 – 1814.3 Ma.

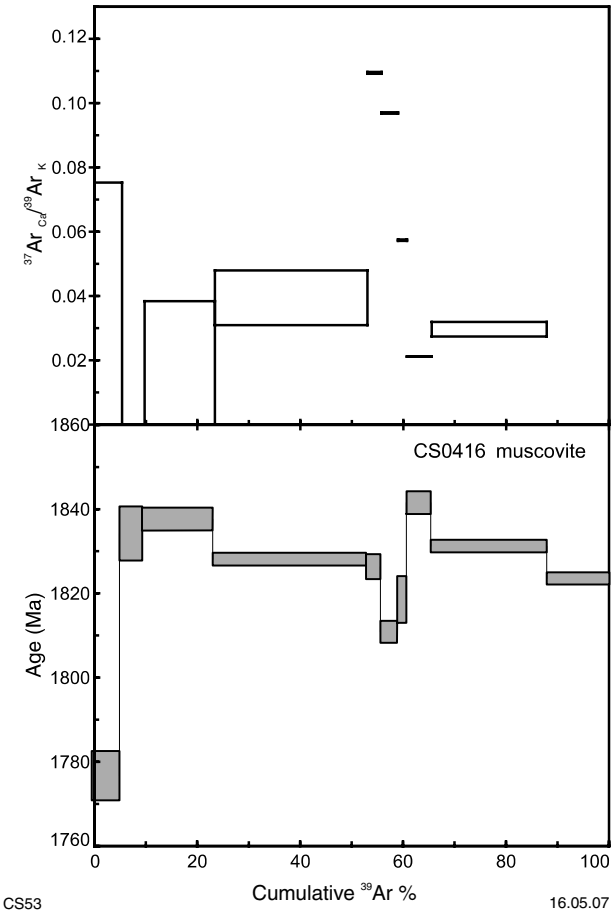

Figure 33. Sample CS0416 (muscovite) ^{40}Ar–^{39}Ar age spectrum and $^{37}Ar_{Ca}$–$^{39}Ar_K$ versus cumulative ^{39}Ar % plot. Individual errors are 1σ (denoted by box height on age spectrum)

Table 2. ^{40}Ar–^{39}Ar data for four samples (CS-491, CS0416, CS0431, and CS0395) from the Jack Hills greenstone belt

Analysis no.	*Age (Ma)*	±	$^{40}Ar^*/^{39}Ar$	±	$^{40}Ar/^{39}Ar$	±	$^{38}Ar/^{39}Ar$	±	$^{37}Ar/^{39}Ar$	±	$^{36}Ar/^{39}Ar$	±	$^{36}Ar/^{40}Ar$	±	^{39}Ar (cm^3)	±	*Cumulative % ^{39}Ar*
CS491 hornblende; six grains, IR laser																	
1	2021.7	6.4	97.49	0.16	99.58	0.16	0.01427	0.00079	1.18350	0.01816	0.00708	0.00001	0.00007	0.00000	6.41E-12	1.03E-14	7.55
2	1932.0	8.7	90.47	0.49	92.61	0.50	0.02256	0.00390	2.21432	0.04158	0.00724	0.00004	0.00008	0.00000	1.30E-12	6.97E-15	9.08
3	2036.6	6.5	98.68	0.18	99.54	0.17	0.01649	0.00017	3.07417	0.06492	0.00288	0.00020	0.00003	0.00000	3.69E-11	4.74E-14	52.60
4	1878.8	99.5	86.47	7.36	104.01	1.52	0.03129	0.01840	7.59965	2.63481	0.05937	0.02454	0.00057	0.00024	2.76E-13	3.78E-15	52.93
5	2051.0	6.8	99.86	0.25	100.76	0.23	0.01728	0.00004	2.97223	0.03018	0.00308	0.00032	0.00003	0.00000	1.06E-11	2.39E-14	65.40
6	2034.3	7.4	98.50	0.34	99.54	0.31	0.01696	0.00005	1.99922	0.03152	0.00352	0.00050	0.00004	0.00001	6.71E-12	2.06E-14	73.31
7	2097.8	7.6	103.72	0.36	104.35	0.26	0.01563	0.00004	1.71616	0.06355	0.00211	0.00085	0.00002	0.00001	5.96E-12	1.44E-14	80.34
8	2158.3	7.5	108.87	0.35	108.87	0.14	0.01525	0.00002	1.77891	0.08820	0.00000	0.00000	0.00000	0.00000	4.75E-12	6.09E-15	85.93
9	2222.8	8.1	114.54	0.45	115.57	0.43	0.01645	0.00090	2.22532	0.02873	0.00346	0.00045	0.00003	0.00000	3.78E-12	1.39E-14	90.38
10	2262.6	7.3	118.16	0.31	118.93	0.24	0.01216	0.00187	2.71554	0.04104	0.00262	0.00066	0.00002	0.00001	2.55E-12	4.78E-15	93.39
11	2562.7	9.6	148.07	0.73	148.83	0.55	0.01498	0.00163	2.68722	0.00980	0.00258	0.00163	0.00002	0.00001	2.07E-12	7.56E-15	95.84
12	2961.4	10.4	196.37	1.00	198.11	0.97	0.01562	0.00096	3.09503	0.03310	0.00591	0.00096	0.00003	0.00000	3.53E-12	1.72E-14	100.00
1 sigma (1σ) errors																	
J value = 0.021200 ± 0.000106																	
Irradiation standard used = Tinto B biotite (409.24 ± 0.71 Ma)																	
CS0416 muscovite; IR laser																	
1	1776.6	8.2	79.03	0.41	79.38	0.22	0.01233	0.00106	0.00950	0.06579	0.00118	0.00118	0.00001	0.00001	5.73E-12	1.59E-14	5.34
2	1834.1	8.6	83.12	0.46	83.33	0.19	0.01278	0.00107	0.00000	0.00000	0.00072	0.00143	0.00001	0.00002	4.72E-12	1.08E-14	9.74
3	1837.5	6.4	83.37	0.20	83.47	0.10	0.01246	0.00033	0.01857	0.01980	0.00034	0.00058	0.00000	0.00001	1.47E-11	1.69E-14	23.41
4	1827.9	5.9	82.68	0.11	82.75	0.07	0.01194	0.00015	0.03945	0.00849	0.00026	0.00027	0.00000	0.00000	3.18E-11	2.57E-14	53.03
5	1826.2	6.4	82.55	0.21	82.55	0.21	0.01153	0.00113	0.10938	0.00028	0.00000	0.00000	0.00000	0.00000	2.99E-12	7.56E-15	55.81
6	1810.7	6.3	81.44	0.18	81.44	0.18	0.01225	0.00100	0.09689	0.00022	0.00000	0.00000	0.00000	0.00000	3.38E-12	7.56E-15	58.96
7	1818.4	8.0	81.99	0.40	82.77	0.30	0.01449	0.00005	0.05736	0.00021	0.00265	0.00089	0.00003	0.00001	1.90E-12	6.97E-15	60.74
8	1841.4	6.4	83.65	0.19	83.74	0.17	0.01270	0.00003	0.02117	0.00004	0.00032	0.00033	0.00000	0.00000	5.16E-12	1.03E-14	65.54
9	1831.1	5.9	82.90	0.10	82.98	0.10	0.01331	0.00016	0.02964	0.00226	0.00027	0.00014	0.00000	0.00000	2.40E-11	2.73E-14	87.88
10	1823.4	5.9	82.35	0.10	82.35	0.07	0.01286	0.00013	0.00000	0.00000	0.00000	0.00000	0.00000	0.00000	1.30E-11	1.07E-14	100.00
1 sigma (1σ) errors																	
J value = 0.021221 ± 0.000106																	
Irradiation standard used = Tinto B biotite (409.24 ± 0.71 Ma)																	
CS0431 biotite; IR laser																	
Grain 1																	
1	1869.2	6.3	85.72	0.18	85.72	0.15	0.01187	0.00030	0.00000	0.00000	0.00000	0.00000	0.00000	0.00000	5.67E-12	1.01E-14	6.51
2	1813.5	6.4	81.68	0.20	81.68	0.17	0.00888	0.00035	0.00000	0.00000	0.00000	0.00000	0.00000	0.00000	4.85E-12	1.01E-14	12.08
3	1818.2	6.6	82.02	0.23	82.01	0.23	0.01058	0.00003	0.06197	0.03067	0.00000	0.00000	0.00000	0.00000	3.59E-12	1.01E-14	16.20
4	1813.9	6.1	81.71	0.16	81.71	0.16	0.01203	0.00002	0.03144	0.01037	0.00000	0.00000	0.00000	0.00000	1.06E-11	2.03E-14	28.38
5	1827.5	7.3	82.69	0.32	82.68	0.32	0.01404	0.00005	0.07550	0.02491	0.00000	0.00000	0.00000	0.00000	2.21E-12	8.45E-15	30.92
6	1841.8	38.9	83.72	2.79	83.72	2.79	0.00000	0.00000	0.00000	0.00000	0.00000	0.00000	0.00000	0.00000	1.83E-13	6.09E-15	31.13
Grain 2																	
2-1	1805.8	5.9	81.13	0.11	81.13	0.11	0.01298	0.00071	0.00000	0.00000	0.00000	0.00000	0.00000	0.00000	4.78E-12	6.09E-15	36.62
2-2	1813.9	5.9	81.71	0.09	81.71	0.09	0.01297	0.00019	0.00000	0.00000	0.00000	0.00000	0.00000	0.00000	2.47E-11	2.75E-14	65.03
2-3	1806.6	5.7	81.19	0.05	81.19	0.05	0.01316	0.00015	0.00000	0.00000	0.00000	0.00000	0.00000	0.00000	2.50E-11	1.36E-14	93.76
2-4	1824.8	6.5	82.49	0.23	82.49	0.21	0.01556	0.00031	0.00000	0.00000	0.00000	0.00000	0.00000	0.00000	5.43E-12	1.36E-14	100.00
1 sigma (1σ) errors																	
J value = 0.021210 ± 0.000106																	
Irradiation standard used = Tinto B biotite (409.24 ± 0.71 Ma)																	

Table 2. (continued)

Analysis no.	*Age (Ma)*	±	$^{40}Ar^*/^{39}Ar$	±	$^{40}Ar/^{39}Ar$	±	$^{38}Ar/^{39}Ar$	±	$^{37}Ar/^{39}Ar$	±	$^{36}Ar/^{39}Ar$	±	*^{39}Ar (cm^3)*	±	*Cumulative % ^{40}A**
CS0395 white mica; in situ, UV laser															
mica 1-1	1787.9	29.8	80.14	2.06	80.30	1.22	0.01976	0.00847	3.08980	1.04700	0.00000	0.00000	5.99E-13	3.78E-15	100.0
mica 1-2	1690.5	26.7	73.44	1.75	82.15	1.04	0.01683	0.00721	3.74933	0.89212	0.02789	0.00481	7.03E-13	3.78E-15	89.6
mica 3-2	1808.6	21.1	81.61	1.45	83.54	0.34	0.01437	0.00160	0.79547	0.05313	0.00619	0.00479	2.12E-12	8.45E-15	97.7
mica 3-3	1789.5	32.2	80.26	2.24	83.26	0.38	0.00997	0.00249	0.99345	0.08291	0.00972	0.00748	1.36E-12	6.09E-15	96.5
mica 3-4	1763.4	20.4	78.43	1.36	81.82	0.30	0.02033	0.00006	1.12632	0.15022	0.01101	0.00452	1.50E-12	4.78E-15	95.9
mica 1-3	1847.4	17.0	84.42	1.17	85.58	0.36	0.01133	0.00005	0.81602	0.14040	0.00357	0.00378	1.79E-12	7.56E-15	98.7
mica 1-4	1869.8	11.7	86.07	0.75	86.13	0.29	0.02104	0.00234	1.20602	0.14033	0.00000	0.00000	1.45E-12	4.78E-15	100.0
mica 1-5	1838.7	18.8	83.78	1.30	84.97	0.71	0.00744	0.00372	1.67297	0.18641	0.00329	0.00372	9.08E-13	7.56E-15	98.7
mica 3-5	1796.5	14.1	80.75	0.92	82.39	0.49	0.00794	0.00265	1.36766	0.15928	0.00495	0.00265	1.28E-12	7.56E-15	98.1

1 sigma (1σ) errors
J value = 0.021137 ± 0.000106
Irradiation standard used = Tinto B biotite (409.24 ± 0.71 Ma)

UV-laser spot analysis sample

White mica dated in situ in sample CS0395 produced a wide spread of ages, from c. 1872 to 1697 Ma (Fig. 35, Table 2). Excluding the youngest age of 1691 Ma that appears to be an outlier, a weighted mean was calculated from the older 8 analyses yielding an age of 1827 ± 32 Ma (95% confidence, MSWD = 4.8). The uncertainties on the analyses are relatively large because of small amounts of gas released from the small white mica grains defining the foliation (Fig. 31d). To obtain more gas a larger than normal (~200 µm) spot size was used, and for most analyses the beam was rastered over an area of approximately 300 to 400 µm along the foliation. This may have resulted in inclusions of other minor K-bearing phases in the rock, thereby giving mixed ages. The relatively high $^{37}Ar_{Ca}/^{39}Ar_K$ ratios (Table 2) of some of the spot analyses indicate that some calcium-bearing phases were sampled during the UV-laser spot ablation.

Interpretation of results

The four samples dated by the ^{40}Ar–^{39}Ar method produced complex age spectra, with most apparent ages of micas dated by the infrared (IR) method ranging from c. 1840 to 1800 Ma (Fig. 36a). These ages are slightly older than, but not inconsistent with, the results from the UV technique, including those from another nine samples dated previously (Figs 36b and 37; Spaggiari et al., in prep.). Most of those analyses are from white micas that define the main foliation, and some were dated in situ. Those samples also gave complex results, but most mica analyses dated by the UV technique yielded apparent ages from c. 1800 to 1700 Ma (Fig. 36b). Two samples indicate some resetting or new mica growth at c. 1200 Ma. Given that only two mica samples were dated by the IR method, the difference between the ages could also be due to those rocks having experienced different stages of movement within different parts of the shear zone network.

Although the data do not readily define specific ages of deformation and cooling, they indicate that the main phase of cooling in the Jack Hills region finished by about 1700 Ma. This is interpreted to be cooling from the main phase of transpressive dextral shearing (i.e. formation of the Cargarah Shear Zone) during the Capricorn Orogeny. The spread in the ages is interpreted to be primarily due to the long and complex deformation history of the belt, including variable movement and reactivation of the shear zone network over a substantial period of time. This has resulted in partial resetting of the grains during deformation, producing heterogeneous distributions of argon both within individual grains and from sample to sample.

Several studies of deformed micas, particularly those using the UV-laser technique, have shown that the formation of microstructures during deformation affects argon retentivity, and simple models of volume diffusion are not adequate (Hodges and Bowring, 1995; Reddy and Potts, 1999; Kramar et al., 2001). Development of microstructures typical of shear zones, such as shear bands, and mica fish where the micas are effectively porphyroclasts, have been shown to produce apparent age

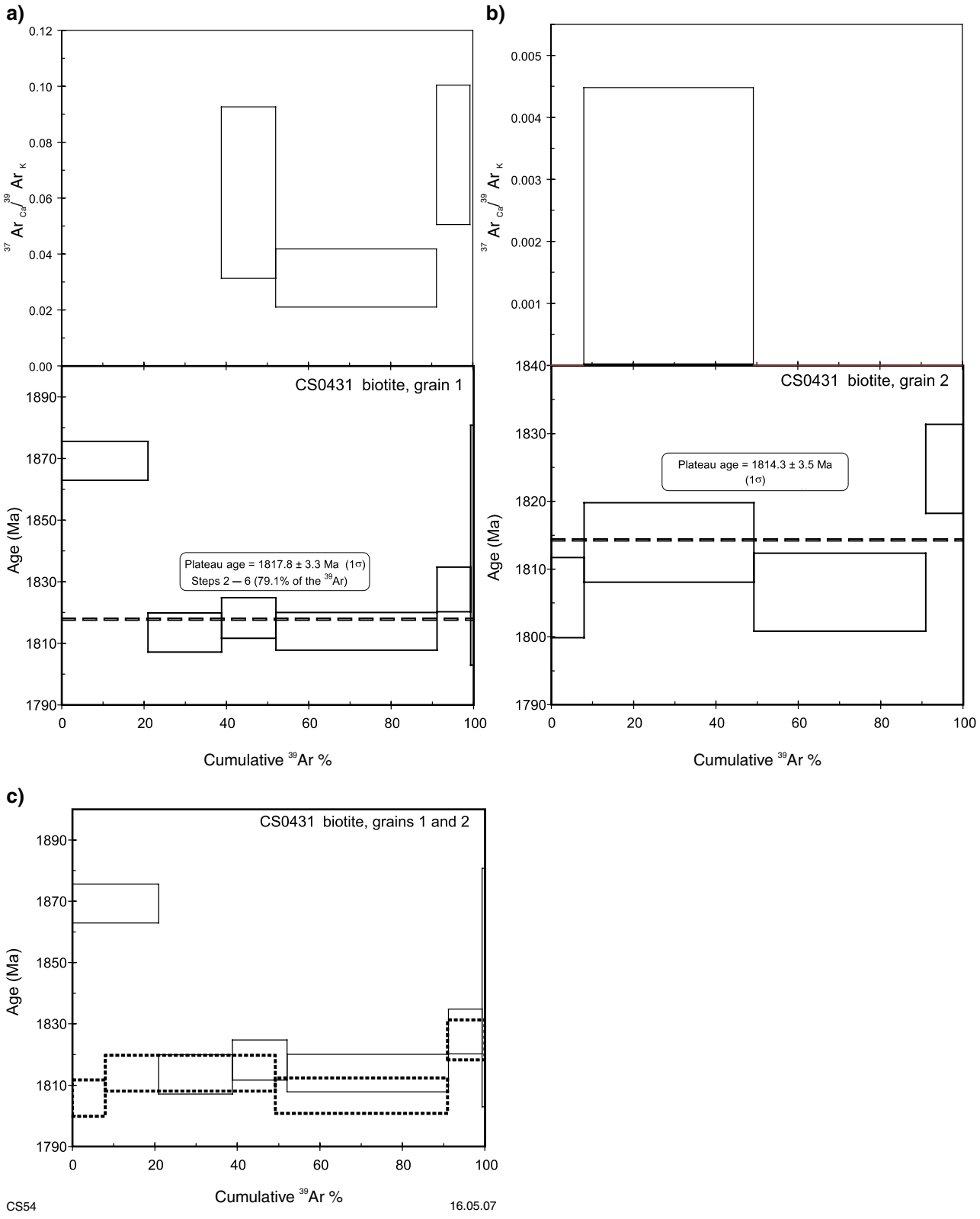

Figure 34. **^{40}Ar–^{39}Ar age spectrum plots for sample CS0431: a) ^{40}Ar–^{39}Ar age spectrum and $^{37}Ar_{Ca}$–$^{39}Ar_K$ versus cumulative %^{39}Ar plot for biotite grain 1. Individual errors are 1σ (denoted by box height on the age spectrum). Steps 2 through 6 gave a plateau age of 1817 ± 3.3 Ma (1σ) representing 79.1% of the ^{39}Ar released; b) ^{40}Ar–^{39}Ar age spectrum for biotite grain 2. Individual errors are 1σ (denoted by box height on the age spectrum). Steps 2 through 4 yielded a plateau age of 1814.3 ± 3.5 Ma (1σ), representing 92% of the ^{39}Ar released; c) ^{40}Ar–^{39}Ar age spectrum from both biotite grains (1 and 2)**

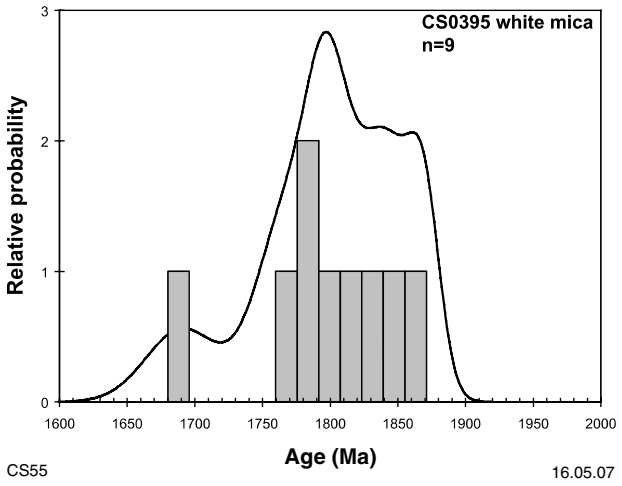

Figure 35. Probability density plot of all UV-laser ages for sample CS0395

groupings defining various deformation events or mixed ages (Kramar et al., 2001; Mulch and Cosca, 2004). Variations in mica composition, produced when micas are partially recrystallized during a deformation event, can also produce different apparent ages (Mulch and Cosca, 2004). Deformation mechanisms that can affect grain sizes of micas are numerous, producing effects such as grain-size reduction, and overgrowths (Reddy and Potts, 1999). These studies show that dating deformation or subsequent cooling from it is complex, particularly in multiply deformed rocks. Although a comprehensive microstructural study has not been undertaken on the samples dated in this study, the structural analysis of the belt shows that it is complex, and the argon systematics would clearly have been affected by deformation. Therefore, although the data are still informative, some dispersion in the results is not surprising.

The possibility of an excess ^{40}Ar component contributing to apparent age variations is difficult to assess because ^{36}Ar (i.e. trapped, nonradiogenic or atmospheric) is negligible. The presence of excess ^{40}Ar produces older apparent ages (e.g. Kelley, 2002). Excess ^{40}Ar, if present, may have come from metamorphic fluids produced during deformation by degassing of minerals that contain a radiogenic ^{40}Ar component (e.g. Reddy et al., 1997). A possible source would be the granitic rocks and gneiss hosting the belt. Meteoric fluids, which may have been plentiful throughout the belt, have been shown to have negligible effects on excess ^{40}Ar content (Kelley, 2002). The very small amounts of ^{36}Ar in the samples mean that inverse isochrons, which may provide a method to check for excess ^{40}Ar (e.g. McDougall and Harrison, 1999), cannot be defined. Hence, any possible effects of ^{40}Ar loss, which would produce younger apparent ages, cannot be assessed.

The wide range of apparent ages from hornblende from sample CS-491 is also probably the result of a long and disturbed history, possibly commencing at about 3.3 or 3.0 Ga. Assuming that the apparent age of the final step of 2961 ± 10 Ma is not due to the effects of excess ^{40}Ar or to phase changes during step-heating, this age would be consistent with known ages of metamorphism and magmatism in the region (e.g. Pidgeon and Wilde, 1998). The sample is interpreted as a metamorphosed dyke within sheared gneiss, and may have intruded the gneiss during its formation, at either 3.3 or 3.0 Ga. Ages between 2050 and 1930 Ma are broadly coincident with the Glenburgh Orogeny (2005–1960 Ma, Occhipinti et al., 2004), which suggests that cooling below the hornblende closure temperature interval (~500°C*, McDougall and Harrison, 1999) did not take place until after that time. Deformation and metamorphism during the Capricorn Orogeny was predominantly at greenschist facies, that is,

* The closure temperature quoted here is an estimate based on other studies. Its calculation would depend on factors such as grain size and cooling rate (McDougall and Harrison, 1999).

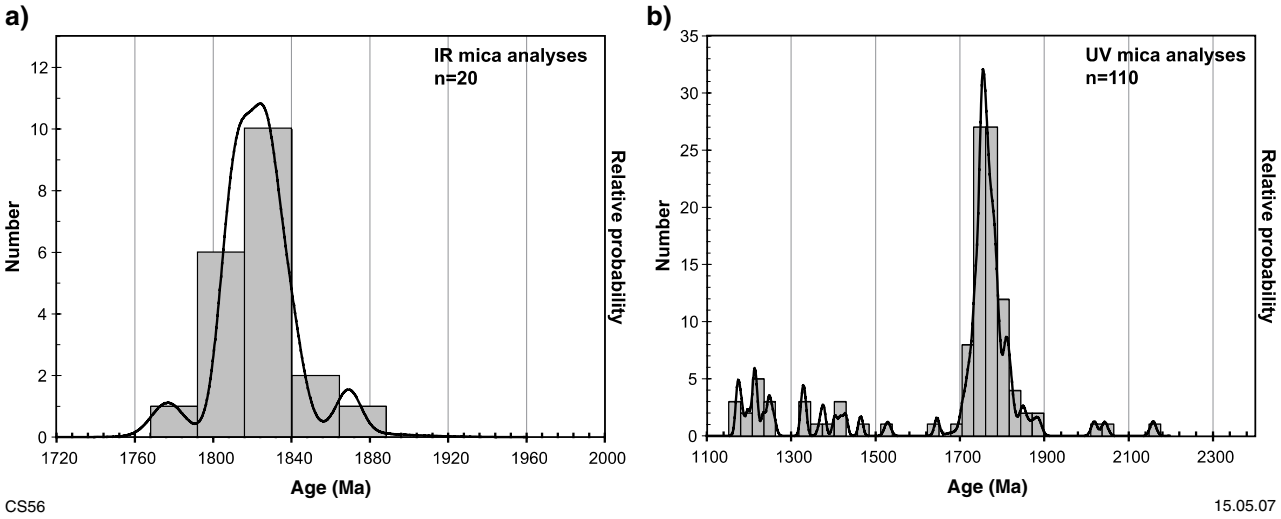

Figure 36. Probability plots comparing infrared and UV-laser ^{40}Ar–^{39}Ar data: a) probability density plot of all ages obtained from infrared analyses; b) probability density plot of all ages obtained from UV-laser analyses, including samples described in Spaggiari et al. (in prep.)

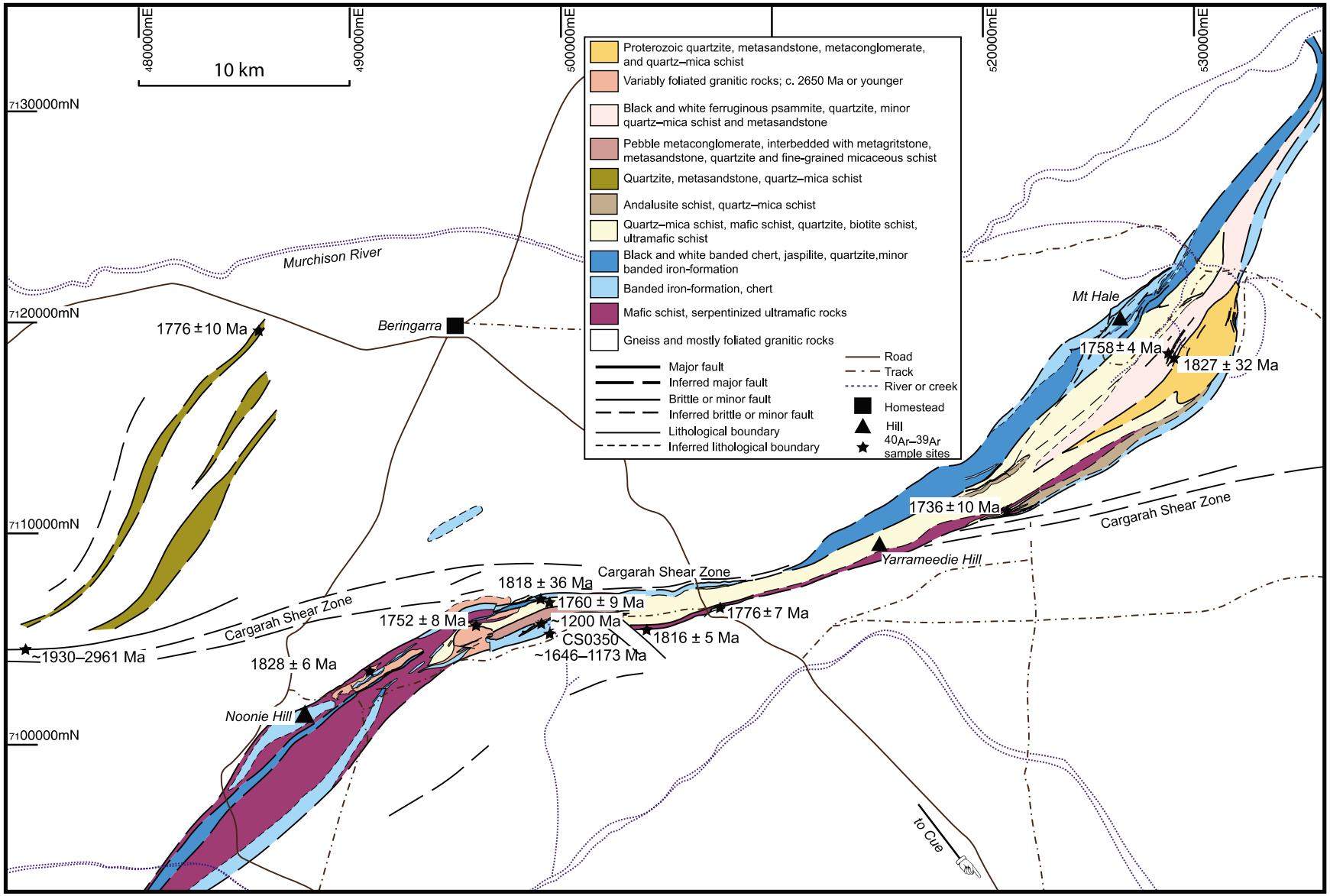

Figure 37. Simplified geological map of the Jack Hills greenstone belt, showing locations and ages of all ^{40}Ar–^{39}Ar samples, including those described in Spaggiari et al. (in prep.)

it probably did not reach temperatures sufficiently high enough to reset the hornblende in this sample. This is consistent with the greenschist overprint on most mafic schist samples.

In summary the ^{40}Ar–^{39}Ar data are interpreted to reflect the complex deformation history shown by the structural data; in particular, variable shear zone movement during the Capricorn Orogeny. This is consistent with the known regional deformation history. Dextral transpression at greenschist facies also occurred during the Capricorn Orogeny within the Errabiddy Shear Zone, which marks the boundary between the Yilgarn Craton and the Glenburgh Terrane (Fig. 1; Occhipinti and Reddy, 2004). The Yarlarweelor Gneiss Complex (Fig. 1), also underwent dextral strike-slip deformation during the Capricorn Orogeny (Sheppard et al., 2003). The ^{40}Ar–^{39}Ar data do not show any evidence of c. 2750–2600 Ma deformation and metamorphism (Myers, 1990), which involved intrusion of Neoarchean granites. This suggests that either most grains were probably completely reset at a later stage, or that the micas dated mostly grew after c. 2600 Ma. The only sample to indicate some possible effects of the Glenburgh Orogeny in the Jack Hills area is the hornblende from CS-491. Whether this marked an earlier phase of deformation, possibly even initiation of the Cargarah Shear Zone, is unknown.

The youngest ^{40}Ar–^{39}Ar data (sample JAW0303, Figs 5, 16b, and 37), indicates that some deformation occurred during emplacement of the dykes associated with the 1210 Ma Marnda Moorn large igneous province. Proterozoic ages of around 1650 Ma have been recorded in biotites dated by the Rb–Sr method throughout the Narryer Terrane and part of the Murchison Domain (Libby et al., 1999). These data also show wide dispersion, which is attributed to the complexity of the biotites and partial resetting.

Discussion and synthesis

Structural, lithological, and geochronological data from the Jack Hills greenstone belt show that it has undergone a long and complex evolution, over more than 1.5 billion years (Table 3). Deposition of the first, and at least part of the second, associations (BIF, chert, quartzite, quartz–mica schist, mafic and ultramafic rocks, pelitic and semipelitic rocks) occurred between c. 3.0 and 2.7 Ga, prior to the intrusion of voluminous monzogranitic rocks across the Yilgarn Craton. Whether the mature clastic association that hosts the 4.0 Ga-and-older detrital zircons was also deposited at this time is unknown, because the detrital zircon geochronology is inconclusive. Alternatively, it may have been deposited after intrusion of the monzogranitic rocks. The rare preservation of recumbent folds in BIF and an early foliation in most rocks of associations 1 and 2, but not in the mature clastic association, are indicative of an early deformation event that occurred prior to intrusion of the monzogranites. This deformation event may have been related to amalgamation of the Narryer Terrane to the Youanmi Terrane, which are stitched by the 2.75 to 2.60 Ga monzogranites. The boundary of the two terranes has been interpreted as the Yalgar Fault (Myers, 1990), but it is not clear as to whether or not this structure was initially formed at that time. The Jack Hills greenstone belt is adjacent to the Yalgar Fault (Fig. 1) and may have formed part of the margin of the Narryer Terrane. The close association of the mafic and ultramafic rocks with

Table 3. Summary of the regional geological events and their effects on the Jack Hills greenstone belt

Age (Ma)	*Orogenic or regional event*	*Effect on Jack Hills greenstone belt*
≥3000	Formation of granitic gneisses and intrusions of granitic rocks in the Narryer Terrane	Formation of basement
c. 3000	Probable time of formation of some greenstones in the Murchison Domain, Yilgarn Craton	Deposition of association 1 (BIF, chert, quartzite, pelitic and semipelitic rocks, mafic and ultramafic rocks) at c. 3000 Ma, or prior to 2750 Ma Deposition of mature clastic rocks at this time?
2750–2600	Intrusion of voluminous monzogranitic rocks across the Yilgarn Craton	Intrusion of monzongranite (e.g. the Blob). Deposition of mature clastic rocks after granite intrusion?
2005–1960	Glenburgh Orogeny	No recognized effects other than detritus in Proterozoic rocks
1830–1780	Capricorn Orogeny	Deposition of Proterozoic sequence, possibly in jogs during shearing. Some rocks may be younger. Major dextral, transpressional shearing (Cargarah Shear Zone)
1680–1620	Mangaroon Orogeny	Reactivation of Cargarah Shear Zone at this time?
c. 1400–1350	No known event	Reactivation of Cargarah Shear Zone at this time?
1210	Marnda Moorn large igneous province	Intrusion of mafic dykes. Semibrittle faulting
1075	Warakurna large igneous province	Intrusion of mafic dykes

BIF, chert, quartzite, and some pelitic and semipelitic rocks may reflect formation of a small rift or marginal basin that was subsequently closed. Alternatively, the Jack Hills greenstone belt may have been part of a broader, more complex, basin that included other greenstones of this age from the Murchison Domain, for example, the Weld Range greenstone belt just south of Jack Hills, and the Mingah Range greenstone belt to the southeast (Fig. 38; Spaggiari, 2006). This would suggest that either the Yalgar Fault is not a terrane boundary or the two terranes were amalgamated prior to deposition of the greenstones.

The next major phase of regional deformation was the Glenburgh Orogeny (c. 2005–1960 Ma), followed by the Capricorn Orogeny (1830–1780 Ma; Occhipinti et al., 2004; Cawood and Tyler, 2004). Whether the Glenburgh Orogeny affected the Jack Hills greenstone belt is unknown. However, given that it was a major event of terrane accretion just north of the belt, some effect is likely. The similarity in structural and metamorphic style between the Errabiddy Shear Zone and the Jack Hills greenstone belt, and the ^{40}Ar–^{39}Ar data, indicate that the Capricorn Orogeny had a major impact on the belt and surrounding region. The Errabiddy Shear Zone is a crustal-scale structure that marks the boundary between the Yilgarn Craton and the Glenburgh Terrane and was initially formed by terrane accretion during the Glenburgh Orogeny, and subsequently reworked at greenschist-facies temperatures during the Capricorn Orogeny (Occhipinti et al., 2004; Occhipinti and Reddy, 2004). The shear zone is interpreted to show evidence of dextral transpression during the Capricorn Orogeny, based on the presence of dextral kinematic indicators such as asymmetric porphyroclasts and a thrust component in the northeastern part of the shear zone where it changes from an east-northeasterly to a north-northeasterly trend (Occhipinti and Reddy, 2004). Although the Errabiddy Shear Zone and the Jack Hills greenstone belt had different early structural histories and are different lithologically, the Errabiddy Shear Zone has a similar dextral sigmoidal geometry and orientation to the Jack Hills greenstone belt. This is interpreted to be a function of similar dextral transpressive shearing (see also Williams, 1986).

SHRIMP geochronology in the Jack Hills greenstone belt shows that some sedimentary rocks were not deposited until at least 1791 ± 21 Ma (Dunn et al., 2005). Because these rocks are deformed this indicates that at least some of the deformation in the belt occurred after that time. Some rocks (and deformation) may be even younger (Cavosie et al., 2004). Paleoproterozoic sedimentary rocks may have been deposited in fault jogs or small pull-apart basins during shearing on the Cargarah Shear Zone, probably during the Capricorn Orogeny, but possibly also later during reactivation. The major compressive stress direction is inferred to have been northwest–southeast and oblique to the belt, which could allow for approximately northeast–southwest oriented pull-aparts to have formed (Fig. 39). Note that the strain rate on the fault system is likely to have been variable over time, and the jogs and associated extensional faults would be overprinted by ongoing shearing. Transpressional deformation may also produce folding and uplift within the shear zone, causing sedimentation during fault movement. Deformation associated with the formation of the Cargarah Shear Zone has been interpreted to extend as far south as the northern end of the Mingah Range greenstone belt (Fig. 38; Spaggiari, 2006). It is possible that the Yalgar Fault, interpreted to be a dextral strike-slip fault (Myers, 1990), was also initiated at this time.

Reactivation of the Cargarah Shear Zone and associated structures, and formation of new semibrittle or brittle structures, occurred after the main phase of shearing, but the timing is poorly constrained. If younger sequences are present in the Jack Hills greenstone belt, they may have been deposited prior to or around this time. The Mangaroon Orogeny (1680–1620 Ma), which has been recognized in the Gascoyne Complex (Sheppard et al., 2005), may have had some effect on the belt. The ^{40}Ar–^{39}Ar data, and Rb–Sr data of Libby et al. (1999), indicate that some deformation may have occurred between c. 1400 to 1350 Ma. Fault activity at around 1200 Ma, indicated by the ^{40}Ar–^{39}Ar data, may have been related to the intrusion of mafic dykes at around 1210 Ma (Wingate et al., 2005). Intrusion of crosscutting mafic dykes at 1075 Ma marks the final stage of substantial tectonic activity in the Jack Hills region.

From this it is clear that the dominant and best preserved phase of deformation is related to shearing that is interpreted to have occurred primarily during the Capricorn Orogeny and had dextral transpressional kinematics. The formation of predominantly dextral S–C foliations, as well as conjugate low-angle shear bands indicate both rotational and flattening components during deformation. Major folds throughout the belt are cut by shears and may also have formed in relation to transpression during progressive deformation, as ongoing oblique compressional stress-tightened fold structures and produced failure and slip (i.e. shearing). However, it is difficult to distinguish whether the folds were pre-existing structures that were subsequently cut by the shearing, or formed in response to it, or both. Coplanar and coaxial overprinting relationships make it difficult to assign specific foliations to tectonic events, but the preservation of multiple foliations in some outcrops, and fold relationships preserved in the BIF unit help define a structural chronology. This has been used to interpret the ^{40}Ar–^{39}Ar data, where the dating of the main shear-related foliations can be compared to age data from other foliation-forming micas and hornblende. This shows that the main phase of cooling, from predominantly upper greenschist-facies temperatures, occurred between c. 1800 and 1700 Ma. Geological and geochronological relationships show that the Jack Hills greenstone belt has undergone a complex depositional and deformational history from c. 3000 to 1075 Ma.

Acknowledgements

The author acknowledges many fruitful discussions with Bob Pidgeon, Simon Wilde, Sandra Occhipinti, Ian Tyler, Craig Buchan, Alan Collins, Ian Fitzsimons, Jo Wartho, Mike Wingate, Steve Reddy, and Peter Cawood. Dave Hollingsworth is thanked for producing the ASTER satellite image. Stereonets were plotted using the Georient

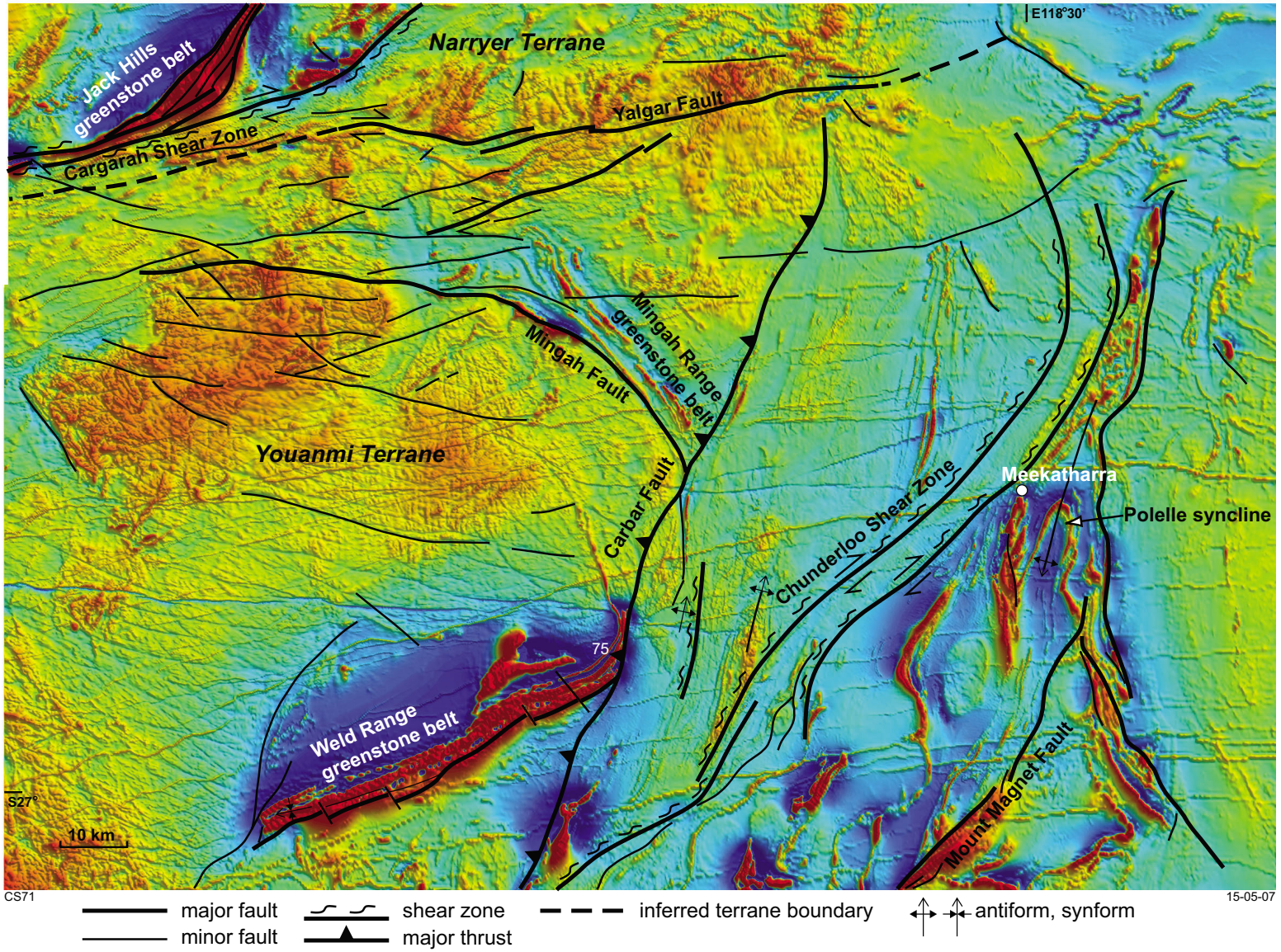

Figure 38. Simplified structural interpretation of the northern Murchison Domain on a reduced to pole, total magnetic intensity image, showing the location of the Yalgar Fault and inferred boundary of the Narryer Terrane and Youanmi Terrane (after Myers and Hocking, 1998; Spaggiari, 2006)

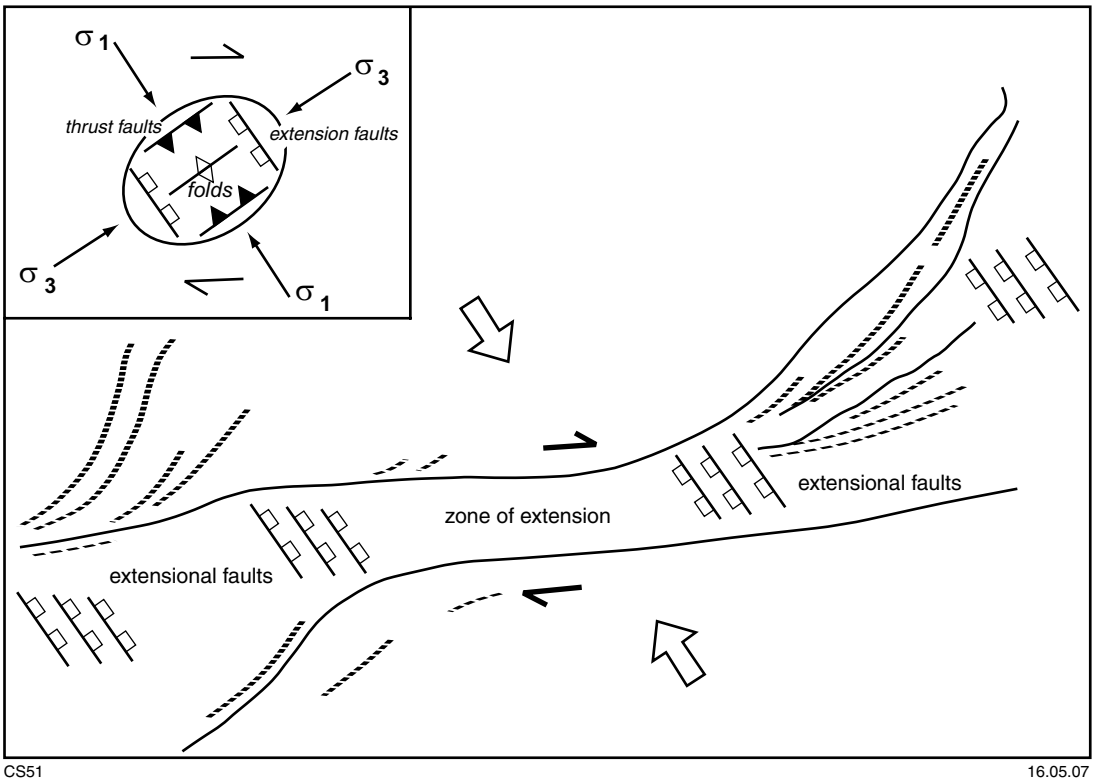

Figure 39. Schematic diagram showing formation of small pull-apart basins or fault jogs in the Jack Hills greenstone belt during dextral strike-slip deformation, in an inferred right-stepping (upper fault to lower fault) wrench system (modified from McClay, 1987). Inset shows the inferred regional strain ellipse associated with the system

program of R. J. Holdcombe, Department of Earth Sciences, University of Queensland. The author thanks Kent Broad for allowing her to use Beringarra Station as home base, and the Walsh family at Mileura Station for their help and hospitality.

References

AMELIN, Y., LEE, D., HALLIDAY, A. N., and PIDGEON, R. T., 1999, Nature of the Earth's earliest crust from hafnium isotopes in single detrital zircons: Nature, v. 399, p. 252–255.

BAXTER, J. L., WILDE, S. A., PIDGEON, R. T., and COLLINS, L. B., 1986, A video presentation of the geological setting of ancient detrital zircons within the Jack Hills Metamorphic Belt, W.A., *in* Eighth Australian Geological Convention — Earth Resources in Time and Space: Geological Society of Australia, Abstracts, v. 15, p. 220.

BOGGS, S., Jr., 1987, Principles of sedimentology and stratigraphy: New York, U.S.A., Macmillan Publishing Company, 784p.

CASSIDY, K. F., CHAMPION, D. C., KRAPEZ, B., BARLEY, M. E., BROWN, S. J. A., BLEWETT, R. S., GROENEWALD, P. B., TYLER, I. M., 2006, A revised geological framework for the Yilgarn Craton: Western Australia Geological Survey, Record 2006/8, 8p.

CAVOSIE, A. J., WILDE, S. A., LIU, D., WEIBLEN, P. W., and VALLEY, J. W., 2004, Internal zoning and U–Th–Pb chemistry of Jack Hills detrital zircons: a mineral record of early Archean to Mesoproterozoic (4348–1576 Ma) magmatism: Precambrian Research, v. 135, p. 251–279.

CAWOOD, P. A., and TYLER, I. M., 2004, Assembling and reactivating the Proterozoic Capricorn Orogen: lithotectonic elements, orogenies, and significance: Precambrian Research, v. 128, p. 201–218.

COMPSTON, W., and PIDGEON, R. T., 1986, Jack Hills, evidence of more very old detrital zircons in Western Australia: Nature, v. 321, p. 766–769.

DUNN, S. J., NEMCHIN, A. A., CAWOOD, P. A., and PIDGEON, R. T., 2005, Provenance record of the Jack Hills Metasedimentary Belt: Source of the Earth's oldest zircons: Precambrian Research v. 138, p. 235–254.

ELIAS, M., 1982, Belele, W.A. (1st edition): Western Australia Geological Survey, 1:250 000 Geological Series Explanatory Notes, 22p.

FLETCHER, I. R., McNAUGHTON, N. J., PIDGEON, R. T., and ROSMAN, K. J. R., 1997, Sequential closure of K–Ca and Rb–Sr isotopic systems in Archaean micas: Chemical Geology, v. 138, p. 289–301.

FROUDE, D. O., IRELAND, T. R., KINNY, P. D., WILLIAMS, I. S., COMPSTON, W., WILLIAMS, I. R., and MYERS, J. S., 1983, Ion microprobe identification of 4100–4200 Myr-old terrestrial zircons: Nature, v. 304, p. 616–618.

HARRISON, T. M., 1981, Diffusion of ^{40}Ar in hornblende: Contributions to Mineralogy and Petrology, v. 78, p. 312–331.

HARRISON, T. M., 1985, Diffusion of ^{40}Ar in biotite: Temperature, pressure and compositional effects: Geochimica et Cosmochimica Acta, v. 49, p. 2461–2468.

HARRISON, T. M., BLICHERT-TOFT, J., MÜLLER, W., ALBAREDE, F., HOLDEN, P., and MOJZSIS, S. J., 2005, Heterogeneous Hadean hafnium: evidence of continental crust at 4.4 to 4.5 Ga: Science, v. 310, p. 1947–1950.

HODGES, K. V., and BOWRING, S. A., 1995, ^{40}Ar/^{39}Ar thermochronology of isotopically zoned micas: Insights from the southwestern USA Proterozoic orogen: Geochimica et Cosmochimica Acta, v. 59, p. 3205–3220.

KELLEY, S., 2002, Excess argon in K–Ar and Ar–Ar geochronology: Chemical Geology, v. 188, p. 1–22.

KINNY, P. D., and NUTMAN, A. P., 1996, Zirconology of the Meeberrie gneiss, Yilgarn Craton, Western Australia: an early Archaean migmatite: Precambrian Research, v. 78, p. 165–178.

KINNY, P. D., WIJBRANS, J. R., FROUDE, D. O., WILLIAMS, I. S., and COMPSTON, W., 1990, Age constraints on the geological evolution of the Narryer Gneiss Complex, Western Australia: Australian Journal of Earth Sciences, v. 37, p. 51–69.

KINNY, P. D., WILLIAMS, I. S., FROUDE, D. O., IRELAND, T. R., and COMPSTON, W., 1988, Early Archaean zircon ages from orthogneisses and anorthosites at Mount Narryer, Western Australia: Precambrian Research, v. 38, p. 325–341.

KRAMAR, N., COSCA, M. A., and HUNZIKER, J. C., 2001, Heterogeneous ^{40}Ar* distributions in naturally deformed muscovite: in situ UV-laser ablation evidence for microstructurally controlled intragrain diffusion: Earth and Planetary Science Letters, v. 192, p. 377–388.

KUIPER, Y. D., 2002, The interpretation of inverse isochron diagrams in ^{40}Ar/^{39}Ar geochronology: Earth and Planetary Science Letters, v. 203, p. 499–506.

LIBBY, W. G., de LAETER, J. R., and ARMSTRONG, R. A., 1999. Proterozoic biotite Rb–Sr dates in the northwestern part of the Yilgarn Craton, Western Australia: Australian Journal of Earth Sciences, v. 46, p. 851–860.

LISTER, G. S., and BALDWIN, S. L., 1996, Modelling the effect of arbitrary P–T–t histories on argon diffusion in minerals using the MacArgon program for the Apple Macintosh: Tectonophysics, v. 253, p. 83–109.

MAAS, R., and McCULLOCH, M. T., 1991, The provenance of Archean clastic metasediments in the Narryer Gneiss Complex, Western Australia: Trace element geochemistry, Nd isotopes, and U–Pb ages for detrital zircons: Geochimica et Cosmochimica Acta, v. 55, p. 1915–1932.

McCLAY, K. R., 1987. The mapping of geological structures: United Kingdom, John Wiley and Sons Ltd., 161p.

McDOUGALL, I., and HARRISON, T. M., 1999, Geochronology and thermochronology by the ^{40}Ar/^{39}Ar method: United Kingdom, Oxford University Press, 269p.

MOJZSIS, S. J., HARRISON, T. M., and PIDGEON, R. T., 2001, Oxygen-isotope evidence from ancient zircons for liquid water at the earth's surface 4,300 Myr ago: Nature, v. 409, p. 178–181.

MULCH, A., and COSCA, M. A., 2004, Recrystallisation or cooling ages: in situ UV-laser ^{40}Ar/^{39}Ar geochronology of muscovite in mylonitic rocks: Journal of the Geological Society, v. 161, p. 573–582.

MYERS, J. S., 1988a, Early Archaean Narryer Gneiss Complex, Yilgarn Craton, Western Australia: Precambrian Research, v. 38, p. 297–307.

MYERS, J. S., 1988b, Oldest known terrestrial anorthosite at Mount Narryer, Western Australia:. Precambrian Research, v. 38, p. 309–323.

MYERS, J. S., 1990, Western Gneiss Terrane, *in* Geology and mineral resources of Western Australia: Western Australia Geological Survey, Memoir 3, p. 13–31.

MYERS, J. S., 1997, Byro, W.A. Sheet SG 50-10 (2nd edition): Western Australia Geological Survey, 1:250 000 Geological Series.

MYERS, J. S., and HOCKING, R. M., 1998, Geological map of Western Australia, 1:2 500 000 scale (13th edition): Western Australia Geological Survey.

MYERS, J. S., and WILLIAMS, I. R., 1985, Early Precambrian crustal evolution at Mount Narryer, Western Australia: Precambrian Research v. 27, p. 153–163.

NELSON, D. R., ROBINSON, B. W., and MYERS, J. S., 2000, Complex geological histories extending for ≥4.0 Ga deciphered from xenocryst zircon microstructures: Earth and Planetary Science Letters, v. 181, p. 89–102.

NUTMAN, A. P., KINNY, P. D., and PRICE, R., 1993, Large-scale crustal structure of the northwestern Yilgarn Craton, Western Australia: Evidence from Nd isotopic data and zircon geochronology: Tectonics, v. 12, p. 971–981.

NUTMAN, A. P., KINNY, P. D., COMPSTON, W., and WILLIAMS, I. S., 1991, SHRIMP U–Pb zircon geochronology of the Narryer Gneiss Complex, Western Australia: Precambrian Research, v. 52, p. 275–300.

OCCHIPINTI, S. A., and REDDY, S. M., 2004, Deformation in a complex crustal-scale shear zone: Errabiddy Shear Zone, Western Australia, *in* Flow processes in faults and shear zones *edited by* G. I. ALSOP, R. E. HOLDSWORTH, K. J. W. McCAFFREY, and M. HAND: Geological Society of London, Special Publications, v. 224, p. 229–248.

OCCHIPINTI, S. A., SHEPPARD, S., PASSCHIER, C., TYLER, I. M., and NELSON, D. R., 2004, Palaeoproterozoic crustal accretion and collision in the southern Capricorn Orogen: the Glenburgh Orogeny: Precambrian Research, v. 128, p. 237–255.

PASSCHIER, C. W., and TROUW, R. A. J., 1996, Micro-tectonics: Berlin, Heidelberg, Springer-Verlag, 289p.

PECK, W. H., VALLEY, J. W, WILDE, S. A., and GRAHAM, C. M., 2001, Oxygen isotope ratios and rare earth elements in 3.3 to 4.4 Ga zircons: Ion microprobe evidence for high $\delta^{18}O$ continental crust and oceans in the early Archean: Geochimica et Cosmochimica Acta, v. 65, p. 4125–4229.

PIDGEON, R. T., and NEMCHIN, A. A., 2006, High abundance of early Archean grains and the age distribution of detrital zircons in a sillimanites bearing quartzite from Mount Narryer, Western Australia: Precambrian Research, v. 150, p. 201–220.

PIDGEON, R. T., and WILDE, S. A., 1998, The interpretation of complex zircon U–Pb systems in Archaean granitoids and gneisses from the Jack Hills, Narryer Gneiss Terrane, Western Australia: Precambrian Research, v. 91, p. 309–332.

PIRAJNO, F., JONES, J. A., HOCKING, R. M., and HALILOVIC, J., 2004, Geology and tectonic evolution of Palaeoproterozoic basins of the eastern Capricorn Orogen, Western Australia: Precambrian Research, v. 128, p. 315–342.

RAMSAY, J. G., and HUBER, M. I., 1983, The techniques of modern structural geology, volume 1: Strain analysis: London, United Kingdom, Academic Press Inc. Ltd., 307p.

REDDY, S. M., KELLEY, S. P., and MAGENNIS, L., 1997, A microstructural and argon laserprobe study of shear zone development at the western margin of the Nanga Parbat-Haramosh Massif, western Himalaya: Contributions to Mineralogy and Petrology, v. 128, p. 16–29.

REDDY, S. M., and POTTS, G. J., 1999, Constraining absolute deformation ages: the relationship between deformation mechanisms and isotope systematics: Journal of Structural Geology, v. 21, p. 1255–1265.

SHEPPARD, S., OCCHIPINTI, S. A., and NELSON, D. R., 2005. Intracontinental reworking in the Capricorn Orogen, Western Australia: the 1680–1620 Mangaroon Orogeny: Australian Journal of Earth Sciences, v. 52, p. 443–460.

SHEPPARD, S., OCCHIPINTI, S. A., and TYLER, I. M., 2003, The relationship between tectonism and composition of granitoid magmas, Yarlarweelor Gneiss Complex, Western Australia: Lithos, v. 66, p. 133–154.

SPAGGIARI, C. V., 2006, Interpreted bedrock geology of the northern Murchison Domain, Youanmi Terrane, Yilgarn Craton: Western Australia Geological Survey, Record 2006/10, 19p.

SPAGGIARI, C. V., WARTHO, J-A., WILDE, S. A., and BODORKOS, S., in prep., Proterozoic development of the northern margin of the Archean Yilgarn Craton: Precambrian Research.

VALLEY, J. W., PECK, W. H., KING, E. M., and WILDE, S. A., 2002, A cool early Earth: Geology, v. 30, p. 351–354.

WARTHO, J-A., REX, D. D., and GUISE, P. G., 1996, Excess argon in amphiboles linked to greenschist facies alteration in the Kamila amphibolite belt, Kohistan Island arc system, northern Pakistan: insights from $^{40}Ar/^{39}Ar$ step-heating and acid leaching experiments: Geology Magazine, v. 133, p. 595–609.

WILDE, S. A., and PIDGEON, R. T., 1990, Geology of the Jack Hills metasedimentary rocks, *in* Third International Archaean Symposium, Perth, Excursion Guidebook *edited by* S. E HO, J. E. GLOVER, J. S. MYERS, and J. R. MUHLING: The University of Western Australia, Geology Department and University Extension, Publication 21, p. 82–95.

WILDE, S. A., VALLEY, J. W., PECK, W. H., and GRAHAM, C. M., 2001, Evidence from detrital zircons for the existence of continental crust and oceans on the Earth 4.4 Gyr ago: Nature, v. 409, p. 175–178.

WILLIAMS, I. R., and MYERS, J. S., 1987, Archaean geology of the Mount Narryer region Western Australia: Western Australia Geological Survey, Report 22, 32p.

WILLIAMS, I. R., WALKER, I. M., HOCKING, R. M., and WILLIAMS, S. J., 1983a, Byro, W.A. (1st edition): Western Australia Geological Survey, 1:250 000 Geological Series Explanatory Notes, 27p.

WILLIAMS, S. J., 1986, Geology of the Gascoyne Province, Western Australia: Western Australia Geological Survey, Report 15, 85p.

WILLIAMS, S. J., WILLIAMS, I. R., and HOCKING, R. M., 1983b, Glenburgh, W.A.: Western Australia Geological Survey, 1:250 000 Geological Series Explanatory Notes, 25p.

WINGATE, M. T. D., MORRIS, P. A., PIRAJNO, F., and PIDGEON, R. T., 2005, Two large igneous provinces in Late Mesoproterozoic Australia, *in* Supercontinents and Earth Evolution Symposium *edited by* M. T. D. WINGATE and S. A. PISAREVSKY: Geological Society of Australia, Abstracts, v. 81, p. 151.

WINGATE, M. T. D., PIRAJNO, F., and MORRIS, P. A., 2004, Warakurna large igneous province: a new Mesoproterozoic large igneous province in west-central Australia: Geology, v. 32, p. 105–108.

WYCHE, S., NELSON, D. R., and RIGANTI, A., 2004, 4350–3130 Ma detrital zircons in the Southern Cross Granite–Greenstone Terrane, Western Australia: implications for the early evolution of the Yilgarn Craton: Australian Journal of Earth Sciences, v. 51, p. 31–45.

Appendix 1

Methodologies for the ^{40}Ar–^{39}Ar geochronology

For the infrared laser step-heating, mineral grains were handpicked, cleaned in methanol, and rinsed in deionized water in an ultrasonic bath. For the UV-laser spot analysis, a polished thick section (100–200 μm thickness) was removed from its glass slide, and the sample rinsed ultrasonically in methanol and subsequently deionized water. Sections of interest 10 mm × 10 mm were broken off the polished thick section. Samples were then individually wrapped in aluminium foil, and all the samples were loaded into an aluminium package. Biotite age standard Tinto B (K–Ar age of 409.24 ± 0.71 Ma (Rex and Guise, 1995) was loaded at 5 mm intervals along the package to monitor the neutron flux gradient. The package was Cd-shielded and irradiated in the 5C position of the McMaster University Nuclear Reactor, Hamilton, Canada, for 89.1 hours. Upon return, the infrared laser step-heating samples were loaded into an ultra-high vacuum laser chamber with a Kovar viewport. The UV-laser spot-analysis samples were loaded into an ultra-high vacuum laser chamber with a Suprasil 2 viewport. All samples were baked to 120°C overnight to remove adsorbed atmospheric argon from the samples and chamber walls.

For the infrared laser step-heating samples, a 110 W Spectron Laser Systems continuous-wave neodymium–yttrium–aluminium–garnet (CW–Nd–YAG) (λ = 1064 nm) laser, fitted with a TEM00 aperture, was used to slowly laser step-heat the mineral sample, at increasing laser powers from 10.0 to 10.2 A (CS-491), 9.9 to 10.1 A (CS0431), and 10.1 to 10.6 A (CS0416). For the UV-laser spot-analysis sample a New Wave Research LUV 213X 4 mJ pulsed quintupled Nd–YAG laser (λ = 213 nm), with a variable spot size of 10–350 μm, and a repetition rate of 10 Hz, was used to ablate the mineral grains. The lasers were fired through a Merchantek computer-controlled X–Y–Z sample chamber stage and microscope system, fitted with a high-resolution CCD camera, 6× computer-controlled zoom, high magnification objective lens, and two light sources for sample illumination.

The gases released by laser heating (or ablation for the UV method) were 'gettered' using 3 SAES AP10 getter pumps to remove all active gases (CO_2, H_2O, H_2, N_2, O_2, CH_4, etc.). The remaining noble gases were equilibrated into a high sensitivity mass spectrometer (MAP 215-50), operated at a resolution of 600, and fitted with a Balzers SEV 217 multiplier. The automated extraction and data acquisition system was computer controlled, using a LabView program. For the infrared laser step-heating samples the mean 4-minute extraction system blank Ar isotope measurements obtained during the experiments were 1.51×10^{-12}, 1.30×10^{-14}, 2.25×10^{-15}, 3.94×10^{-14}, and 1.52×10^{-14} cm^3 STP (standard temperature and pressure) for ^{40}Ar, ^{39}Ar, ^{38}Ar, ^{37}Ar, and ^{36}Ar respectively. For the UV-laser spot-analysis sample the mean 4-minute extraction system blank Ar isotope measurements obtained during the experiments were 3.82×10^{-12}, 1.49×10^{-14}, 5.41×10^{-15}, 5.95×10^{-14}, and 3.11×10^{-14} cm^3 STP for ^{40}Ar, ^{39}Ar, ^{38}Ar, ^{37}Ar, and ^{36}Ar respectively. Samples were corrected for mass spectrometer discrimination and nuclear interference reactions. Errors quoted on the ages are 1 sigma, and Ar–Ar ages were calculated using the decay constant quoted by Steiger and Jäger (1977). J values and uncertainties are noted on the sample Ar–Ar data tables. The Ar–Ar data presented in this study were collected at the Western Australian Argon Isotope Facility, operated by a consortium consisting of Curtin University and the University of Western Australia.

References

REX, D. C., and GUISE, P. G., 1995, Evaluation of argon standards with special emphasis on time scale measurements, *in* Phanerozoic Time Scale *edited by* G. S. ODIN: Bull. Liais. Inform. IUGS Subcommission on Geochronology, v. 13, p. 21–23.

STEIGER, R. J., and JÄGER, E., 1977, Subcommission on geochronology: Convention on the use of decay constants in geo- and cosmochronology: Earth and Planetary Science Letters, v. 36, p. 359–362.

SPAGGIARI

Structural and lithological evolution of the Jack Hills greenstone belt, Narryer Terrane, Yilgarn Craton, Western Australia

RECORD 2007/3

This Record is published in digital format (PDF) and is available online at: www.doir.wa.gov.au/GSWA/publications. Laser-printed copies can be ordered from the Information Centre for the cost of printing and binding.

Further details of geological publications and maps produced by the Geological Survey of Western Australia can be obtained by contacting:

Information Centre
Department of Industry and Resources
100 Plain Street
East Perth WA 6004
Phone: (08) 9222 3459 Fax: (08) 9222 3444

www.doir.wa.gov.au/GSWA/publications

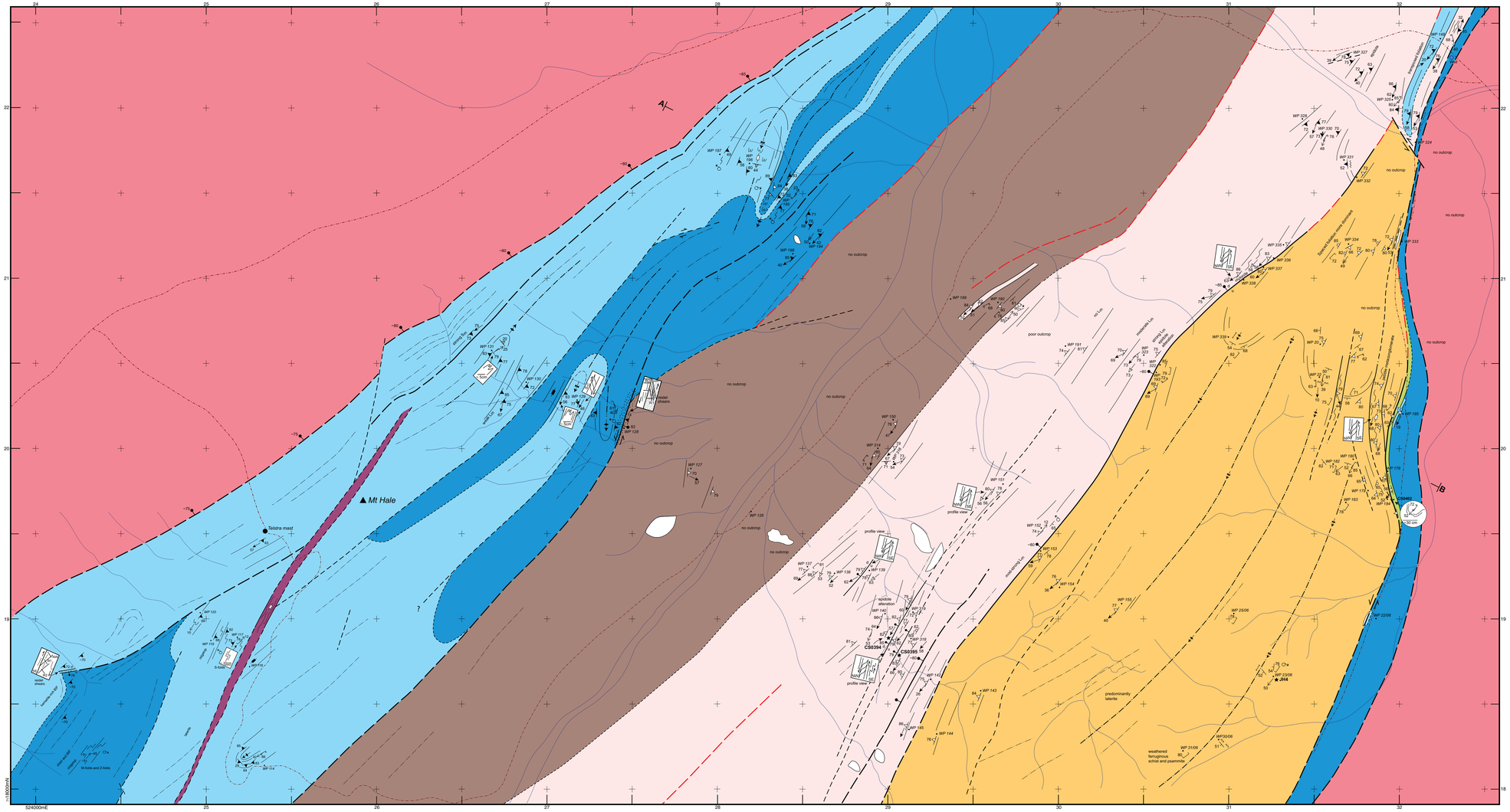

Lithological units

- dolerite or gabbro plug, sill or dyke
- felsic dyke
- quartz veins
- (Proterozoic) fine-grained micaceous schist, quartz–mica schist, quartzite
- (Proterozoic) quartzite, metasandstone, metaconglomerate, quartz–mica schist, ferruginous schist
- muscovite granite and pegmatite, pegmatite
- granitic rocks
- black and white ferruginous psammite, quartzite, jaspilitic chert, minor quartz–mica schist and metasandstone
- fine-grained micaceous schist, quartz–mica schist, quartzite
- pebble metaconglomerate, interbedded with metagritstone, metasandstone, quartzite and fine-grained micaceous schist
- interbedded metasandstone, quartzite, metagritstone, minor pebble metaconglomerate, and fine-grained micaceous schist
- andalusite schist, quartz–mica schist
- fine-grained micaceous schist, quartz–mica schist, quartzite, sometimes interleaved with mafic or ultramafic schist
- quartzite or chert, black and white banded chert, jaspilite, minor quartz–mica schist, banded iron-formation
- banded iron-formation, chert
- mafic schist (mostly hornblende- or actinolite-rich), chlorite schist, commonly interleaved with quartz–mica or biotite schist, and ultramafic rocks
- serpentinized ultramafic rocks, silicified ultramafic rocks; mafic schist
- gneiss, foliated granitic rocks, pegmatite, mafic and ultramafic schist

Structural symbols

Fault

- major fault with dip; inferred major fault
- reverse or thrust fault with dip; inferred reverse or thrust fault
- fault or unconformity, or both
- brittle or minor fault with dip; inferred brittle or minor fault
- brittle fault zone
- dextral strike slip movement (section only)
- sinistral strike-slip movement (section only)

Geological boundary

- contact interpreted from satellite image
- lithological boundary; inferred lithological boundary

Structural symbols

Fold

- axial trace of fold hinges
- fold with axial surface and plunge
- antiform; synform
- fold vergence (to next antiform) S_0>S_m

Bedding

- inclined
- vertical
- overturned
- bedding (section only)

Trend of bedding or foliation

- trend lines
- trend lines of anastomosing foliation, often associated with shearing
- trend lines from aerial photo or satellite image interpretation
- early cleavage (section only)
- crenulation cleavage (section only)
- gneissic fabric (section only)

Metamorphic foliation, showing strike and dip

- early foliation; vertical
- compositional banding (BIF and chert); parallel to main foliation (S_{m1}) vertical
- gneissic layering
- main foliation (S_{m1}); vertical
- crenulation cleavage (S_{DC}); vertical
- 2nd generation crenulation cleavage; vertical
- spaced foliation (S_{DC}); vertical
- shear bands

Lineation, showing trend and plunge

- intersection lineation (bedding and main foliation L_0=S_{m1})
- crenulation intersection lineation (L_S=S_{DC})
- pebble elongation
- mineral lineation (L_{m1})
- rodding lineation

- section lines
- younging direction
- sample locality
- GPS waypoint
- creek
- secondary road or track
- hill
- locality

1:250 000 SHEET INDEX

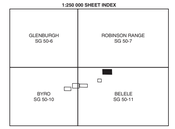

Compiled by C.V. Spaggiari 2003–04
Cartography by C.V. Spaggiari and A. Blake

Published by the Geological Survey of Western Australia. PDF available on website at www.doir.wa.gov.au/GSWA/publications

The recommended reference for this map is:
SPAGGIARI, C. V., 2007, Northeastern area of the Jack Hills greenstone belt, *in* Structural and lithological evolution of the Jack Hills greenstone belt, Narryer Terrane, Yilgarn Craton, Western Australia: Western Australia Geological Survey, Record 2007/3, Plate 1

Department of Industry and Resources
FRANCIS LOGAN, M.L.A.
MINISTER FOR RESOURCES

Geological Survey of Western Australia
TIM GRIFFIN
EXECUTIVE DIRECTOR

500 0 1
Metres Kilometre

UNIVERSAL TRANSVERSE MERCATOR PROJECTION
HORIZONTAL DATUM: GEODETIC DATUM OF AUSTRALIA 1994
VERTICAL DATUM: AUSTRALIAN HEIGHT DATUM
Grid lines indicate 500 metre interval of the Map Grid Australia Zone 50

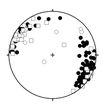

Main foliation (S_m):
all rocks, black dots, n=111;
BIF–chert: S_m / banding, squares, n=36; banding, open dots, n=5;
girdle: 136/26NE,
beta axis: 64–226

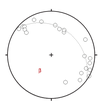

Bedding: metasedimentary rocks, n=21
girdle: 126/36NE,
beta axis: 54–216

Early foliation: metasedimentary rocks, crosses, n=6;
early spaced foliation in quartzite, diamonds, n=3

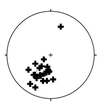

Mineral lineation (L_m):
BIF–chert, crosses, n=22;
intersection lineation, triangle, n=1

Late folds (fold banding or post-S_m): all rocks,
axial planes, n=15

Late folds (fold banding or post-S_m): all rocks,
fold axes, n=13

Mineral lineation (L_m):
quartzite, open crosses, n=31;
mafic schist, dot, n=1; quartz–mica schist, black crosses, n=5;
intersection lineation, quartzite, triangles, n=7

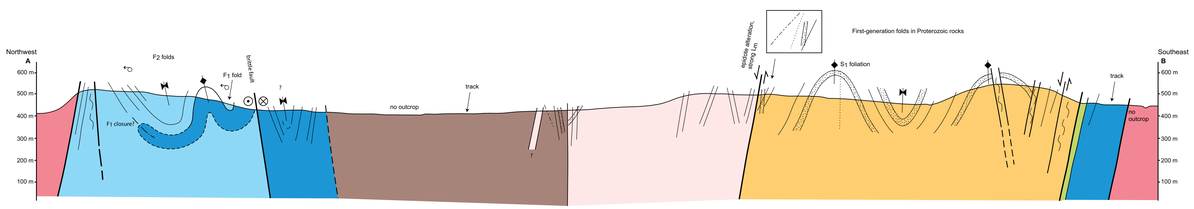

GEOLOGICAL SURVEY OF WESTERN AUSTRALIA
RECORD 2007/3 PLATE 1

PLATE 1
NORTHEASTERN AREA OF THE JACK HILLS GREENSTONE BELT

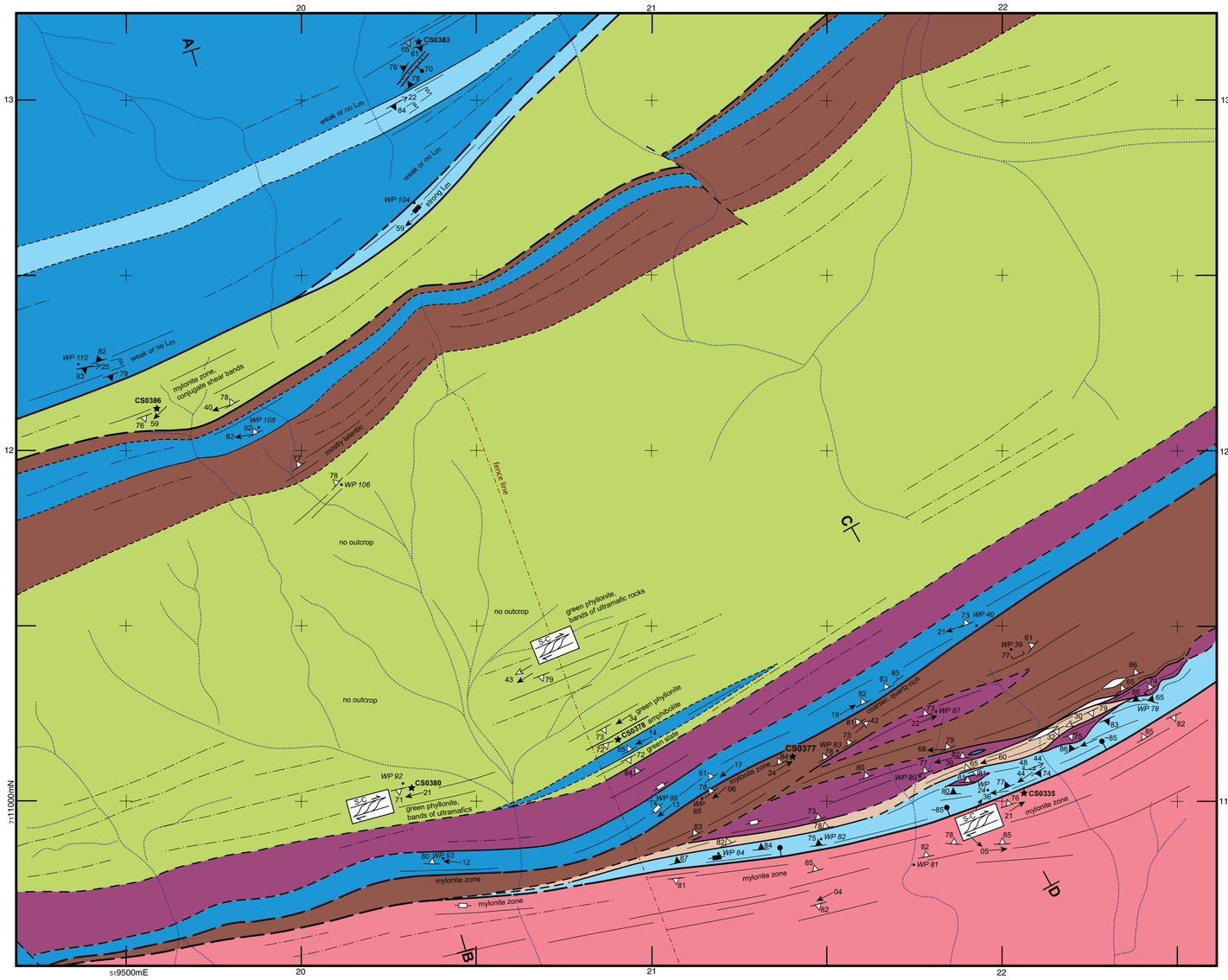

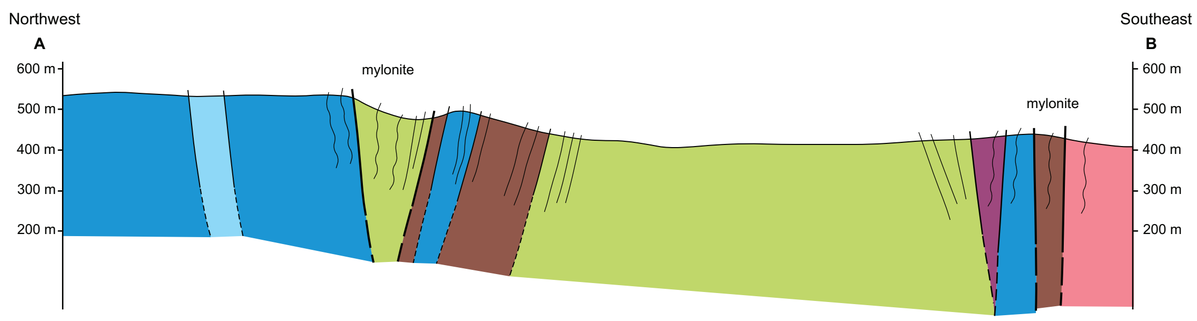

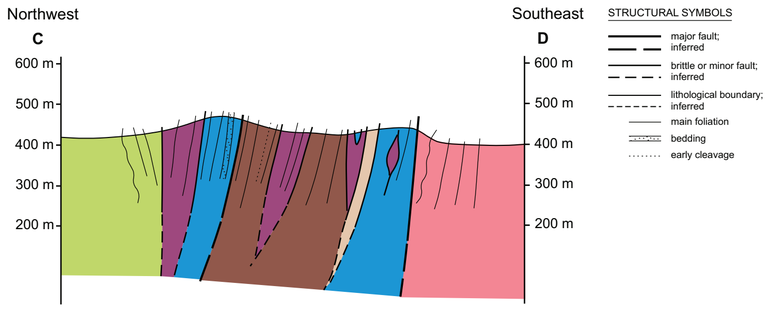

Lithological units

- dolerite or gabbro plug, sill or dyke
- felsic dyke
- quartz veins
- (Proterozoic) fine-grained micaceous schist, quartz–mica schist, quartzite
- (Proterozoic) quartzite, metasandstone, metaconglomerate, quartz–mica schist, ferruginous schist
- muscovite granite and pegmatite, pegmatite
- granitic rocks
- black and white ferruginous psammite, quartzite, jaspilitic chert, minor quartz–mica schist and metasandstone
- fine-grained micaceous schist, quartz–mica schist, quartzite
- pebble metaconglomerate, interbedded with metagritstone, metasandstone, quartzite and fine-grained micaceous schist
- interbedded metasandstone, quartzite, metagritstone, minor pebble metaconglomerate, and fine-grained micaceous schist
- andalusite schist, quartz–mica schist
- fine-grained micaceous schist, quartz–mica schist, quartzite, sometimes interleaved with mafic or ultramafic schist
- quartzite or chert, black and white banded chert, jaspilite, minor quartz–mica schist, banded iron-formation
- banded iron-formation, chert
- mafic schist (mostly hornblende- or actinolite-rich), chlorite schist, commonly interleaved with quartz–mica or biotite schist, and ultramafic rocks
- serpentinized ultramafic rocks, silicified ultramafic rocks, mafic schist
- gneiss, foliated granitic rocks, pegmatite, mafic and ultramafic schist

Structural symbols

Fault

- major fault with dip; inferred major fault
- reverse or thrust fault with dip; inferred reverse or thrust fault
- fault or unconformity, or both
- brittle or minor fault with dip; inferred brittle or minor fault
- brittle fault zone
- dextral strike slip movement (section only)
- sinistral strike-slip movement (section only)

Geological boundary

- contact interpreted from satellite image
- lithological boundary; inferred lithological boundary

Structural symbols

Fold

- axial trace of fold hinges
- fold with axial surface and plunge
- antiform; synform
- fold vergence (to next antiform) S_O/S_m

Bedding

- inclined
- vertical
- overturned
- bedding (section only)

Trend of bedding or foliation

- trend lines
- trend lines of anastomosing foliation, often associated with shearing
- trend lines from aerial photo or satellite image interpretation
- early cleavage (section only)
- crenulation cleavage (section only)
- gneissic fabric (section only)

Metamorphic foliation, showing strike and dip

- early foliation; vertical
- compositional banding (BIF and chert); parallel to main foliation (S_m); vertical
- gneissic layering
- main foliation (S_m); vertical
- crenulation cleavage (S_{cc}); vertical
- 2nd generation crenulation cleavage; vertical
- spaced foliation (S_{cc}); vertical
- shear bands

Lineation, showing trend and plunge

- intersection lineation (bedding and main foliation L_O/S_m)
- crenulation intersection lineation (LS_{cc})
- pebble elongation
- mineral lineation (L_m)
- rodding lineation
- section lines
- younging direction
- sample locality
- GPS waypoint
- creek
- secondary road or track
- hill
- locality

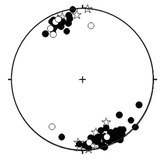

Main foliation (S_m):
all rocks except granitic, black dots, n=63;
granitic rocks, stars, n=14
BIF–chert: S_m / banding, open dots, n=8;
mean principle orientation of S_m: 066/85N

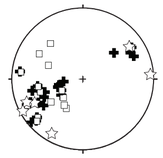

Mineral lineation (L_m):
schists and ultramafics, black crosses, n=14;
BIF–chert, squares, n=14;
granite and gneiss, open crosses, n=6

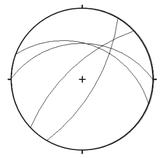

Late folds (fold banding or post-S_m):
BIF–chert, axial planes, n=4

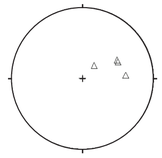

Late folds (fold banding or post-S_m):
BIF–chert, fold axes, n=4

1:250 000 SHEET INDEX

Compiled by C.V. Spaggiari 2003–04
Cartography by C.V. Spaggiari and A. Blake

Published by the Geological Survey of Western Australia. PDF available on website at www.doir.wa.gov.au/GSWA/publications

The recommended reference for this map is:
SPAGGIARI, C. V., 2007 East-central area of the Jack Hills greenstone belt, *in* Structural and lithological evolution of the Jack Hills greenstone belt, Narryer Terrane, Yilgarn Craton, Western Australia: Western Australia Geological Survey, Record 2007/3, Plate 2

Department of Industry and Resources
FRANCIS LOGAN, M.L.A.
MINISTER FOR RESOURCES

Geological Survey of Western Australia
TIM GRIFFIN
EXECUTIVE DIRECTOR

500 Metres 0 1 Kilometre

UNIVERSAL TRANSVERSE MERCATOR PROJECTION
HORIZONTAL DATUM: GEODETIC DATUM OF AUSTRALIA 1994
VERTICAL DATUM: AUSTRALIAN HEIGHT DATUM
Grid lines indicate 500 metre interval of the Map Grid Australia Zone 50

GEOLOGICAL SURVEY OF WESTERN AUSTRALIA
RECORD 2007/3 PLATE 2

PLATE 2
EAST-CENTRAL AREA OF THE JACK HILLS GREENSTONE BELT

Lithological units

- dolerite or gabbro plug, sill or dyke
- felsic dyke
- quartz veins
- (Proterozoic) fine-grained micaceous schist, quartz–mica schist, quartzite
- (Proterozoic) quartzite, metasandstone, metaconglomerate, quartz–mica schist, ferruginous schist
- muscovite granite and pegmatite, pegmatite
- granitic rocks
- black and white ferruginous psammite, quartzite, jaspilitic chert, minor quartz–mica schist and metasandstone
- fine-grained micaceous schist, quartz–mica schist, quartzite
- pebble metaconglomerate, interbedded with metagritstone, metasandstone, quartzite and fine-grained micaceous schist
- interbedded metasandstone, quartzite, metagritstone, minor pebble metaconglomerate, and fine-grained micaceous schist
- andalusite schist, quartz–mica schist
- fine-grained micaceous schist, quartz–mica schist, quartzite, sometimes interleaved with mafic or ultramafic schist
- quartzite or chert, black and white banded chert, jaspilite, minor quartz–mica schist, banded iron-formation
- banded iron-formation, chert
- mafic schist (mostly hornblende- or actinolite-rich), chlorite schist, commonly interleaved with quartz–mica or biotite schist, and ultramafic rocks
- serpentinized ultramafic rocks, silicified ultramafic rocks, mafic schist
- gneiss, foliated granitic rocks, pegmatite, mafic and ultramafic schist

Structural symbols

Fault

- major fault with dip; inferred major fault
- reverse or thrust fault with dip; inferred reverse or thrust fault
- fault or unconformity, or both
- brittle or minor fault with dip; inferred brittle or minor fault
- brittle fault zone
- dextral strike slip movement (section only)
- sinistral strike-slip movement (section only)

Geological boundary

- contact interpreted from satellite image
- lithological boundary; inferred lithological boundary

Structural symbols

Fold

- axial trace of fold hinges
- fold with axial surface and plunge
- antiform; synform
- fold vergence (to next antiform) S_o/S_m

Bedding

- inclined
- vertical
- overturned
- bedding (section only)

Trend of bedding or foliation

- trend lines
- trend lines of anastomosing foliation, often associated with shearing
- trend lines from aerial photo or satellite image interpretation
- early cleavage (section only)
- crenulation cleavage (section only)
- gneissic fabric (section only)

Metamorphic foliation, showing strike and dip

- early foliation; vertical
- compositional banding (BIF and chert); parallel to main foliation (S_m); vertical
- gneissic layering
- main foliation (S_m); vertical
- crenulation cleavage (S_{cc}); vertical
- 2nd generation crenulation cleavage; vertical
- spaced foliation (S_{cc}); vertical
- shear bands

Lineation, showing trend and plunge

- intersection lineation (bedding and main foliation L_o/S_m)
- crenulation intersection lineation (L_{Scc})
- pebble elongation
- mineral lineation (L_m)
- rodding lineation
- section lines
- younging direction
- sample locality
- GPS waypoint
- creek
- secondary road or track
- hill
- locality

Compiled by C.V. Spaggiari 2003–04
Cartography by C.V. Spaggiari and A. Blake

Published by the Geological Survey of Western Australia. PDF available on website at www.doir.wa.gov.au/GSWA/publications

The recommended reference for this map is:
SPAGGIARI, C. V., 2007, Central area of the Jack Hills greenstone belt, *in* Structural and lithological evolution of the Jack Hills greenstone belt, Narryer Terrane, Yilgarn Craton, Western Australia: Western Australia Geological Survey, Record 2007/3, Plate 3

Department of Industry and Resources
FRANCIS LOGAN, M.L.A.
MINISTER FOR RESOURCES

Geological Survey of Western Australia
TIM GRIFFIN
EXECUTIVE DIRECTOR

500 Metres — 0 — 1 Kilometre

UNIVERSAL TRANSVERSE MERCATOR PROJECTION
HORIZONTAL DATUM: GEODETIC DATUM OF AUSTRALIA 1994
VERTICAL DATUM: AUSTRALIAN HEIGHT DATUM
Grid lines indicate 500 metre interval of the Map Grid Australia Zone 50

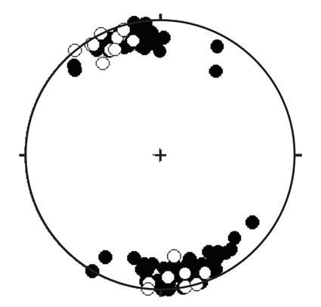

All rocks: main foliation (S_m), black dots, n=90; BIF–chert: S_m / banding, open dots, n=18; mean principle orientation of S_m: 078/78N

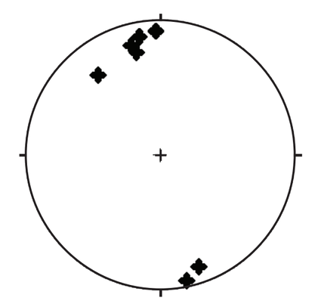

Metasedimentary and mafic schists: early foliation, n=7

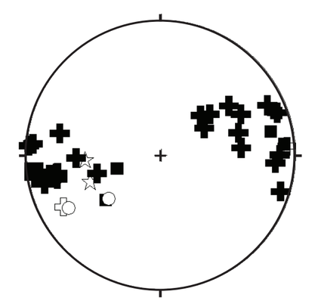

Mineral lineations (L_m): quartzite, stars, n=2; mafic and quartz–mica schists, black crosses, n=24; ultramafics, open dots, n=2; BIF–chert, squares, n=14; granite and gneiss, open crosses, n=2

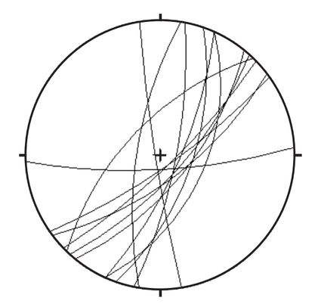

Late folds (fold banding or post-S_m): all rocks, axial planes, n=13

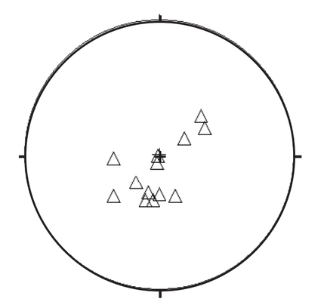

Late folds (fold banding or post-S_m): all rocks, fold axes, n=13

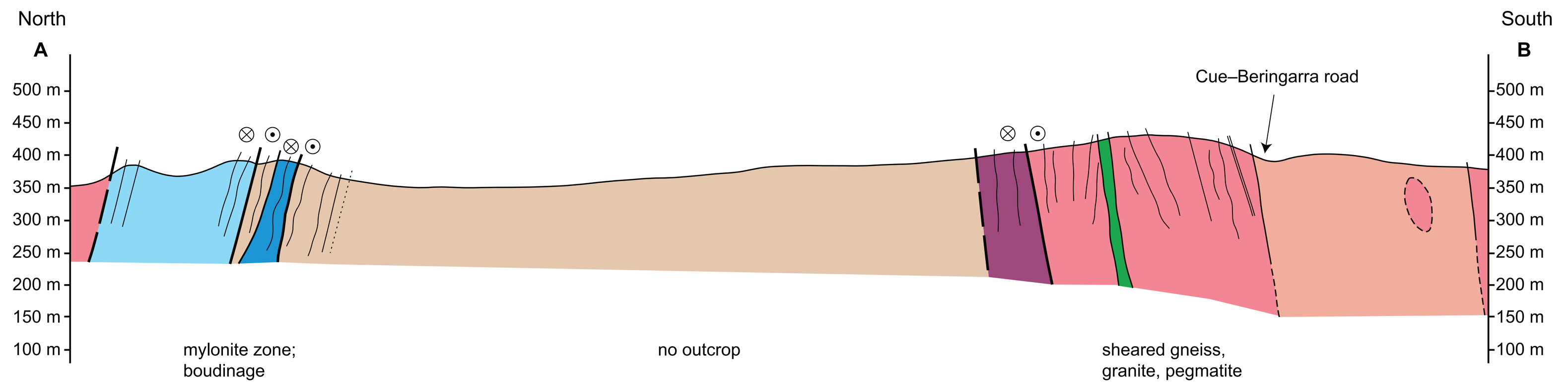

GEOLOGICAL SURVEY OF WESTERN AUSTRALIA
RECORD 2007/3 PLATE 3

PLATE 3
CENTRAL AREA OF THE JACK HILLS GREENSTONE BELT

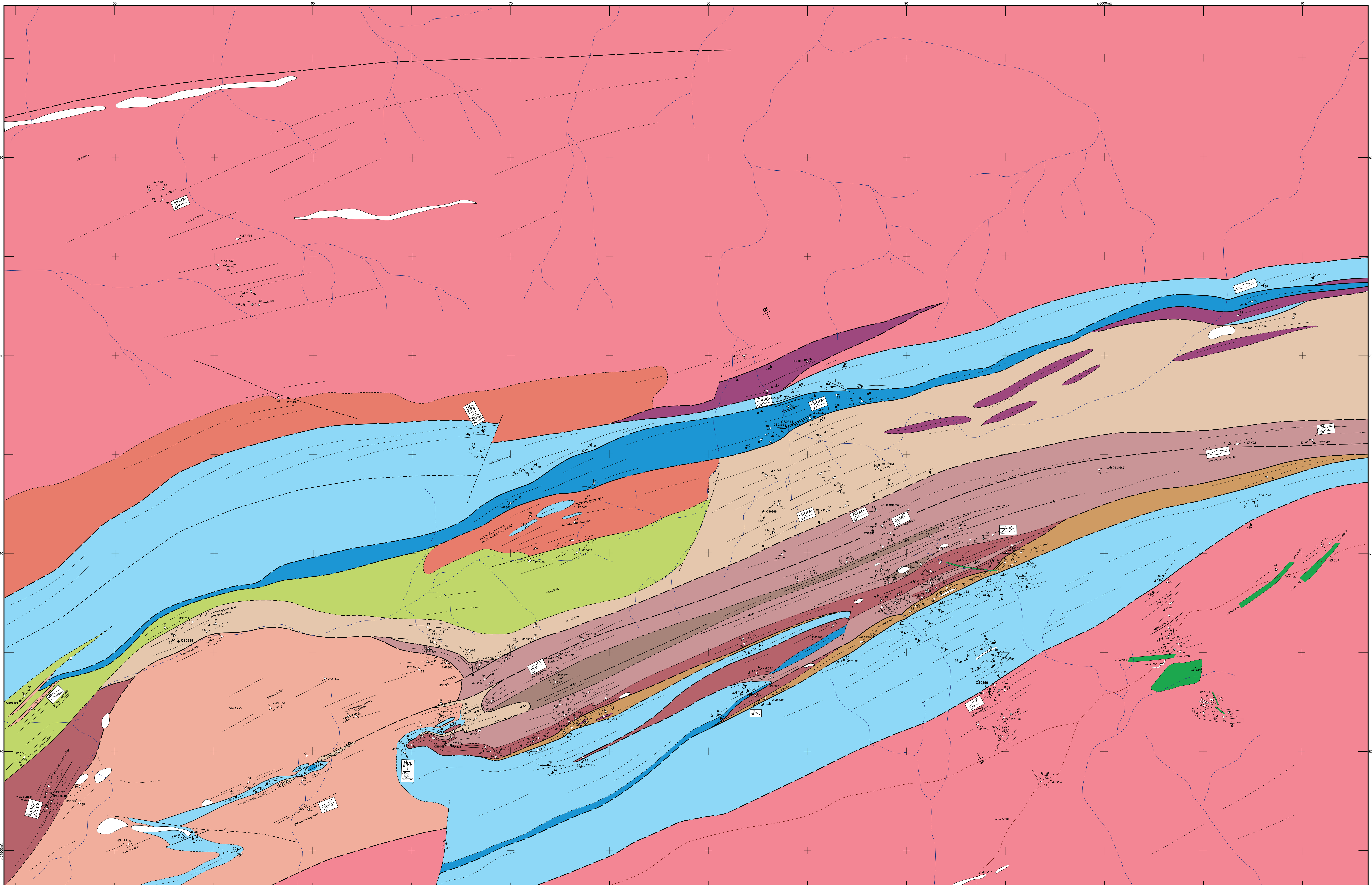

Lithological units

- dolerite or gabbro plug, sill or dyke
- felsic dyke
- quartz veins
- (Proterozoic) fine-grained micaceous schist, quartz–mica schist, quartzite
- (Proterozoic) quartzite, metasandstone, metaconglomerate, quartz–mica schist, ferruginous schist
- muscovite granite and pegmatite, pegmatite
- granitic rocks
- black and white ferruginous psammite, quartzite, jaspilitic chert, minor quartz–mica schist and metasandstone
- fine-grained micaceous schist, quartz–mica schist, quartzite
- pebble metaconglomerate, interbedded with metagritstone, metasandstone, quartzite and fine-grained micaceous schist
- interbedded metasandstone, quartzite, metagritstone, minor pebble metaconglomerate, and fine-grained micaceous schist
- andalusite schist, quartz–mica schist
- fine-grained micaceous schist, quartz–mica schist, quartzite, sometimes interleaved with mafic or ultramafic schist
- quartzite or chert, black and white banded chert, jaspilite, minor quartz–mica schist, banded iron-formation
- banded iron-formation, chert
- mafic schist (mostly hornblende- or actinolite-rich), chlorite schist, commonly interleaved with quartz–mica or biotite schist, and ultramafic rocks
- serpentinized ultramafic rocks, silicified ultramafic rocks, mafic schist
- gneiss, foliated granitic rocks, pegmatite, mafic and ultramafic schist

Structural symbols

Fault
- major fault with dip; inferred major fault
- reverse or thrust fault with dip; inferred reverse or thrust fault
- fault or unconformity, or both
- brittle or minor fault with dip; inferred brittle or minor fault
- brittle fault zone
- dextral strike slip movement (section only)
- sinistral strike-slip movement (section only)

Geological boundary
- contact interpreted from satellite image
- lithological boundary; inferred lithological boundary

Structural symbols

Fold
- axial trace of fold hinges
- fold with axial surface and plunge
- antiform; synform
- fold vergence (to next antiform) S_o/S_m

Bedding
- inclined
- vertical
- overturned
- bedding (section only)

Trend of bedding or foliation
- trend lines
- trend lines of anastomosing foliation, often associated with shearing
- trend lines from aerial photo or satellite image interpretation
- early cleavage (section only)
- crenulation cleavage (section only)
- gneissic fabric (section only)

Metamorphic foliation, showing strike and dip
- early foliation; vertical
- compositional banding (BIF and chert); parallel to main foliation (S_m); vertical
- gneissic layering
- main foliation (S_m); vertical
- crenulation cleavage (S_{cc}); vertical
- 2nd generation crenulation cleavage; vertical
- spaced foliation (S_{cc}); vertical
- shear bands

Lineation, showing trend and plunge
- intersection lineation (bedding and main foliation L_o/S_m)
- crenulation intersection lineation (LS_{cc})
- pebble elongation
- mineral lineation (L_m)
- rodding lineation
- section lines
- younging direction
- sample locality
- GPS waypoint
- creek
- secondary road or track
- hill
- locality

1:250 000 SHEET INDEX

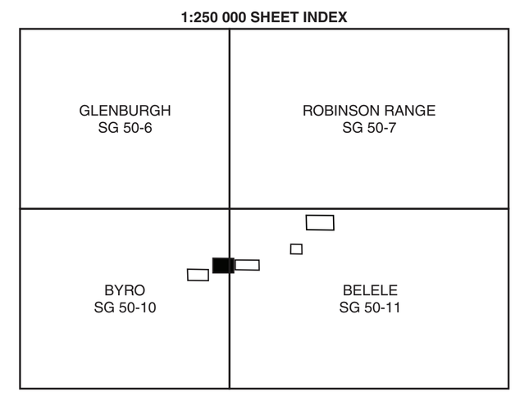

Compiled by C.V. Spaggiari 2003–04
Cartography by C.V. Spaggiari and A. Blake

Published by the Geological Survey of Western Australia. PDF available on website at www.doir.wa.gov.au/GSWA/publications

The recommended reference for this map is:
SPAGGIARI, C. V., 2007, West-central area of the Jack Hills greenstone belt, *in* Structural and lithological evolution of the Jack Hills greenstone belt, Narryer Terrane, Yilgarn Craton, Western Australia: Western Australia Geological Survey, Record 2007/3, Plate 4

Department of Industry and Resources
FRANCIS LOGAN, M.L.A.
MINISTER FOR RESOURCES

Geological Survey of Western Australia
TIM GRIFFIN
EXECUTIVE DIRECTOR

500 Metres 0 1 Kilometre

UNIVERSAL TRANSVERSE MERCATOR PROJECTION
HORIZONTAL DATUM: GEODETIC DATUM OF AUSTRALIA 1994
VERTICAL DATUM: AUSTRALIAN HEIGHT DATUM
Grid lines indicate 500 metre interval of the Map Grid Australia Zone 50

GEOLOGICAL SURVEY OF WESTERN AUSTRALIA
RECORD 2007/3 PLATE 4

PLATE 4
WEST-CENTRAL AREA OF THE JACK HILLS GREENSTONE BELT

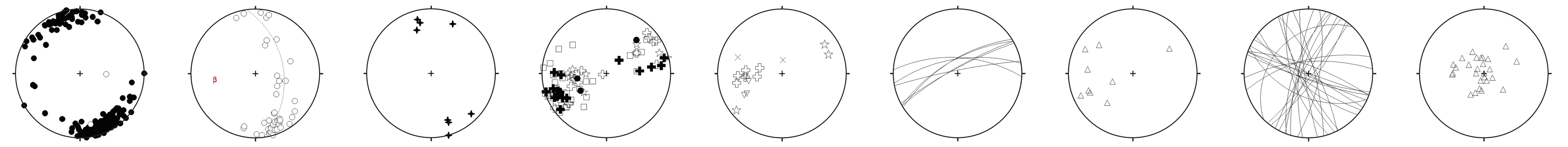

Main foliation (S_m): all rocks, black dots, n=214; BIF–chert: S_m / banding, open dots, n=2; mean principle orientation: 067/84 NW

Bedding: metasedimentary rocks, n=45; calculated girdle: 172/54E calculated beta axis: 36–262

Early foliation: metasedimentary, mafic and ultramafic rocks, n=8

Mineral lineation (L_m): quartzite–conglomerate, stars, n=11; schists, black crosses, n=16; ultramafic rocks, dots, n=3; BIF–chert, squares, n=32; granite and gneiss, open crosses, n=18

Quartzite–conglomerate: intersection lineation (S_o–S_m), triangles, n=5; pebble elongation, open crosses, n=6; BIF–chert: crenulation lineation, crosses, n=2; gneissic mineral lineation, stars, n=3

BIF: axial planes defined by main foliation (S_m), n=7

BIF: fold axes where axial planes are defined by main foliation (S_m), n=9

All rocks: late folds (fold banding or post-main foliation (S_m)), axial planes, n=28

All rocks: late folds (fold banding or post-main foliation (S_m)), fold axes, n=28

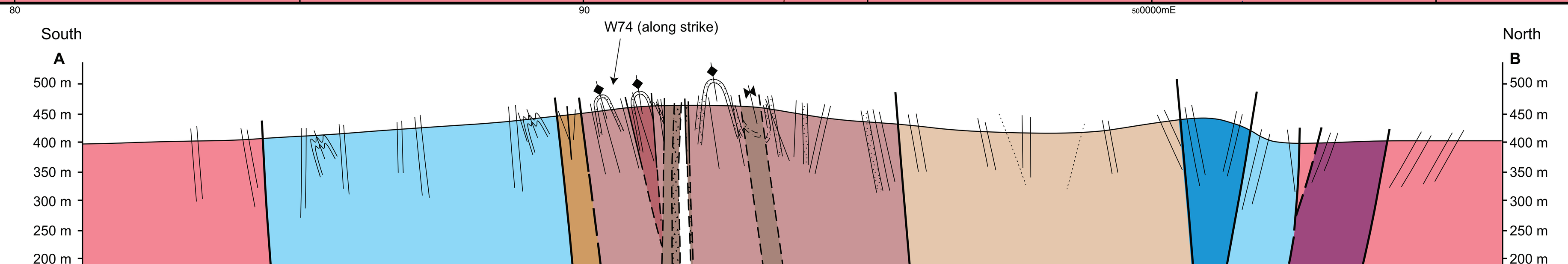

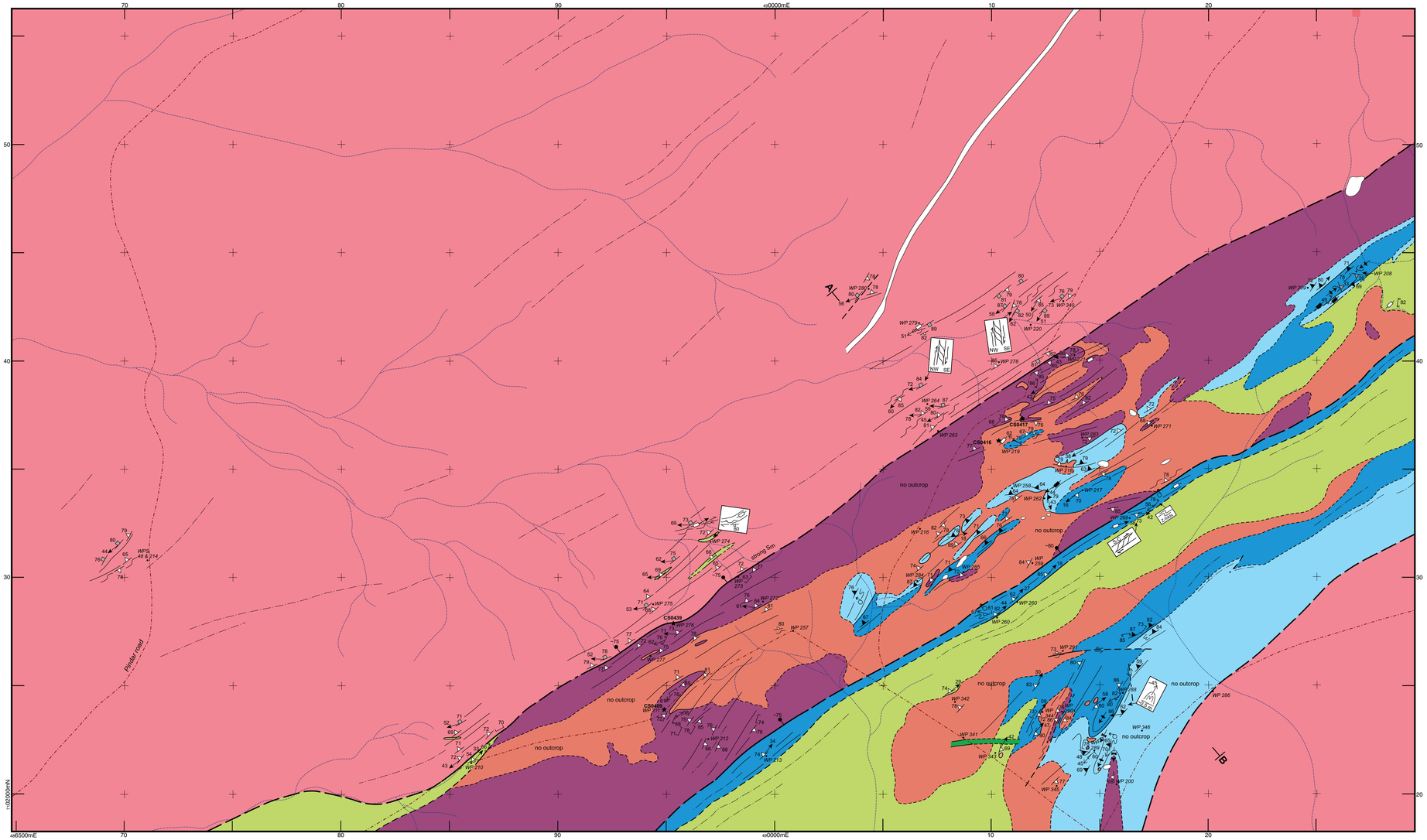

Lithological units

- dolerite or gabbro plug, sill or dyke
- felsic dyke
- quartz veins
- (Proterozoic) fine-grained micaceous schist, quartz–mica schist, quartzite
- (Proterozoic) quartzite, metasandstone, metaconglomerate, quartz–mica schist, ferruginous schist
- muscovite granite and pegmatite, pegmatite
- granitic rocks
- black and white ferruginous psammite, quartzite, jaspilitic chert, minor quartz–mica schist and metasandstone
- fine-grained micaceous schist, quartz–mica schist, quartzite
- pebble metaconglomerate, interbedded with metagritstone, metasandstone, quartzite and fine-grained micaceous schist
- interbedded metasandstone, quartzite, metagritstone, minor pebble metaconglomerate, and fine-grained micaceous schist
- andalusite schist, quartz–mica schist
- fine-grained micaceous schist, quartz–mica schist, quartzite, sometimes interleaved with mafic or ultramafic schist
- quartzite or chert, black and white banded chert, jaspilite, minor quartz–mica schist, banded iron-formation
- banded iron-formation, chert
- mafic schist (mostly hornblende- or actinolite-rich), chlorite schist, commonly interleaved with quartz–mica or biotite schist, and ultramafic rocks
- serpentinized ultramafic rocks, silicified ultramafic rocks, mafic schist
- gneiss, foliated granitic rocks, pegmatite, mafic and ultramafic schist

Structural symbols

Fault
- major fault with dip; inferred major fault
- reverse or thrust fault with dip; inferred reverse or thrust fault
- fault or unconformity, or both
- brittle or minor fault with dip; inferred brittle or minor fault
- brittle fault zone
- dextral strike slip movement (section only)
- sinistral strike-slip movement (section only)

Geological boundary
- contact interpreted from satellite image
- lithological boundary; inferred lithological boundary

Structural symbols

Fold
- axial trace of fold hinges
- fold with axial surface and plunge
- antiform; synform
- fold vergence (to next antiform) S_O/S_M

Bedding
- inclined
- vertical
- overturned
- bedding (section only)

Trend of bedding or foliation
- trend lines
- trend lines of anastomosing foliation, often associated with shearing
- trend lines from aerial photo or satellite image interpretation
- early cleavage (section only)
- crenulation cleavage (section only)
- gneissic fabric (section only)

Metamorphic foliation, showing strike and dip
- early foliation; vertical
- compositional banding (BIF and chert); parallel to main foliation (S_M); vertical
- gneissic layering
- main foliation (S_M): vertical
- crenulation cleavage (S_{CC}): vertical
- 2nd generation crenulation cleavage; vertical
- spaced foliation (S_{CC}): vertical
- shear bands

Lineation, showing trend and plunge
- intersection lineation (bedding and main foliation L_O/S_M)
- crenulation intersection lineation ($L_{S_{CC}}$)
- pebble elongation
- mineral lineation (L_M)
- rodding lineation

- section lines
- younging direction
- sample locality
- GPS waypoint
- creek
- secondary road or track
- hill
- locality

1:250 000 SHEET INDEX

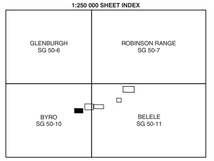

Compiled by C.V. Spaggiari 2003–04
Cartography by C.V. Spaggiari and A. Blake

Published by the Geological Survey of Western Australia. PDF available on website at www.doir.wa.gov.au/GSWA/publications

The recommended reference for this map is:
SPAGGIARI, C. V., 2007, Northwestern area of the Jack Hills greenstone belt, *in* Structural and lithological evolution of the Jack Hills greenstone belt, Narryer Terrane, Yilgarn Craton, Western Australia: Western Australia Geological Survey, Record 2007/3, Plate 5

Department of Industry and Resources
FRANCIS LOGAN, M.L.A.
MINISTER FOR RESOURCES

Geological Survey of Western Australia
TIM GRIFFIN
EXECUTIVE DIRECTOR

500 0 1
Metres Kilometre

UNIVERSAL TRANSVERSE MERCATOR PROJECTION
HORIZONTAL DATUM: GEODETIC DATUM OF AUSTRALIA 1994
VERTICAL DATUM: AUSTRALIAN HEIGHT DATUM
Grid lines indicate 500 metre interval of the Map Grid Australia Zone 50

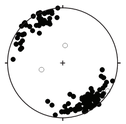

Main foliation (S_M): all rocks, black dots, n=120;BIF–chert, banding, open dots, n=3; mean principle orientation of S_M: 056/84NW

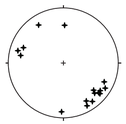

Early foliation: all rocks, n=19

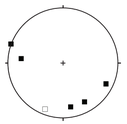

Late folds (fold banding or post-S_M): all rocks except gneiss, axial planes, n=5; gneiss, open square, n=1

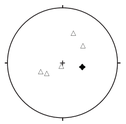

Late folds (fold banding or post-S_M): all rocks except gneiss, fold axes, n=5; gneiss, open square, n=1

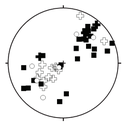

Mineral lineation (L_M): schists, black crosses, n=3; ultramafic rocks, dots, n=6; BIF–chert, squares, n=26; granite and gneiss, open crosses, n=13

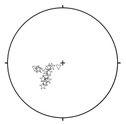

Intersection lineation, triangles, n=2; gneissic layering, stars, n=11

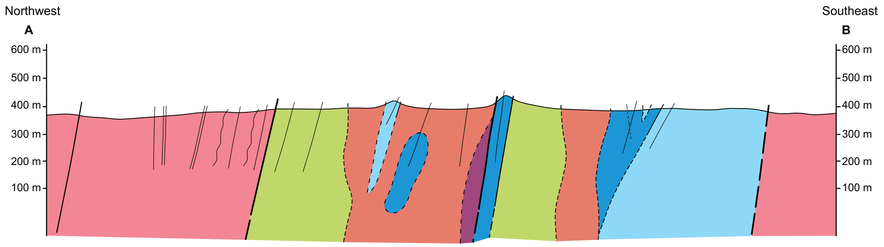

GEOLOGICAL SURVEY OF WESTERN AUSTRALIA
RECORD 2007/3 PLATE 5

PLATE 5
SOUTHWESTERN AREA OF THE JACK HILLS GREENSTONE BELT